NACA

RESEARCH MEMORANDUM

TRANSONIC INVESTIGATION OF YAWED WINGS OF ASPECT RATIOS 3 AND 6 WITH A SEARS-HAACK BODY AND WITH SYMMETRICAL AND ASYMMETRICAL BODIES INDENTED FOR A MACH NUMBER OF 1.20

By George H. Holdaway and Elaine W. Hatfield

Ames Aeronautical Laboratory
Moffett Field, Calif.

NATIONAL ADVISORY COMMITTEE FOR AERONAUTICS

WASHINGTON

June 30, 1958

NATIONAL ADVISORY COMMITTEE FOR AERONAUTICS

RESEARCH MEMORANDUM

TRANSONIC INVESTIGATION OF YAWED WINGS OF ASPECT RATIOS 3 AND 6 WITH A SEARS-HAACK BODY AND WITH SYMMETRICAL AND ASYMMETRICAL BODIES INDENTED FOR A MACH NUMBER OF 1.20

By George H. Holdaway and Elaine W. Hatfield

SUMMARY

This investigation, which emphasized the experimental and predicted wave-drag characteristics of wing-body combinations, was conducted at a Reynolds number per foot of about 4,000,000. Two yawed wings, each with an average sweep of about 40°, were tested with various bodies and the results were compared with existing data for similar models with swept-back wings. An 8-percent-thick yawed wing of aspect ratio 6 was tested with a fineness-ratio-11 Sears-Haack body, a symmetrically indented body designed for a Mach number of 1.20, and an asymmetrical M = 1.20 indented body. An aspect-ratio-3 yawed wing with a streamwise thickness of about 5 percent was tested with a fineness-ratio-12.5 Sears-Haack body and a symmetrical M = 1.20 indented body.

In general, the effects of changing the plan form of a wing from sweptback to yawed were similar for either aspect ratio. With or without body contouring the drag coefficients were reduced at transonic speeds and increased to a lesser extent at subsonic and supersonic speeds by yawing the wings. Inboard loading on the sweptforward panel and outboard loading on the sweptback panel of the yawed wings caused negative rolling moments near zero lift. Predictions of the wave drag were satisfactory for the aspect-ratio-3 wings and unsatisfactory for the aspect-ratio-6 wings either sweptback or yawed.

INTRODUCTION

Experiment and theory (e.g., refs. 1 through 6) have demonstrated that the supersonic wave drag can be kept low by using slender configurations with smooth longitudinal distributions of volume. Usually the

wave drag of the configurations was improved by the proper removal or addition of volume to the body. Another possibility for reducing wave drag exists - that of merely redistributing the wing volume. Since a yawed wing has its volume distributed over a greater streamwise length than a sweptback wing with similar panels, the yawed wing might be expected to have lower wave drag. The primary purpose of this investigation was to measure the drag of two yawed wings in combination with several bodies. The wings had aspect ratios of 3 and 6 with streamwise thickness-chord ratios of about 5 and 8 percent, respectively. Tests of the latter thicker wing were of additional interest because theoretical computations were not expected to apply and the relative magnitude of the experimental changes in wave drag in comparison with estimated values were felt to be of interest.

Because of the asymmetry of a yawed wing, an asymmetrical body contour was devised and tested with the aspect-ratio-6 wing. The basis for the design is indicated by the plan view of this yawed wing in sketch (a). As outlined in reference 2, the desired body indentation

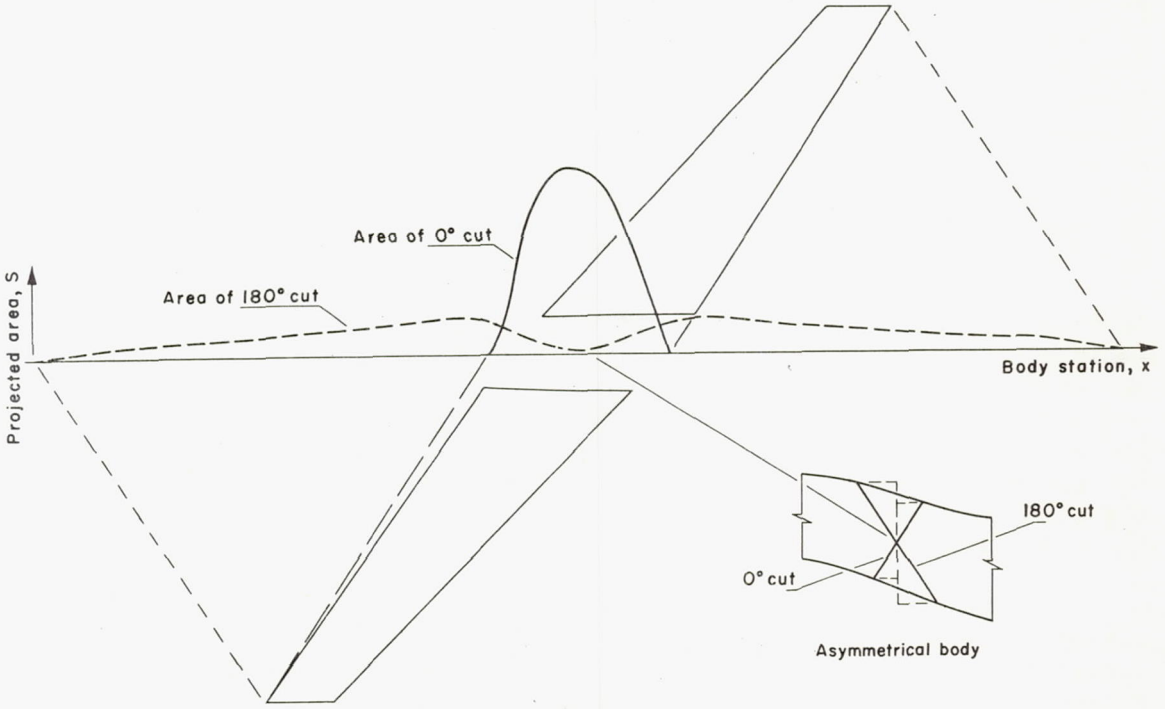

Sketch (a)

for a wing-body combination at a specified supersonic Mach number is based on an average wing area obtained from all cuts tangent to the Mach cone for each particular body station. As shown in the sketch, a curved body could compensate for the different wing areas resulting from cuts made 180° apart. A secondary purpose in testing the asymmetrical wing-body combination was the possibility that the pressure-term contribution

which appears in the wave-drag equation of reference 4, but is neglected in that of reference 2, would contribute to the wave-drag reduction.

The investigation included the measurement of the surface pressures on all bodies and wings. Data for comparable sweptback wings (with symmetrical bodies) were obtained from references 7 and 8. Test data were obtained for an angle-of-attack range of $\pm 4^{\circ}$, a Mach number range of 0.80 to 1.20, and a Reynolds number per foot of about 4,000,000.

The symbols used in the report are presented in appendix A.

MODELS AND TESTS

Yawed wings of aspect ratios 6 and 3, each with an average sweep of roughly 40°, were used with various bodies for this investigation. The wings were fabricated of solid steel and covered by plastic impregnated glass cloth containing pressure tubes. A sketch of the aspect-ratio-6 yawed wing with a Sears-Haack body with a closed-body fineness ratio of 11 is shown in figure 1. This body is, by definition, a minimum-wave-drag body for transonic speeds for prescribed volume and length; its equation is given in figure 1. A similar body was used with the aspect-ratio-3 wing, but in this case the closed-body fineness ratio was 12.5. Details of the aspect-ratio-3 yawed wing are given in figure 2(a). In both figures 1 and 2(a), note the comparable sweptback wings indicated by dashed lines.

The yawed wings were also used with the basic Sears-Haack bodies symmetrically indented for minimum wave drag at $M = 1.20$ by the procedures given in reference 2. The indentations for the yawed wings neglected a small portion of the wing tip when it was projected ahead of the body nose for some roll-angle cuts. These indented-body radii are listed in table I. A photograph of the aspect-ratio-3 yawed wing with the indented body is shown in figure 2(b). The cross-sectional area distributions normal to the free stream for the various combinations are shown in figures 3 and 4.

Asymmetrical bodies indented for $M = 1.20$ were designed by a method discussed in appendix B. Only the asymmetrical body for the aspect-ratio-6 wing was constructed and tested for reasons to be discussed in the next section. Geometric details are presented in table II and figure 5(a), and a photograph of the model is presented in figure 5(b). The body cross-sections in this case are elliptical with a ratio of the horizontal to the vertical axis of 2 to 1. (This ratio is altered near the body base to approach circular sections to accommodate the circular model-support sting.)

Wing-pressure orifices were located as shown in figure 6. Pressure orifices were located on the symmetrical bodies as shown in figure 7. The locations of the pressure orifices on the asymmetrical body are shown in table III and figure 8.

The models were tested in the Ames 14-foot transonic wind tunnel which is of the closed-return type with perforated walls in the test section. A sketch of the high-speed region of this test facility is presented in figure 9. The flexible walls ahead of the test section produce the convergent-divergent nozzle required to generate supersonic Mach numbers up to 1.20. This tunnel is similar to the smaller Ames 2- by 2-foot transonic wind tunnel which is described in detail in reference 9. One exception, however, is that the 14-foot tunnel is not of the variable-density type, but operates at atmospheric pressure. The models are mounted on a sting and the forces are measured as electrical outputs from a strain-gage balance located within the model. Transition of the boundary layer was fixed for each body by Carborundum grit (size 200) distributed over 1 inch of the body nose as can be seen in figures 2(b) and 5(b).

Force data, wing pressures, and body pressures were obtained over an angle-of-attack range of about $\pm 4^{\circ}$. The Reynolds number per foot of the tests was about 4,000,000 throughout the Mach number range of 0.80 to 1.20. The tunnel blockage of the models was in each case less than one-half of 1 percent, and the data should be relatively free of wall interference as indicated by reference 9. All aerodynamic coefficients are based on the complete plan-form area of the particular wing for which the results apply. The pitching moments were computed about the moment centers listed in figures 1 and 2. These moment centers were selected as the average of the locations of the quarter chords of the mean aerodynamic chords of the sweptback and sweptforward panels. The drag coefficients were adjusted by equating the base pressures to free-stream static pressure. The magnitudes of the base-drag coefficients for this investigation were comparable to those presented in reference 8 for similar base conditions.

The wave-drag component of the zero-lift drag coefficient at supersonic speeds was estimated using the harmonic analysis method of reference 5. The zero-lift rise in the drag coefficients above the subsonic level at $M = 0.80$ was assumed to be directly comparable to the wave drag, because sample theoretical computations for each wing model showed a friction-drag-coefficient variation (from $M = 0.80$ to $M = 1.20$) which was of the same order as the estimated accuracy of the experimental data of $C_{D_o} = \pm 0.0005$. For the symmetrical bodies the wave drag was computed for the bodies to closure and then corrected for the portion of the body cut off for sting mounting as was done in reference 8. This correction was equal to a C_{D_o} of -0.0006 for the aspect-ratio-3 wing and -0.0010 for the aspect-ratio-6 wing. For the asymmetrical bodies the wave drag was computed for the bodies as cut off, with the area curves arbitrarily faired to have zero slopes at the base of the model.

RESULTS AND DISCUSSION

The results will be discussed in two major divisions with primary emphasis on the wave drag. The first section will be concerned with force measurements and the last section with zero-lift pressure coefficients. The pressure data are used primarily as an aid in interpreting the force data.

Aerodynamic Characteristics

Plots of the basic data for the aspect-ratio-6 yawed wing with the asymmetrical M = 1.20 indented body are shown in figure 10. These data were selected as representative, although this was the only configuration which had significant (although small) yawing-moment (fig. 10(e)) and side-force coefficients (fig. 10(f)). The aerodynamic coefficients of the various models with the aspect-ratio-6 wing are presented in figure 11, and similar data for the models with the aspect-ratio-3 wing are presented in figure 12. The drag polars presented in figures 11(c) and 12(c) clearly indicate that the indentations were effective in reducing the drag at all supersonic Mach numbers and at lifting conditions as well as at zero lift. The subsonic drag data for the symmetrical M = 1.20 indented body with the aspect-ratio-6 yawed wing (fig. 11(c)) appear to be too low because of the lack of agreement with the unindented configuration at M = 0.80. Unfortunately, data for the indented configuration were not obtained at M = 0.90 and 0.94. The supersonic drag data were checked at zero lift by a separate run at M = 1.195. The drag at zero lift will be discussed later.

Lift and moments.- In general the lift and moment curves were more nonlinear for the asymmetrical body with the aspect-ratio-6 yawed wing (fig. 11) than for any other model. The assumption of a center-of-pressure location which was an average of the locations of the quarter chords of the mean aerodynamic chords of the sweptforward and sweptback panels was quite good at subsonic Mach numbers for the aspect-ratio-6 yawed wing and at M = 1.05 for the aspect-ratio-3 yawed wing as shown by the pitching-moment data of figures 11(b) and 12(b).

Of particular interest were the rolling-moment data of figures 11(d) and 12(d). Generally, for each yawed wing the rolling moments decreased with an increase in positive lift. The pressure data, which will be presented later, showed that the sweptforward panel had greater inboard loading and the sweptback wing had the greater outboard loading which accounts for the negative rolling moments. Some penalty in drag would probably be incurred in providing lateral trim for these configurations.

The lift curves for the two yawed wings with their respective Sears-Haack bodies were sufficiently linear that the slopes could be measured and are compared in figure 13 with values from references 6 and 7 for comparable sweptback-wing-body combinations. Relative to their comparable (same wing sections and volume) sweptback wings the aspect-ratio-6 yawed wing was superior at supersonic Mach numbers and the aspect-ratio-3 yawed wing was inferior at most Mach numbers.

Zero-lift-drag.- In comparison with sweptback wings, the yawed wings have cross-sectional area distributions normal to the free stream (see fig. 14) that are equivalent to longer and thinner bodies and were therefore expected to have lower wave drag at $M = 1.00$. These expectations were realized as shown in figure 15. In both cases the yawed wings had lower drag at transonic speeds and higher drag at both subsonic and supersonic speeds than the sweptback-wing models. The higher drag for the yawed wings at subsonic speeds might be the result of separated flow near the wing-body juncture. The higher drag at supersonic speeds was not predicted theoretically and is probably a result of the reduced sweep of the leading edge of the sweptforward panel. As shown in table IV the leading-edge stagnation pressures on the sweptforward panel at $M = 1.20$ were 30 to 60 percent greater than those on the sweptback one.

As mentioned previously the symmetrical $M = 1.20$ indentations were successful in reducing the supersonic drag of the yawed wings and, in particular, at the zero-lift coefficients as shown in figure 16. These results for the aspect-ratio-3 yawed wing with the indented body are replotted in figure 17 with zero-lift drag coefficients from reference 8 for the sweptback wing and similarly indented body. It is apparent that at the design Mach number of 1.20 the indentation for the yawed wing did not alleviate the greatly increased drag of the yawed wing in comparison with the sweptback wing.

Although the theoretical predictions for the aspect-ratio-6 wing with the asymmetrically indented body indicated an increase in wave-drag coefficient at $M = 1.20$ of 0.0020 in comparison with the symmetrically indented model, the experimental results indicated no penalty. This result may be noted from the zero-lift drag coefficients of figure 18 and the drag-rise coefficients of figure 19. Figure 19 includes the results for the aspect-ratio-6 wing with the basic Sears-Haack body. From figure 19 it may be noted that the wave drag was reduced by the asymmetrical contouring relative to the basic body by 10 to 40 percent at all the supersonic Mach numbers. No quantitative wave-drag comparisons should be made relative to the symmetrically indented configuration because of the uncertainty of the subsonic data.

Figure 20 shows that the computed zero-lift drag for the aspect-ratio-6 sweptback wing was not in agreement with experimental values from reference 7. This is also true for the yawed wing (fig. 21). These results illustrate that the method of reference 5 cannot be relied on to

estimate accurately the wave drag of relatively high-aspect-ratio wings of this thickness. Figures 22(a) and (b) show that the calculations are reliable for the aspect-ratio-3 wing. The computations for this wing are more accurate for the indented configuration which has the more optimum area curves. The little peak in the computed curve is at the Mach number for which the leading edge of the sweptforward-wing panel is sonic.

Effect of oblique-force term, $\beta L(x,\theta)/2q$.- The body of the asymmetrically indented model tested was sufficiently asymmetrical relative to normal aircraft design that a check of the size of the oblique-force term of reference 4 at $M = 1.20$ and zero lift was of practical interest. The size of this term at zero lift would probably (but not necessarily) be a maximum at the highest test Mach number because the term is a direct function of β and goes to zero at $M = 1.00$. The pressures on the body used to compute the oblique-force term are shown in figure 23. The orifice locations are given in figure 8 and table III. As a result of the relative thinness of the wing, the oblique-force-term contribution from the wing should be negligible at zero lift. The oblique-force terms obtained from the pressure coefficients for various cutting-plane angles, θ, are shown in figure 24, and the equivalent area distributions for two representative θ angles of 0° and 180° are presented in figure 25. Although the area curves for each θ angle were altered slightly by introducing the equivalent areas of the oblique-force term, the over-all effect on the computed wave-drag coefficients was negligible for $M = 1.20$.

Pressure Results

Summary plots of some of the more interesting wing pressure coefficients at zero lift are presented in figures 26 through 29. The pressure coefficients near the wing-body juncture are of interest relative to techniques such as reference 7 for reducing the interference effects near a wing root at high subsonic and transonic speeds. The curves of figures 26 and 27 show that the sweptforward panels, in comparison with the sweptback panels, have juncture pressure coefficients which would be expected to give more favorable drag interference with the bodies (particularly at $M = 1.00$). The general effect of the asymmetrical indented body on the wing pressure near the wing-body juncture (shown in fig. 26) was to reduce the pressure coefficients almost as if the wing were thinner.

A comparison of the wing pressure coefficients at three spanwise stations on the sweptback wing, the sweptback panel, and the sweptforward panel is made in figure 28 for the aspect-ratio-6 wings and in figure 29 for the aspect-ratio-3 wings. The results for the wings of different aspect ratios are similar. These pressure data clearly demonstrate the large inboard loading on the sweptforward panel and the large outboard

loading on the sweptback panel or the sweptback wing. These loadings explain the negative rolling moments near zero lift obtained from the force measurements. The wing pressure coefficients for the sweptback panel generally approached the values for the sweptback wing.

The wing pressure coefficients at zero lift for the aspect-ratio-6 yawed wing with various bodies are given in detail in figures 30 through 32 and present a direct comparison between sweptback and sweptforward panels. The body pressure coefficients for the aspect-ratio-6 yawed wing at zero lift are presented in figure 33. Similarly, the wing pressure coefficients for the aspect-ratio-3 yawed wing models are presented in figures 34 and 35 and the body pressure coefficients in figure 36.

CONCLUDING REMARKS

In general, the effects on the drag characteristics of a model obtained by changing a sweptback wing to a yawed wing were similar for either the aspect-ratio-6 or -3 wings. Without body contouring, drag-coefficient reductions at a Mach number near 1.00 of about 0.0050 to 0.0100 were obtained by yawing the wings. Yawing the wings caused increases in the drag coefficients at subsonic Mach numbers of about 0.0015 to 0.0030 and at $M = 1.20$ of about 0.0035 to 0.0060. In each case the lower values are for the aspect-ratio-3 wing which had the larger wing area and the thinner sections. With a symmetrical $M = 1.20$ indented body, the aspect-ratio-3 yawed wing again had lower drag at transonic speeds and higher drag at $M = 1.20$ relative to a comparable indentation for a sweptback wing. For both yawed wings the $M = 1.20$ indentations reduced the supersonic wave drag without an increase in drag at $M = 1.00$.

Predictions of the wave drag were satisfactory for aspect-ratio-3 wings and unsatisfactory for the aspect-ratio-6 wings, either sweptback or yawed. Although the theoretical predictions for the aspect-ratio-6 wing with the asymmetrically indented body indicated an increase in wave-drag coefficient of 0.0020 in comparison with the symmetrically indented model, the experimental results indicated qualitatively no penalty.

Introducing the equivalent area curves obtained from the oblique-force term at zero lift to the area curves analyzed for $M = 1.20$ had a negligible effect on the predicted wave drag.

Ames Aeronautical Laboratory
National Advisory Committee for Aeronautics
Moffett Field, Calif., Mar. 3, 1958

APPENDIX A

SYMBOLS

A	wing aspect ratio
b	model span
C_D	drag coefficient
C_{D_o}	zero-lift drag coefficient
ΔC_{D_o}	rise of C_{D_o} above subsonic level at $M = 0.80$ or theoretical wave-drag coefficients
C_L	lift coefficient
C_l	rolling-moment coefficient
C_m	pitching-moment coefficient, measured about the average of the locations of the quarter chords of the mean aerodynamic chords of the sweptback and sweptforward panels
C_n	yawing-moment coefficient
C_p	pressure coefficient, $\frac{p-p_\infty}{q_\infty}$
C_Y	side-force coefficient
c	local chord of wing, measured parallel to the x axis
c'	local chord of design airfoil section of the aspect-ratio-3 wing, measured perpendicular to $\Lambda = 39.45^\circ$ line
$\bar{c}$	mean aerodynamic chord
c_j	juncture chord, measured in x direction from point of intersection of wing leading edge and body
d	distance from asymmetrical body mean center line to reference line, x axis
e	perpendicular distance from xz plane through body mean center line to surface of asymmetrical body for different θ as shown in figure 5(a)

$L(x,\theta)$ resultant force (on the obliquely cut section) normal to the free stream and parallel to the plane θ = constant (ref. 4)

l length of theoretical body to closure

M free-stream Mach number

N number of terms or harmonics used in the theoretical computations of wave drag

p local static pressure on the model

p_∞ free-stream static pressure

q_∞ free-stream dynamic pressure

R Reynolds number

r radius of body

r_o radius of Sears-Haack body at $\frac{l}{2}$; maximum radius

S projection of S_S on a plane perpendicular to the x axis

S_S area formed by cutting configuration with planes tangent to the Mach cone

x,y,z Cartesian coordinates as conventional body axes (measured from the body reference line for the asymmetrical body)

α angle of attack

β $\sqrt{M^2-1}$

θ angle between the positive y axis and the projection of the tangent to the Mach cone in the yz plane; also roll angle

Λ sweep angle

ξ distance in the x direction measured from the intersection of the wing leading edge and the body

ψ angle in the xy plane between the intercept with the xy plane of the cutting planes tangent to the Mach cone and the positive y axis

APPENDIX B

DESIGN OF THE ASYMMETRICAL BODY

It has been shown that the wave drag of a configuration for a Mach number greater than 1 is a function of cross-sectional area cuts of planes tangent to the Mach cone (ref. 2); that is, at a particular Mach number the average of the wave-drag components of all of the area cuts will be the drag for that Mach number.

Previous methods of indentation have been to optimize the drag for a particular Mach number with a body shape which is constant for all θ angles (a body of revolution). The body of revolution was indented

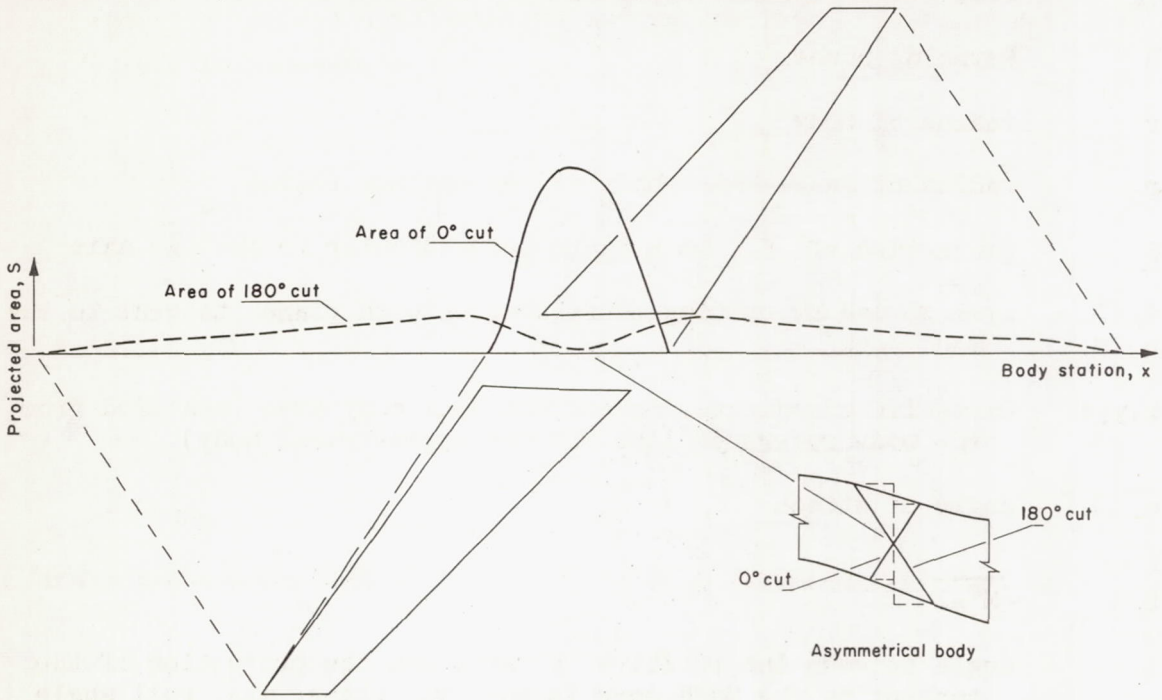

Sketch (a)

symmetrically for the average of the wing areas computed from each θ area cut of the Mach cone. However, for the yawed wing the individual wing areas vary greatly from the average (sketch (a)), so it was thought that for this configuration an asymmetrical indentation might produce lower wave drag than the conventional symmetrical type of indentation. For the asymmetrically indented body the cross-sectional area contribution of the body would be more for some θ cuts than for others. The body contribution would be designed to complement the cross-sectional area contribution of the wings (sketch (a)).

The following procedure was used in designing the asymmetrical body for the aspect-ratio-6 yawed wing. The area distribution of a Sears-Haack body (minimum wave drag at transonic speeds for prescribed volume and length) was taken to be a desirable distribution for the wing-body combination for each θ cut. The design Mach number was chosen to be $M = 1.20$. The most desirable area distribution of body cross section for each roll angle or θ cut would be obtained if the computed wing area for each θ cut were subtracted from the Sears-Haack area distribution.

Optimizing all cuts at once presented numerous problems, so it was decided to begin with one or two cuts. It was thought that if the body shape could be improved for two extreme cuts ($\theta = 0^\circ$ and 180°), the cuts in between might also be improved. A body with an asymmetrical shape such as the one shown below would create the desired effect; that is small body area for 0° and large body area at 180°. The 90° cut would have an area falling between the two extremes as was also desirable.

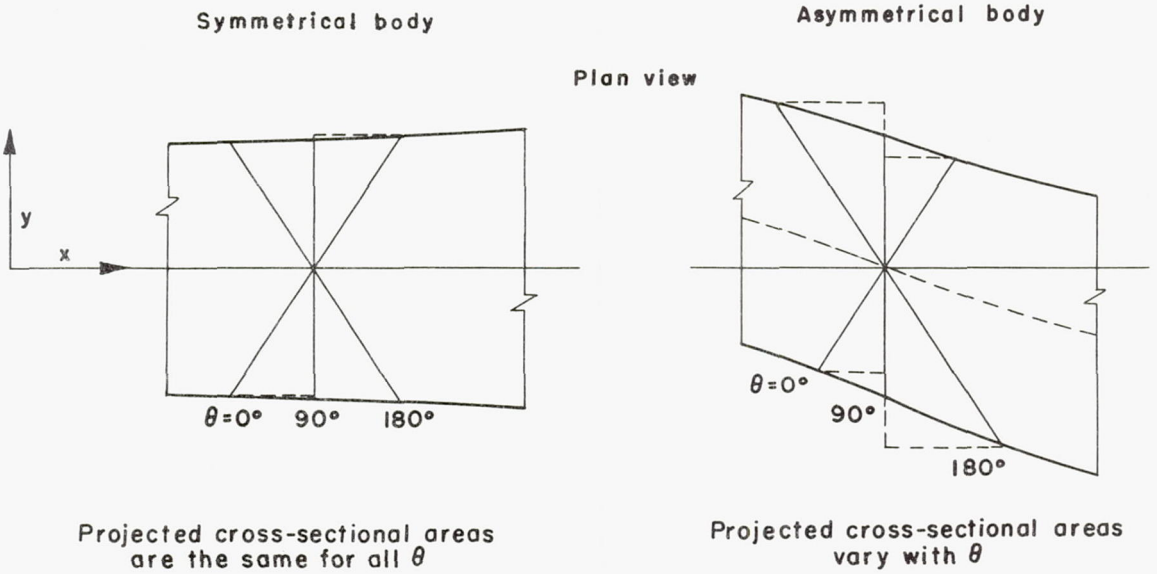

Sketch (b)

The vertical height of this body was assumed to be small in comparison with the horizontal, an elliptic shape with a ratio of 1 to 2 was chosen; thus the $\theta = 90^\circ$ cut became approximately equal to the $M = 1.00$ cut; and the vertical heights of all cuts were approximately the same. To aid in calculation, the maximum thickness of the elliptical cut was assumed to lie on the body reference line and the projected areas were assumed to be elliptical. The errors introduced were calculated and found to be small.

The method chosen to obtain the asymmetrical shape was to leave the $\theta = 90^\circ$ area distribution constant and shear the body in the y direction along planes perpendicular to the x axis in such a way as to

obtain the desired area for the other two cuts, $\theta = 0^\circ$ and $\theta = 180^\circ$. For the aspect-ratio-6 yawed wing, the body area distribution selected for the $\theta = 90^\circ$ cut was the same as that for the symmetrical average indented body for $M = 1.20$, and for the $\theta = 180^\circ$ cut, the Sears-Haack area distribution less the aspect-ratio-6 yawed wing area for the $\theta = 180^\circ$ cut was used. It was felt that the average distribution for the $\theta = 90^\circ$ cut would aid in satisfying both the $\theta = 0^\circ$ and $\theta = 180^\circ$ desired area distribution.

The contouring was not successful in lowering the complete drag for the design Mach number. The individual components of the wave drag were affected as explained below. The contouring succeeded in smoothing the $\theta = 180^\circ$ cut distribution as shown in figure 37 and it would have been a Sears-Haack distribution as desired except for newly exposed wing volume due to the contouring. The magnitude of the $\theta = 0^\circ$ cut distribution was lowered; however, the slopes of the area curves were not improved and, consequently, the computed drag was not lowered, in fact, there was an increase. The calculated drag component for the $\theta = 90^\circ$ cut which should have remained the same as for the symmetrical average indented body was somewhat worsened due to newly exposed wing areas. Similar computations with comparable results were made for the aspect-ratio-3 wing. Changes in the area curves are shown in figure 38 and the computed drag for the asymmetrical shape is shown in figure 22.

REFERENCES

1. Whitcomb, Richard T.: A Study of the Zero-Lift Drag-Rise Characteristics of Wing-Body Combinations Near the Speed of Sound. NACA Rep. 1273, 1956. (Supersedes NACA RM L52H08)

2. Jones, Robert T.: Theory of Wing-Body Drag at Supersonic Speeds. NACA Rep. 1284, 1956. (Supersedes NACA RM A53H18a)

3. Holdaway, George H.: An Experimental Investigation of Reduction in Transonic Drag Rise at Zero Lift by the Addition of Volume to the Fuselage of a Wing-Body-Tail Configuration and a Comparison With Theory. NACA RM A54F22, 1954.

4. Lomax, Harvard: The Wave Drag of Arbitrary Configurations in Linearized Flow as Determined by Areas and Forces in Oblique Planes. NACA RM A55A18, 1955.

5. Holdaway, George H., and Mersman, William A.: Application of Tchebichef Form of Harmonic Analysis to the Calculation of Zero-Lift Wave Drag of Wing-Body-Tail Combinations. NACA RM A55J28, 1956.

6. Holdaway, George H.: Additional Comparisons Between Computed and Measured Transonic Drag-Rise Coefficients at Zero Lift for Wing-Body-Tail Configurations. NACA RM A55F06, 1955.

7. McDevitt, John B., and Taylor, Robert A.: An Investigation of Wing-Body Juncture Interference Effects at Transonic Speeds for Several Swept-Wing and Body Combinations. NACA RM A57A02, 1957.

8. Holdaway, George H., and Hatfield, Elaine W.: Investigation of Symmetrical Body Indentations Designed to Reduce the Transonic Zero-Lift Wave Drag of a 45° Swept Wing With an NACA 64A006 Section and With a Thickened Leading-Edge Section. NACA RM A56K26, 1957.

9. Spiegel, Joseph M., and Lawrence, Leslie F.: A Description of the Ames 2- by 2-Foot Transonic Wind Tunnel and Preliminary Evaluation of Wall Interference. NACA RM A55I21, 1956.

TABLE I.- COORDINATES FOR THE SYMMETRICAL M = 1.20 INDENTED BODIES
[Dimensions in inches]

Body for aspect-ratio-6 wing				Body for aspect-ratio-3 wing			
Station, x	Radius, r	Station, x	Radius, r	Station, x	Radius, r	Station, x	Radius, r
0	0	42.22	3.676	0	0	60.00	4.048
.92	.282	44.00	3.725	3.00	.719	63.00	4.103
2.31	.564	45.00	3.769	6.00	1.235	66.00	4.115
4.61	.993	46.20	3.817	10.00	1.805	70.00	4.089
5.02	1.048	49.00	3.896	14.00	2.261	73.00	4.033
6.93	1.374	50.82	3.917	18.00	2.644	76.00	3.948
9.24	1.726	55.44	3.884	22.00	2.957	79.00	3.834
11.87	2.074	60.06	3.776	26.00	3.207	82.00	3.694
13.86	2.313	63.38	3.641	28.00	3.307	85.00	3.529
18.48	2.752	64.68	3.573	30.00	3.398	87.00	3.404
23.10	3.054	69.30	3.301	32.00	3.445	88.73	3.286
26.63	3.203	70.24	3.230	34.00	3.491	90.00	3.195
27.72	3.232	73.92	2.932	36.00	3.497	93.00	2.958
28.00	3.231	78.54	2.479	38.00	3.506	96.00	2.675
28.50	3.223	80.53	2.243	40.00	3.561	98.62	2.397
29.06	3.205	83.16	1.902	42.00	3.614	100.14	2.230
30.00	3.226	85.47	1.561	44.00	3.656	101.81	2.020
31.00	3.267	87.38	1.236	46.00	3.696	103.48	1.799
32.34	3.336	87.79	1.165	49.00	3.753	105.15	1.562
32.81	3.365	90.09	.688	50.00	3.775	106.82	1.298
36.96	3.583	91.48	.333	52.00	3.824	108.49	1.023
39.00	3.640	92.40	0	54.00	3.877	110.15	.679
40.00	3.653			55.00	3.908	111.37	.397
41.00	3.664			56.25	3.948	112.49	0
41.58	3.672			58.00	3.995		

TABLE II.- COORDINATES FOR THE ASYMMETRICAL M = 1.20 INDENTED BODY

[Dimensions in inches]

Horizontal ordinates			Radial ordinates[1]																				Distribution from reference line to body mean center line
			θ = 0°		θ = 5.625°		θ = 11.25°		θ = 22.5°		θ = 33.75°		θ = 45°		θ = 56.25°		θ = 67.5°		θ = 78.75°		θ = 90°		
x	+y	-y	e	z	e	z	e	z	e	z	e	z	e	z	e	z	e	z	e	z	e	z	d
2	0.714	0.714	0.714	0	0.701	0.069	0.663	0.132	0.550	0.228	0.428	0.286	0.319	0.319	0.226	0.339	0.145	0.350	0.071	0.355	0	0.357	0
4	1.210	1.210	1.210	0	1.187	.117	1.124	.224	.932	.386	.725	.484	.541	.541	.383	.574	.245	.592	.120	.602	0	.605	0
5	1.480	1.480	1.480	0	1.452	.143	1.375	.274	1.140	.472	.887	.593	.662	.662	.469	.702	.300	.725	.147	.737	0	.740	0
6	1.712	1.712	1.712	0	1.680	.165	1.591	.316	1.318	.546	1.026	.686	.766	.766	.543	.812	.347	.838	.169	.852	0	.856	0
8	2.170	2.100	2.135	0	2.095	.206	1.984	.395	1.644	.681	1.279	.855	.955	.955	.677	1.012	.433	1.045	.211	1.062	0	1.068	.035
10	2.680	2.450	2.565	0	2.517	.248	2.383	.474	1.975	.818	1.537	1.027	1.147	1.147	.813	1.216	.520	1.256	.254	1.276	0	1.283	.115
12	3.260	2.650	2.955	0	2.899	.286	2.746	.546	2.276	.943	1.770	1.183	1.322	1.322	.936	1.401	.599	1.447	.293	1.470	0	1.478	.305
14	3.890	2.680	3.285	0	3.223	.317	3.052	.607	2.530	1.048	1.968	1.315	1.469	1.469	1.041	1.558	.666	1.608	.325	1.634	0	1.643	.605
15	4.240	2.640	3.440	0	3.375	.332	3.196	.636	2.649	1.097	2.061	1.377	1.538	1.538	1.090	1.631	.698	1.684	.340	1.711	0	1.720	.800
16	4.600	2.550	3.575	0	3.508	.345	3.322	.661	2.753	1.140	2.142	1.431	1.599	1.599	1.133	1.695	.725	1.750	.354	1.779	0	1.788	1.025
18	5.420	2.250	3.835	0	3.763	.371	3.563	.709	2.953	1.223	2.298	1.535	1.715	1.715	1.215	1.819	.778	1.878	.380	1.908	0	1.918	1.585
20	6.260	1.840	4.050	0	3.974	.391	3.763	.748	3.119	1.292	2.426	1.621	1.811	1.811	1.283	1.921	.821	1.983	.401	2.015	0	2.025	2.210
22	6.790	1.630	4.210	0	4.131	.407	3.912	.778	3.242	1.343	2.522	1.685	1.883	1.883	1.334	1.996	.854	2.061	.417	2.095	0	2.105	2.580
24	7.020	1.650	4.335	0	4.253	.419	4.028	.801	3.338	1.383	2.597	1.735	1.939	1.939	1.374	2.056	.879	2.123	.429	2.157	0	2.168	2.685
25	7.020	1.760	4.390	0	4.307	.424	4.079	.811	3.381	1.400	2.630	1.757	1.963	1.963	1.391	2.082	.890	2.149	.435	2.184	0	2.195	2.630
26	6.980	1.950	4.465	0	4.381	.431	4.149	.825	3.438	1.424	2.675	1.787	1.997	1.997	1.415	2.117	.906	2.186	.442	2.222	0	2.233	2.515
28	6.750	2.450	4.600	0	4.511	.444	4.266	.849	3.523	1.459	2.732	1.826	2.035	2.035	1.440	2.155	.921	2.223	.449	2.258	0	2.269	2.150
30	6.380	3.050	4.715	0	4.614	.454	4.339	.863	3.531	1.463	2.705	1.808	1.999	1.999	1.407	2.106	.897	2.167	.437	2.197	0	2.207	1.665
32	5.850	3.740	4.795	0	4.697	.463	4.430	.881	3.632	1.504	2.799	1.870	2.076	2.076	1.466	2.193	.936	2.259	.456	2.293	0	2.304	1.055
34	5.240	4.500	4.870	0	4.777	.471	4.521	.899	3.740	1.549	2.905	1.941	2.163	2.163	1.534	2.295	.981	2.369	.479	2.407	0	2.418	.370
35	4.920	4.920	4.920	0	4.828	.476	4.574	.910	3.796	1.572	2.956	1.975	2.208	2.208	1.566	2.343	1.002	2.420	.489	2.459	0	2.471	0
36	4.600	5.370	4.985	0	4.892	.482	4.637	.922	3.851	1.595	3.002	2.006	2.244	2.244	1.591	2.381	1.019	2.460	.497	2.500	0	2.513	-.385
38	3.940	6.200	5.070	0	4.978	.490	4.722	.939	3.932	1.629	3.084	2.061	2.300	2.300	1.632	2.443	1.046	2.525	.511	2.567	0	2.580	-1.130
40	3.340	6.940	5.140	0	5.046	.497	4.785	.952	3.982	1.649	3.109	2.077	2.326	2.326	1.656	2.470	1.057	2.553	.516	2.595	0	2.608	-1.800
42	2.840	7.600	5.220	0	5.120	.504	4.844	.964	4.004	1.659	3.109	2.077	2.317	2.317	1.640	2.455	1.049	2.533	.512	2.573	0	2.586	-2.380
44	2.500	8.130	5.315	0	5.211	.513	4.926	.980	4.063	1.683	3.148	2.103	2.343	2.343	1.657	2.480	1.059	2.558	.517	2.598	0	2.610	-2.815
45	2.380	8.370	5.375	0	5.270	.519	4.983	.991	4.110	1.703	3.185	2.128	2.371	2.371	1.677	2.510	1.073	2.589	.523	2.630	0	2.642	-2.995
46	2.270	8.570	5.420	0	5.315	.524	5.028	1.000	4.154	1.720	3.223	2.153	2.401	2.401	1.699	2.543	1.087	2.624	.530	2.665	0	2.678	-3.150
48	2.130	8.860	5.495	0	5.391	.531	5.106	1.016	4.232	1.753	3.292	2.200	2.457	2.457	1.741	2.606	1.114	2.690	.544	2.734	0	2.748	-3.365
50	2.060	8.980	5.520	0	5.416	.533	5.129	1.020	4.251	1.761	3.307	2.210	2.469	2.469	1.749	2.618	1.120	2.703	.546	2.746	0	2.760	-3.460
52	2.050	9.020	5.535	0	5.431	.535	5.143	1.023	4.262	1.765	3.316	2.216	2.475	2.475	1.754	2.625	1.123	2.710	.548	2.754	0	2.768	-3.485
54	1.994	8.964	5.479	0	5.378	.530	5.100	1.014	4.241	1.757	3.310	2.211	2.476	2.476	1.756	2.628	1.125	2.716	.549	2.761	0	2.775	-3.485
55	1.979	8.909	5.444	0	5.346	.526	5.073	1.009	4.228	1.751	3.306	2.209	2.476	2.476	1.758	2.631	1.127	2.720	.550	2.766	0	2.780	-3.465
56	1.960	8.812	5.386	0	5.291	.521	5.027	1.000	4.202	1.741	3.295	2.201	2.472	2.472	1.758	2.630	1.127	2.721	.551	2.768	0	2.783	-3.426
58	1.915	8.610	5.263	0	5.174	.510	4.927	.980	4.147	1.718	3.271	2.186	2.465	2.465	1.757	2.630	1.129	2.725	.552	2.775	0	2.790	-3.347
60	1.820	8.350	5.085	0	5.006	.493	4.783	.951	4.064	1.683	3.234	2.161	2.453	2.453	1.756	2.628	1.131	2.730	.554	2.783	0	2.800	-3.265
62	1.667	8.050	4.859	0	4.789	.472	4.594	.914	3.950	1.636	3.180	2.125	2.432	2.432	1.751	2.621	1.132	2.733	.555	2.792	0	2.810	-3.191
64	1.517	7.717	4.617	0	4.558	.449	4.390	.873	3.821	1.583	3.115	2.081	2.407	2.407	1.745	2.611	1.132	2.734	.557	2.799	0	2.820	-3.100
65	1.420	7.503	4.462	0	4.409	.434	4.256	.847	3.734	1.546	3.069	2.051	2.387	2.387	1.738	2.602	1.132	2.733	.558	2.803	0	2.825	-3.041
66	1.340	7.332	4.336	0	4.288	.422	4.148	.825	3.661	1.516	3.030	2.024	2.370	2.370	1.733	2.594	1.132	2.732	.558	2.806	0	2.830	-2.996
68	1.150	6.901	4.026	0	3.987	.393	3.874	.771	3.471	1.438	2.923	1.953	2.321	2.321	1.716	2.569	1.129	2.726	.559	2.812	0	2.840	-2.875
70	.943	6.460	3.702	0	3.671	.362	3.584	.713	3.260	1.350	2.796	1.868	2.258	2.258	1.693	2.534	1.125	2.715	.560	2.817	0	2.850	-2.758
72	.690	6.010	3.350	0	3.328	.328	3.263	.649	3.014	1.248	2.638	1.763	2.175	2.175	1.660	2.484	1.117	2.696	.561	2.820	0	2.860	-2.660
74	.400	5.540	2.970	0	2.955	.291	2.909	.579	2.730	1.131	2.444	1.633	2.065	2.065	1.612	2.413	1.104	2.666	.561	2.821	0	2.873	-2.570

[1]See figure 5 and appendix A for definitions of nomenclature used.

TABLE III.- COORDINATES FOR LOCATIONS OF PRESSURE ORIFICES ON THE UPPER SURFACE OF THE ASYMMETRICAL M = 1.20 INDENTED BODY

[Dimensions in inches]

$\theta = 0^\circ$			$\theta = 22.5^\circ$			$\theta = 45^\circ$			$\theta = 90^\circ$			$\theta = 135^\circ$			$\theta = 157.5^\circ$			$\theta = 180^\circ$		
x	y	z	x	y	z	x	y	z	x	y	z	x	y	z	x	y	z	x	y	z
4.97	1.47	0							4.00	0	0.61							3.27	-1.09	0
9.70	2.60	0				8.71	1.07	0.62				7.42	-0.89	0.90				6.77	-1.86	0
14.76	4.15	0							12.24	.34	1.50							10.35	-2.49	0
20.21	6.34	0				18.25	3.39	1.74	16.82	1.24	1.85	15.57	-.64	1.56				14.23	-2.67	0
24.68	7.03	0							21.68	2.54	2.09							18.58	-2.12	0
28.45	6.67	0				26.91	4.39	2.02	25.70	2.56	2.22	24.47	.71	1.96				22.93	-1.61	0
31.90	5.88	0	31.24	4.89	1.49	30.36	3.56	2.00	29.24	1.86	2.22	28.07	.11	2.03	27.22	-1.19	1.45	26.62	-2.09	0
33.57	5.38	0	32.91	4.47	1.54	32.06	3.11	2.08	30.92	1.39	2.24	29.81	-.29	2.00	28.94	-1.59	1.46	28.31	-2.55	0
35.22	4.85	0	34.59	3.93	1.56	33.74	2.59	2.15				31.46	-.81	2.04	30.62	-2.06	1.47	29.98	-3.04	0
37.68	4.05	0	37.06	3.10	1.61	36.18	1.79	2.25	35.00	0	2.47	33.86	-1.94	2.16	33.03	-2.97	1.52	32.42	-3.90	0
40.18	3.29	0	39.43	2.33	1.64	38.63	.96	2.31				36.19	-2.71	2.25	35.36	-3.96	1.58	34.80	-4.84	0
42.78	2.70	0	42.05	1.62	1.66	41.12	.17	2.32	39.84	-1.75	2.61	38.58	-3.65	2.31	37.72	-4.96	1.62	37.13	-5.86	0
45.54	2.32	0	44.76	1.14	1.70	43.72	-.42	2.34				41.06	-4.46	2.32	40.14	-5.82	1.65	39.53	-6.78	0
47.44	2.16	0	46.63	.95	1.73	45.54	-.69	2.39	44.12	-2.84	2.61	42.78	-4.88	2.32	41.80	-6.33	1.66	41.14	-7.34	0
51.37	2.06	0				49.36	-.98	2.47	47.78	-3.35	2.74	46.29	-5.61	2.42				44.53	-8.26	0
55.32	1.97	0				53.32	-1.03	2.47	51.69	-3.49	2.77	50.07	-5.93	2.46				48.11	-8.87	0
63.05	1.59	0				61.49	-.77	2.44	59.83	-3.28	2.80	58.15	-5.81	2.47				56.16	-8.80	0
70.57	.87	0				69.66	-.51	2.27	68.09	-2.87	2.84	66.47	-5.33	2.36				65.02	-7.51	0
74.00	0	1.44							72.24	-2.65	2.86							69.66	-6.54	0

Note: (a) The vertical dimensions, z, for $\theta = 0^\circ$ and 180°, with exception of station 74.00 of $\theta = 0^\circ$, are shown in the idealized position. These points were moved upward 1/8 inch as necessary to clear the horizontal parting plane of the body or the wing juncture with the body.

(b) The actual lengths of the wing-body-juncture chords were used in computing ξ/c_j used in the plots of the body pressure data: sweptback panel c_j = 13.91 inches; sweptforward panel c_j = 12.75 inches.

(c) See figure 5 and appendix A for definitions of nomenclature used.

TABLE IV.- WING LEADING-EDGE PRESSURES AS INDICATED BY x/c = 0 ORIFICE

Aspect-ratio-6 wing with Sears-Haack body							
Mach number \ $\frac{y}{b/2}$	Sweptforward panel				Sweptback panel		
	0.139	0.194	0.500	0.938	0.139	0.194	0.500
0.8	0.749	0.720	0.730	0.683	0.565	0.519	0.486
.9	.798	.756	.760	.735	.597	.544	.482
.96	.841	.788	.787	.774	.627	.575	.495
1.00	.868	.816	.802	.802	---	.547	.520
1.04	.898	.851	.833	.829	.634	.565	.511
1.10	.978	.923	.904	.874	.665	.642	.585
1.20	1.006	.941	.903	.857	.725	.645	.573
Aspect-ratio-6 wing with symmetrical M = 1.20 indented body							
.8	.732	.704	.719	.691	.562	.520	.507
.9	---	---	---	---	---	---	---
.96	.814	.760	.783	.778	.617	.577	.537
1.00	.824	.773	.778	.788	.591	.541	.563
1.04	.867	.808	.822	.827	.611	.559	.529
1.10	.902	.844	.854	.831	.641	.599	.559
1.20	.968	.909	.887	.865	.732	.658	.606
Aspect-ratio-6 wing with asymmetrical M = 1.20 indented body							
.8	.775	.743	.779	.882	---	.701	.544
.9	.803	.781	.759	.710	---	.684	.594
.96	.830	.790	.778	.744	---	.737	.599
1.00	.869	.814	.804	.893	---	.773	.575
1.04	.898	.844	.839	.959	---	.761	.585
1.10	.917	.873	.889	.924	---	.787	.599
1.20	.952	.915	.943	.939	---	.841	.612

Aspect-ratio-3 wing with Sears-Haack body						
Mach number \ $\frac{y}{b/2}$	Sweptforward panel			Sweptback panel		
	0.179	0.505	0.888	0.179	0.244	0.505
0.8	0.856	0.791	0.871	0.535	0.469	0.613
.9	.905	.828	.905	.567	.613	.640
.95	.935	.847	.931	.589	.719	.658
1.00	.953	.869	.961	.564	.770	.631
1.05	.994	.908	.990	.600	.902	.641
1.10	1.015	.928	.994	.637	.997	.663
1.20	1.081	.965	1.045	.664	1.373	.699
Aspect-ratio-3 wing with symmetrical M = 1.20 indented body						
.8	.770	.791	.846	.554	---	.494
.9	.815	.829	.884	.588	---	.519
.95	.844	.844	.907	.608	---	.536
1.00	.875	.873	.935	.596	---	.565
1.05	.913	.896	.961	.625	---	.542
1.10	.946	.924	.982	.660	---	.545
1.20	1.009	.964	1.003	.695	---	.600

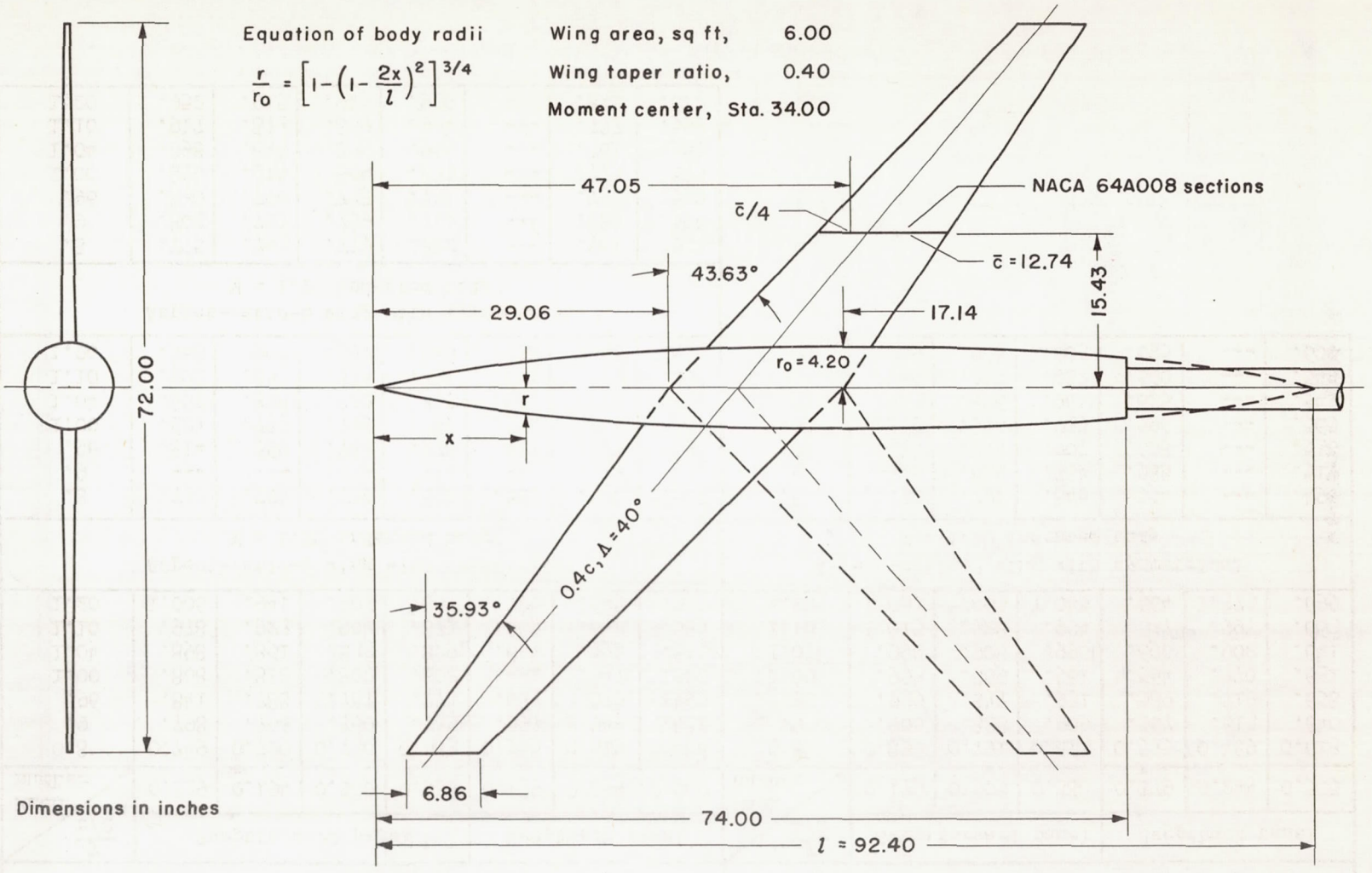

Figure 1.- Aspect-ratio-6 yawed wing with the fineness-ratio-11 Sears-Haack body.

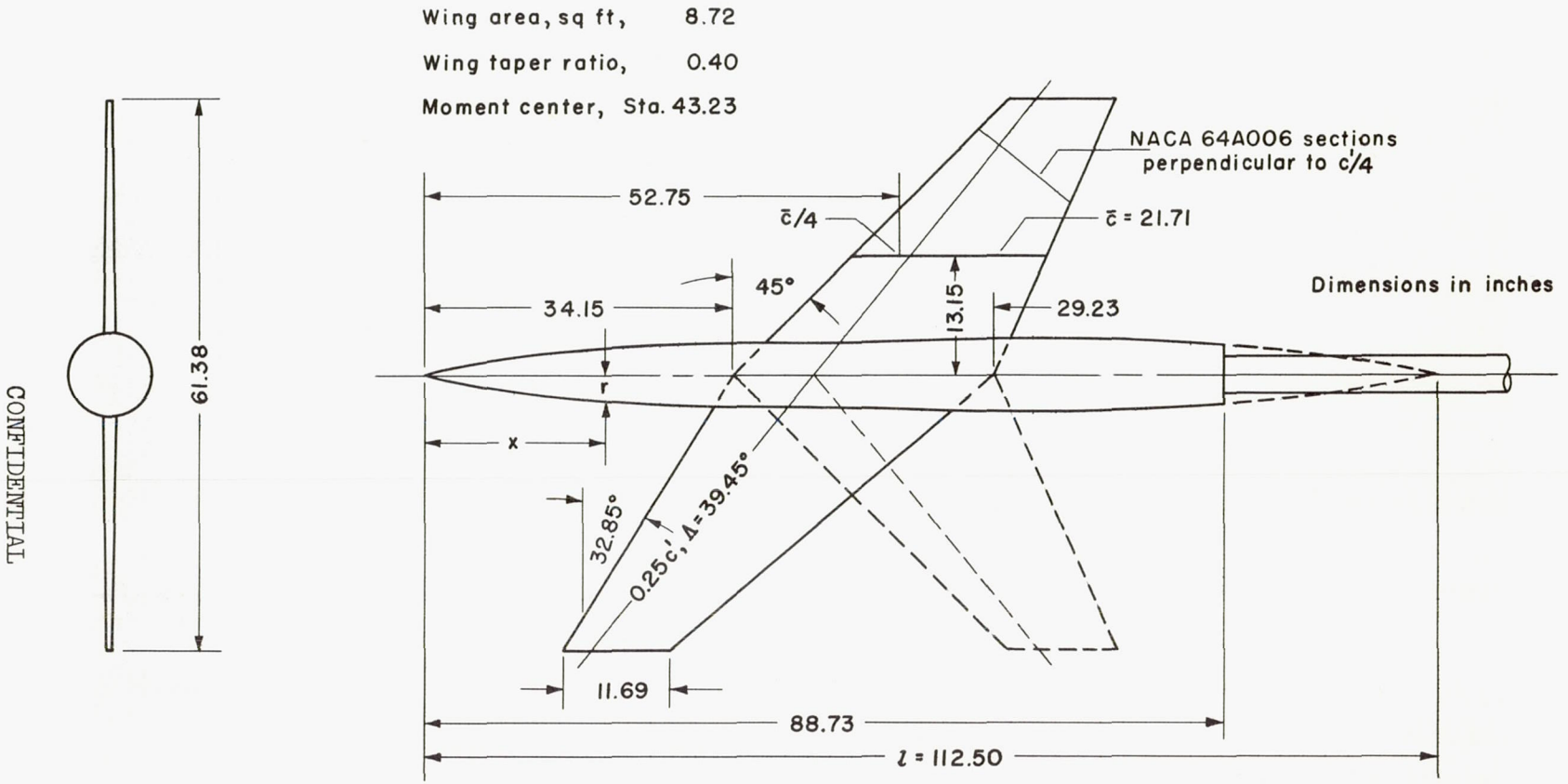

(a) Geometric details.

Figure 2.- Aspect-ratio-3 yawed wing with the symmetrical M = 1.20 indented body.

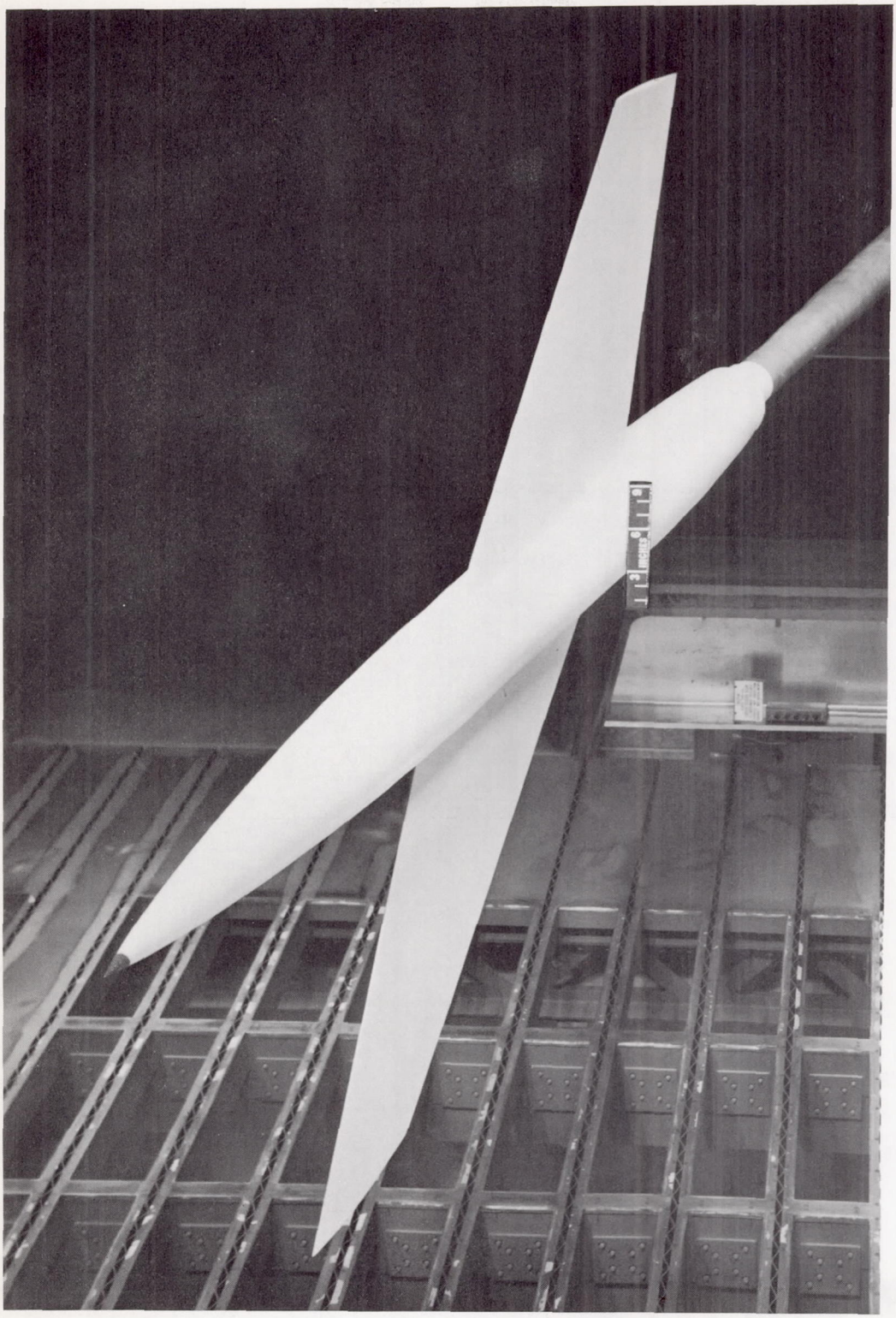

A-21680.1

(b) Model in wind tunnel.

Figure 2.- Concluded.

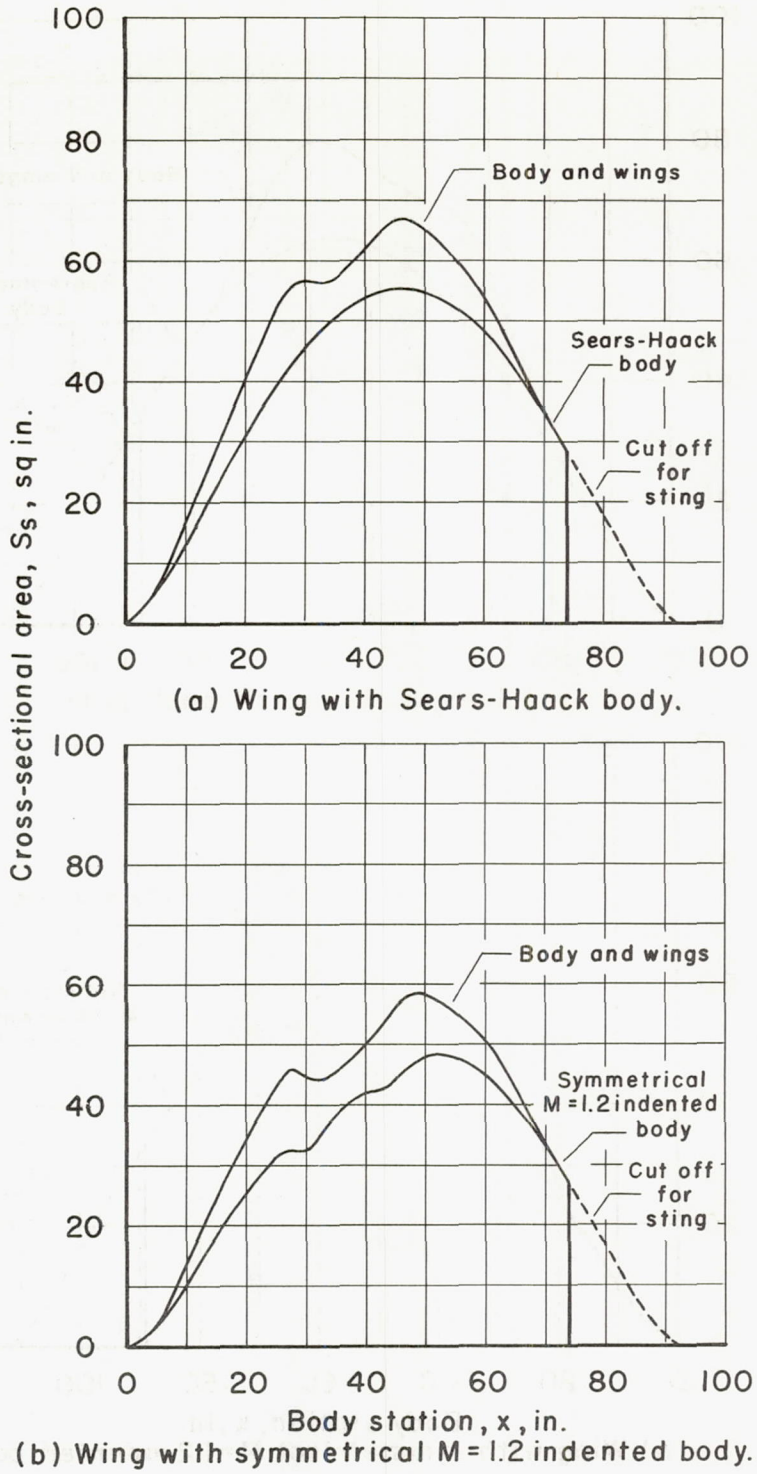

Figure 3.- Cross-sectional area distributions for the aspect-ratio-6 yawed wing with its Sears-Haack body and symmetrical M = 1.20 indented body.

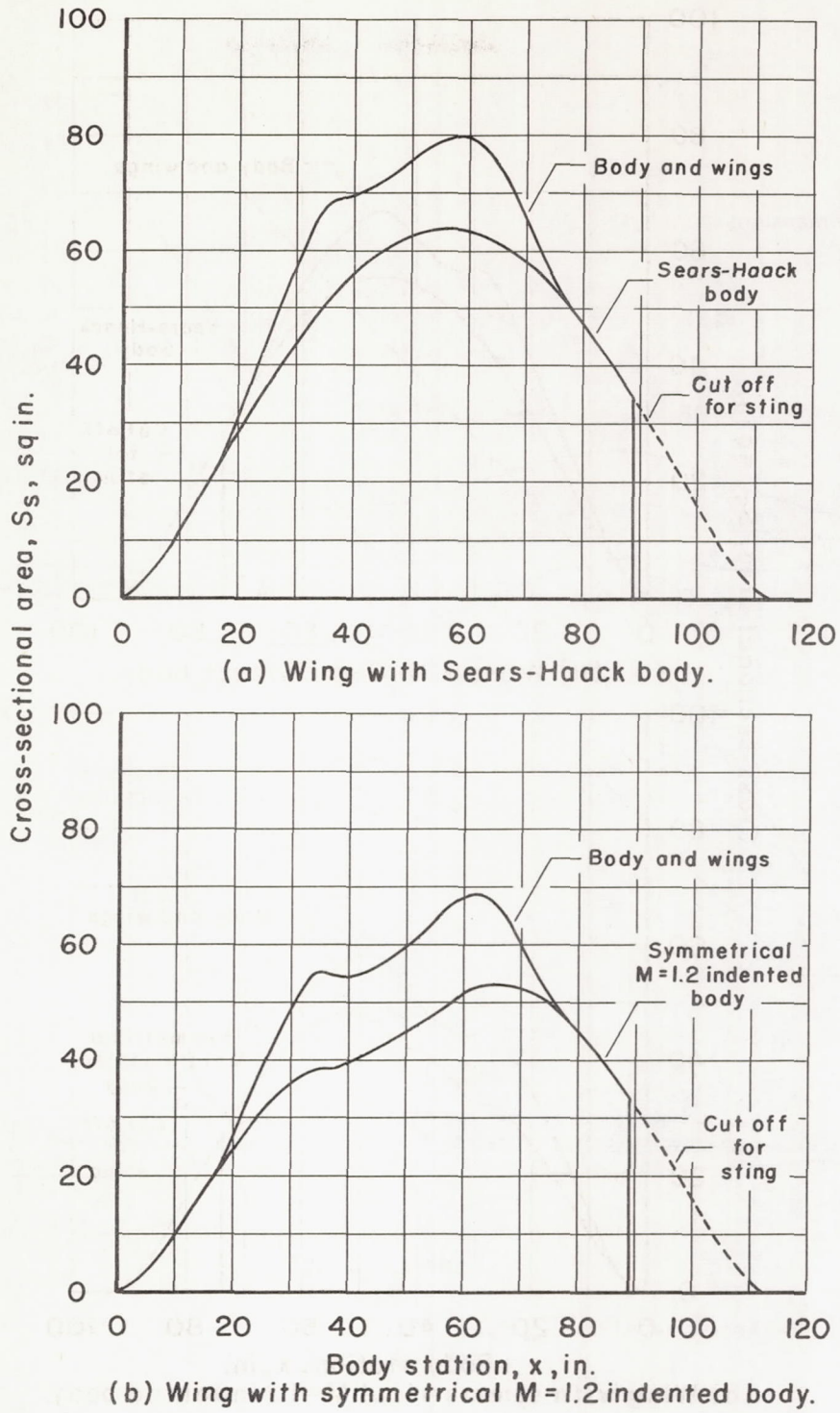

Figure 4.- Cross-sectional area distributions for the aspect-ratio-3 yawed wing with its Sears-Haack body and symmetrical M = 1.20 indented body.

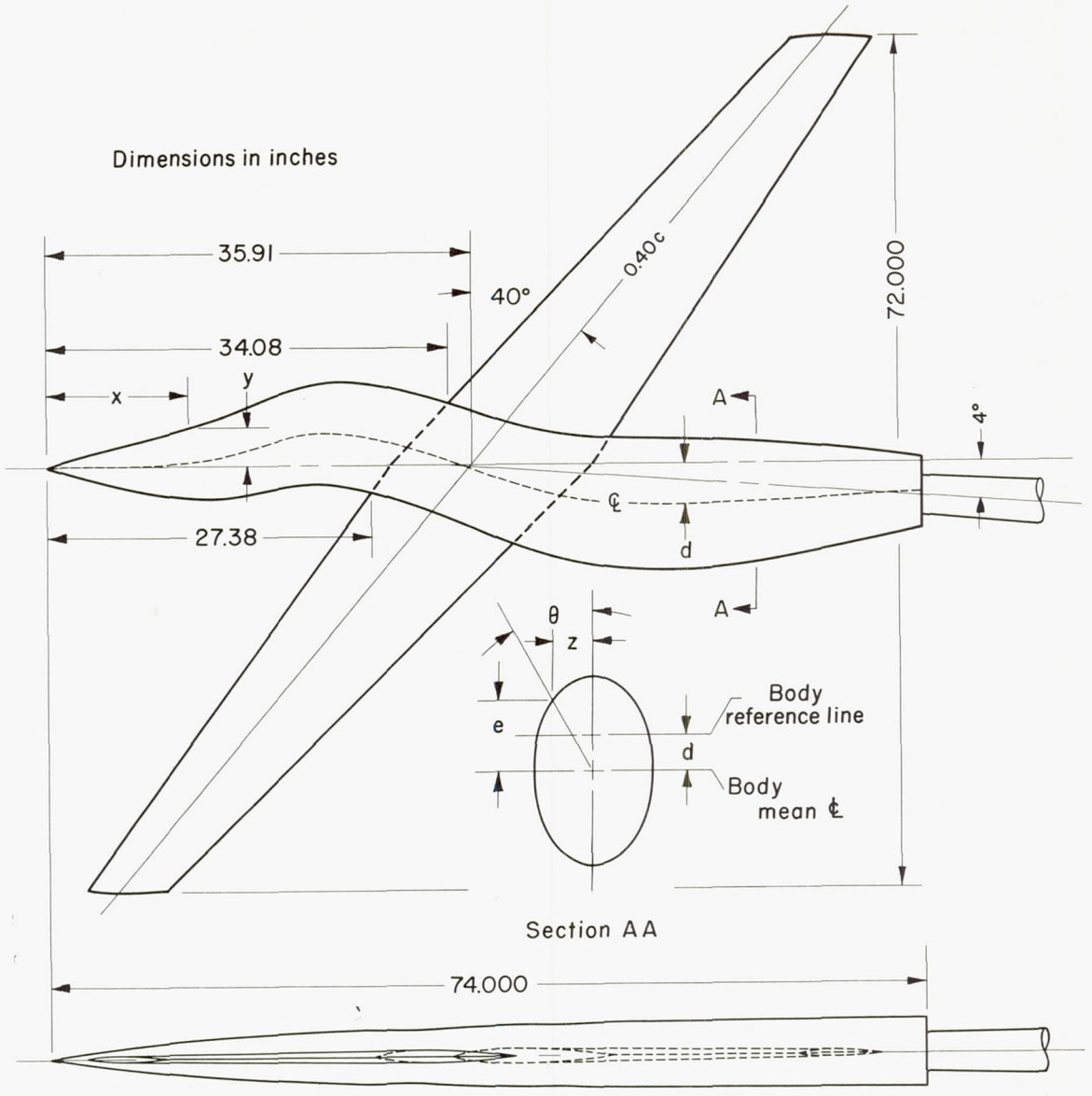

(a) Geometric details.

Figure 5.- Aspect-ratio-6 yawed wing with the asymmetrical M = 1.20 indented body.

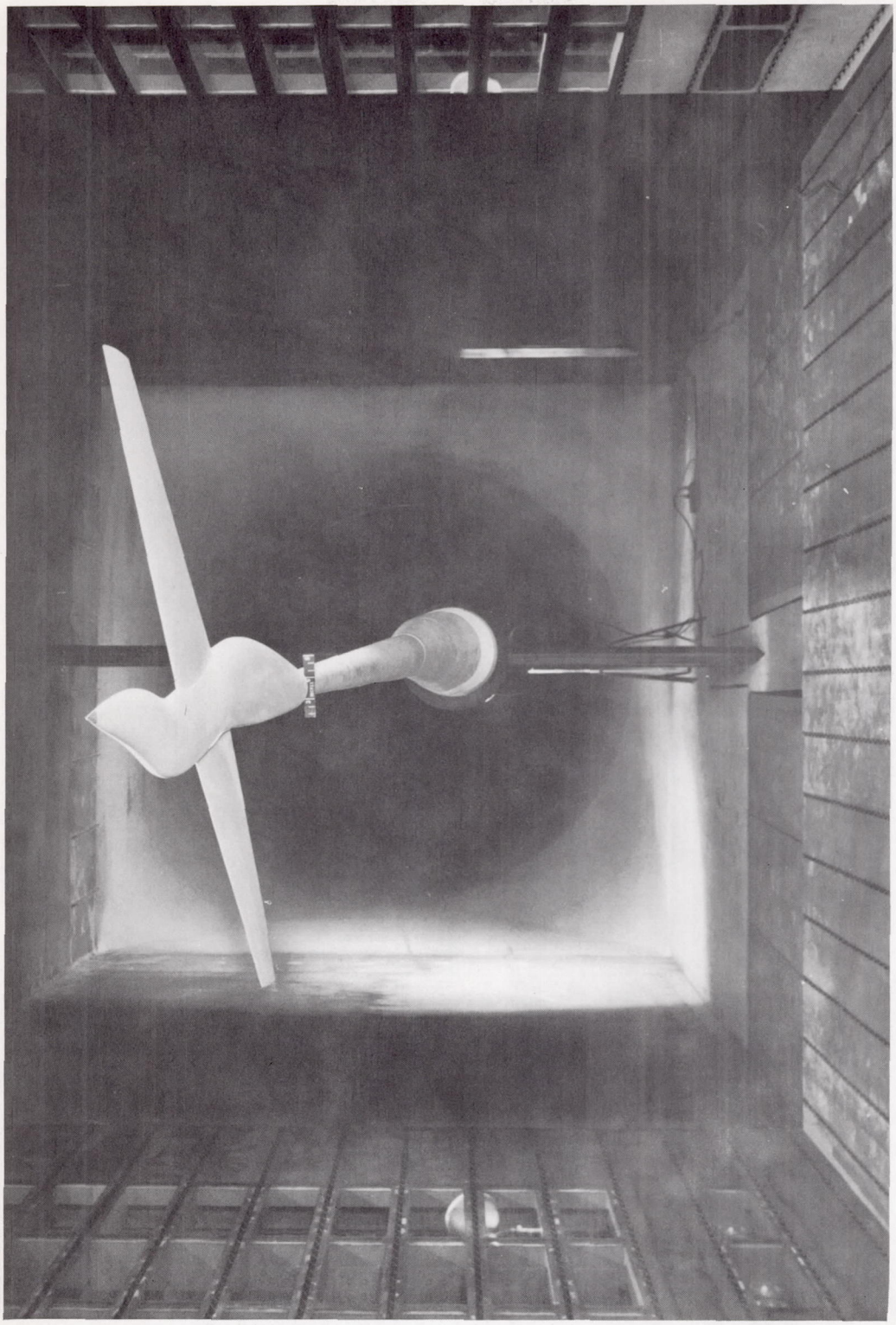

A-21920.1

(b) Model in wind tunnel.

Figure 5.- Concluded.

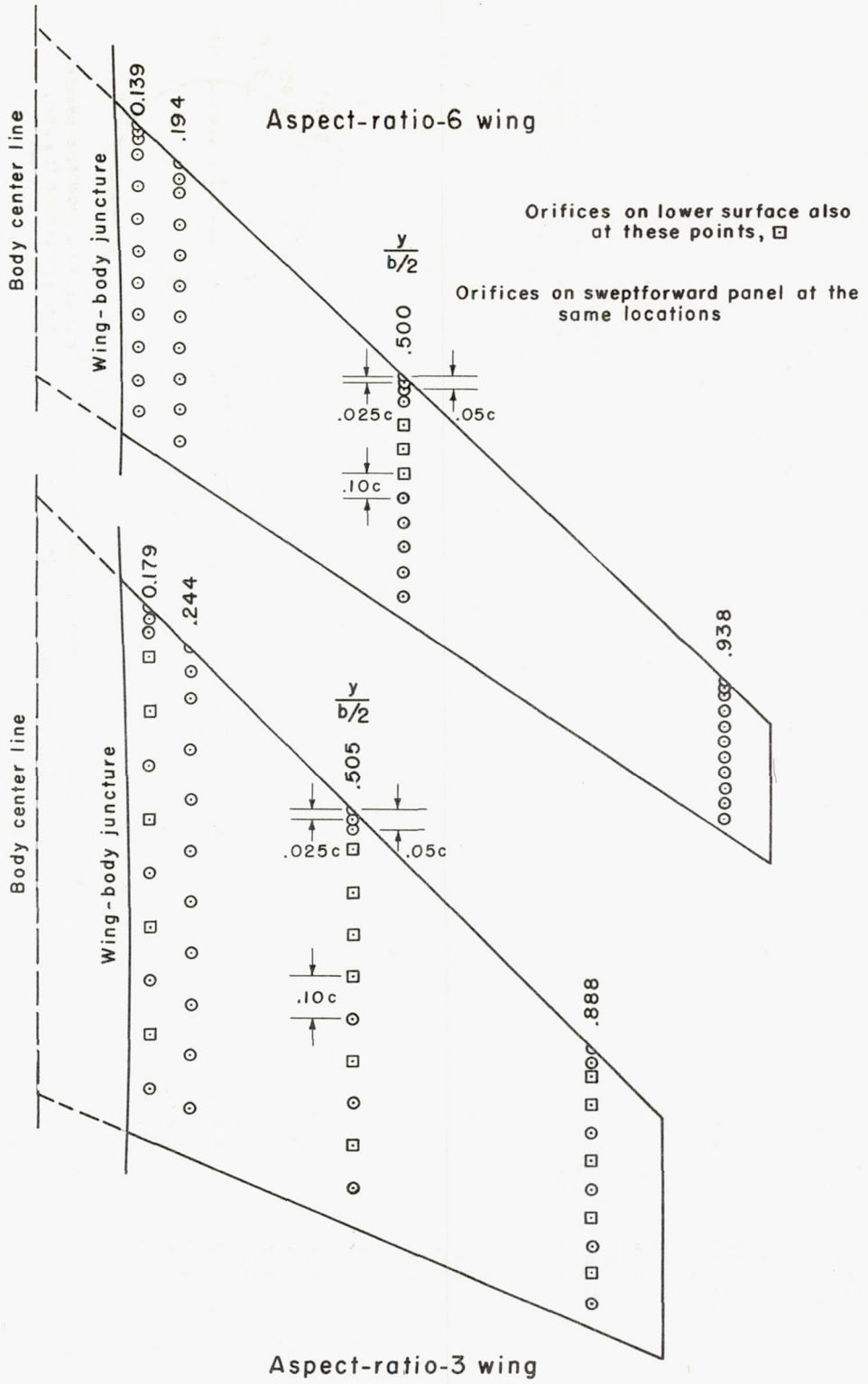

Figure 6.- Location of wing pressure orifices.

x inches	ξ/c_j Basic body	ξ/c_j Indented body
3.00	-1.902	-1.858
9.00	-1.527	-1.483
15.00	-1.152	-1.108
21.00	-0.777	-0.733
24.73	-0.544	-0.500
27.93	-0.344	-0.300
29.53	-0.244	-0.200
31.13	-0.144	-0.100
32.73	-0.044	0
33.53	0.001	0.050
34.33	.006	.100
35.93	.156	.200
37.53	.256	.300
39.13	.356	.400
40.73	.456	.500
42.33	.556	.600
43.93	.656	.700
45.53	.756	.800
47.13	.856	.900
48.73	.956	1.000
50.33	1.056	1.100
51.93	1.156	1.200
55.13	1.356	1.400
58.33	1.556	1.600
61.53	1.756	1.800
64.73	1.956	2.000
67.93	2.156	2.200

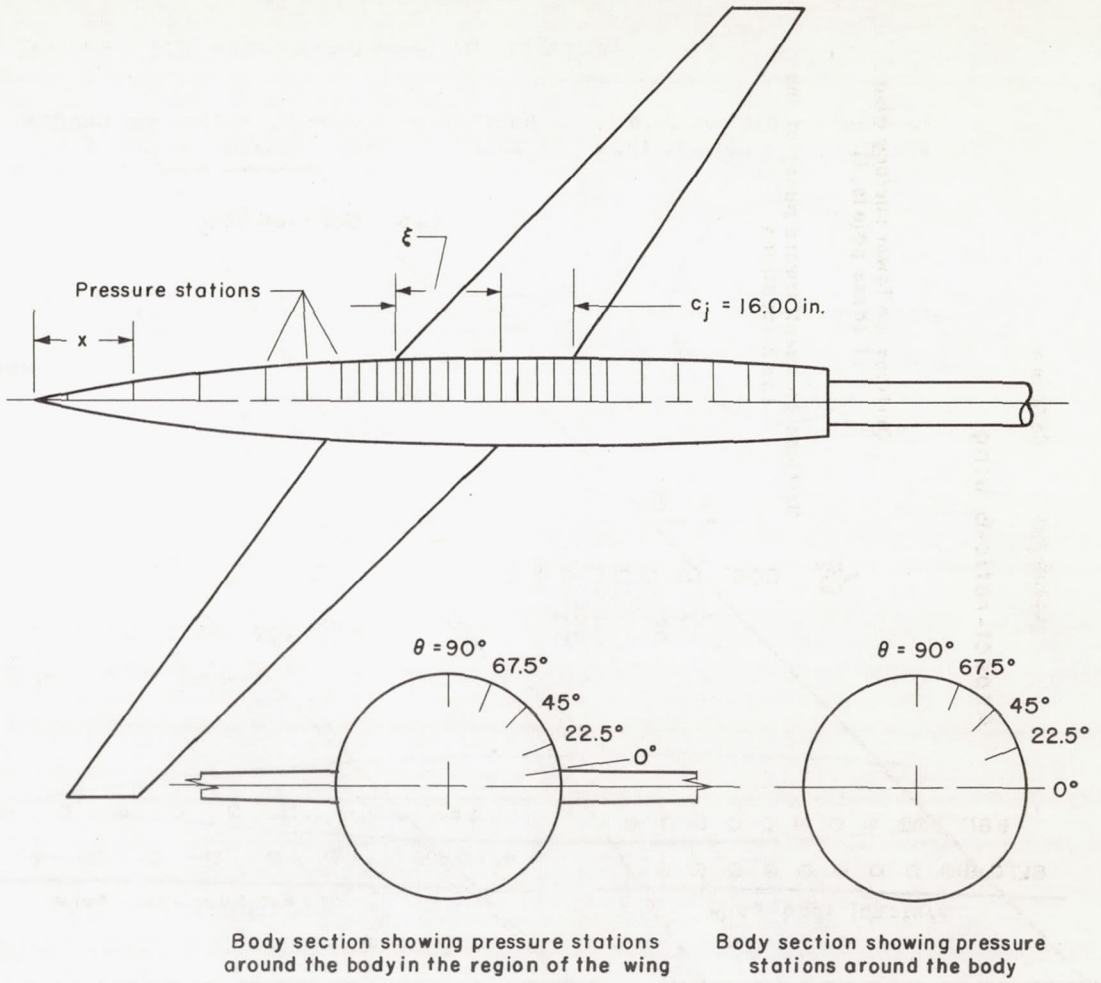

(a) Bodies with aspect-ratio-6 yawed wing.

Figure 7.- Location of pressure orifices on symmetrical bodies.

x inches	ξ/c_j Basic body	ξ/c_j Indented body
4.20	-1.354	-1.266
7.43	-1.202	-1.146
17.44	-0.830	-0.775
24.85	-0.556	-0.500
30.24	-0.356	-0.300
32.94	-0.256	-0.200
35.63	-0.156	-0.100
36.98	-0.106	-0.050
38.33	-0.056	0
39.68	-0.006	0.050
41.03	0.045	.100
43.72	.144	.200
46.42	.244	.300
49.11	.344	.400
51.81	.444	.500
54.51	.544	.600
57.12	.644	.700
59.90	.744	.800
62.59	.844	.900
63.94	.894	.950
65.29	.944	1.000
66.64	.994	1.050
67.99	1.044	1.100
70.68	1.144	1.200
73.38	1.244	1.300
76.07	1.344	1.400
81.47	1.544	1.600
86.86	1.744	1.800

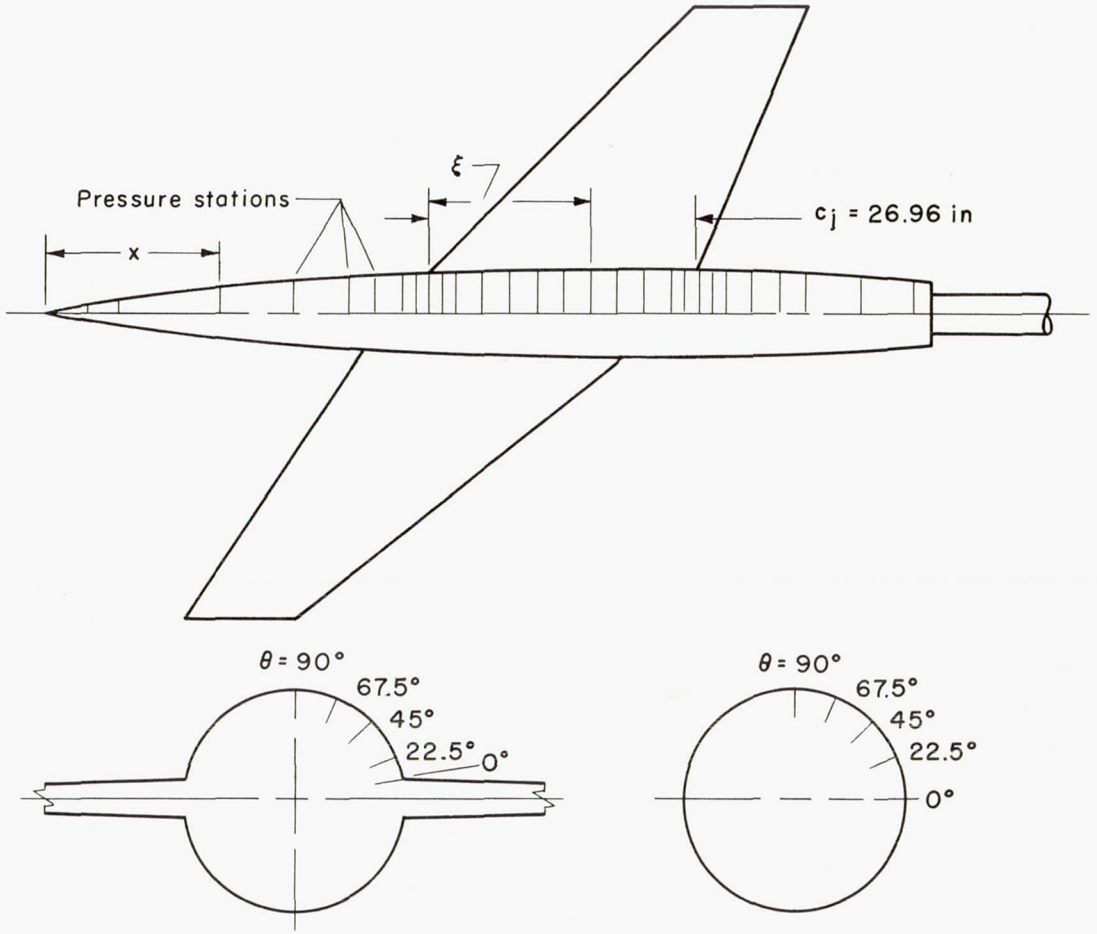

Body section showing pressure stations around the body in the region of the wing

Body section showing pressure stations around the body

(b) Bodies with aspect-ratio-3 yawed wing.

Figure 7.- Concluded.

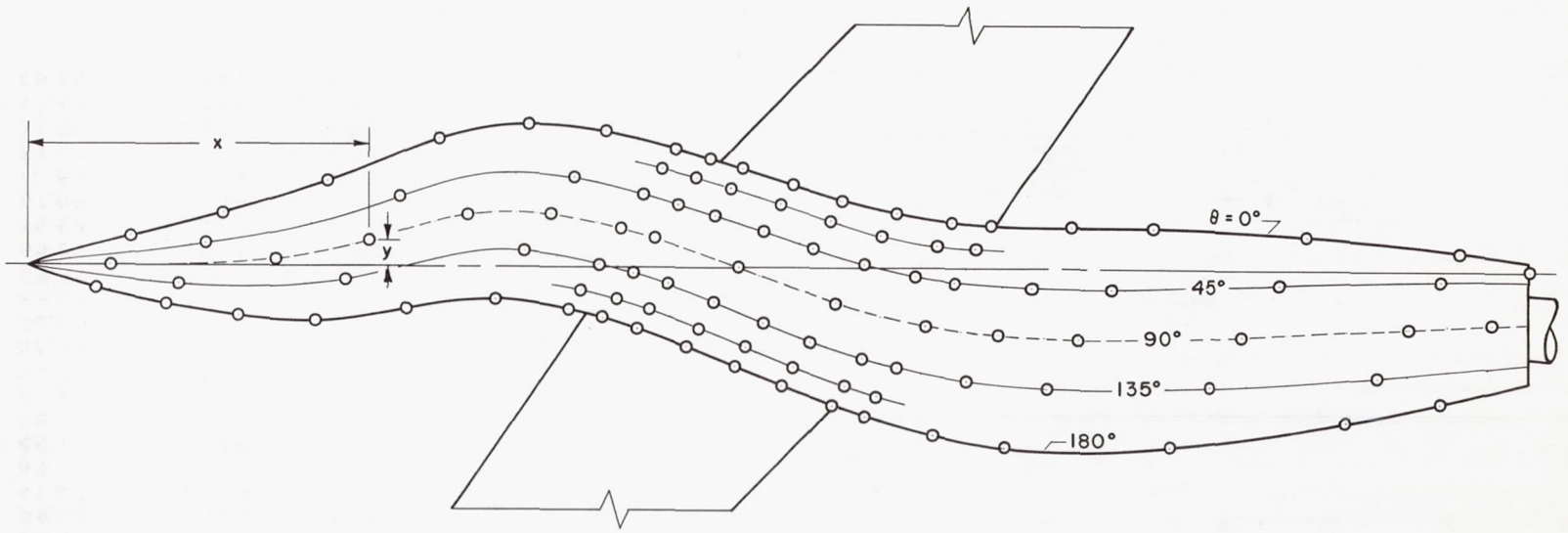

Figure 8.- Location of body pressure orifices on the asymmetrical M = 1.20 indented body used with the aspect-ratio-6 yawed wing. (See table III for specific body stations.)

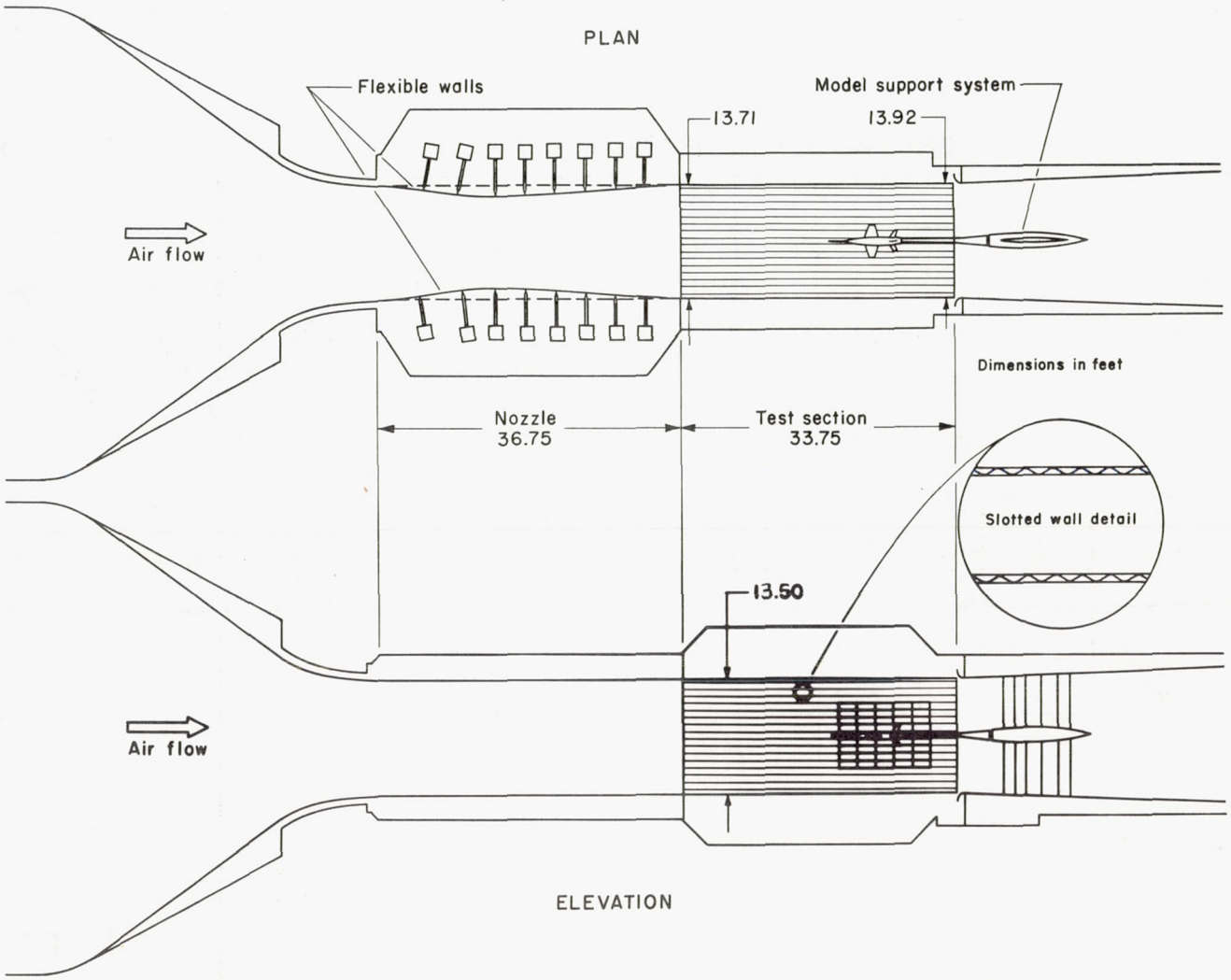

Figure 9.- Two views of the high-speed region of the Ames 14-foot transonic wind tunnel.

CONFIDENTIAL

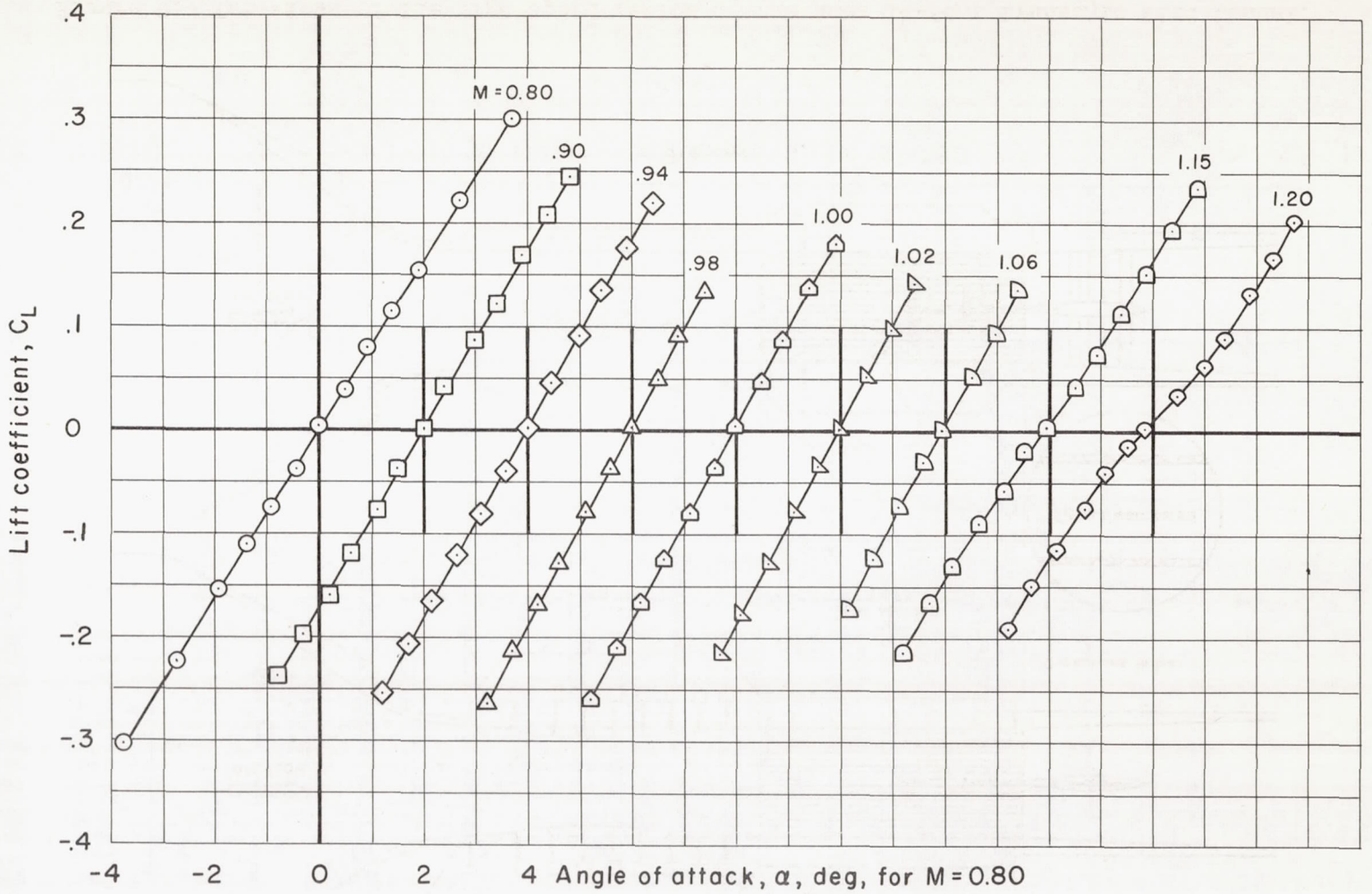

(a) C_L vs. α

Figure 10.- Aerodynamic characteristics of the aspect-ratio-6 yawed wing with an asymmetrical M = 1.20 indented body.

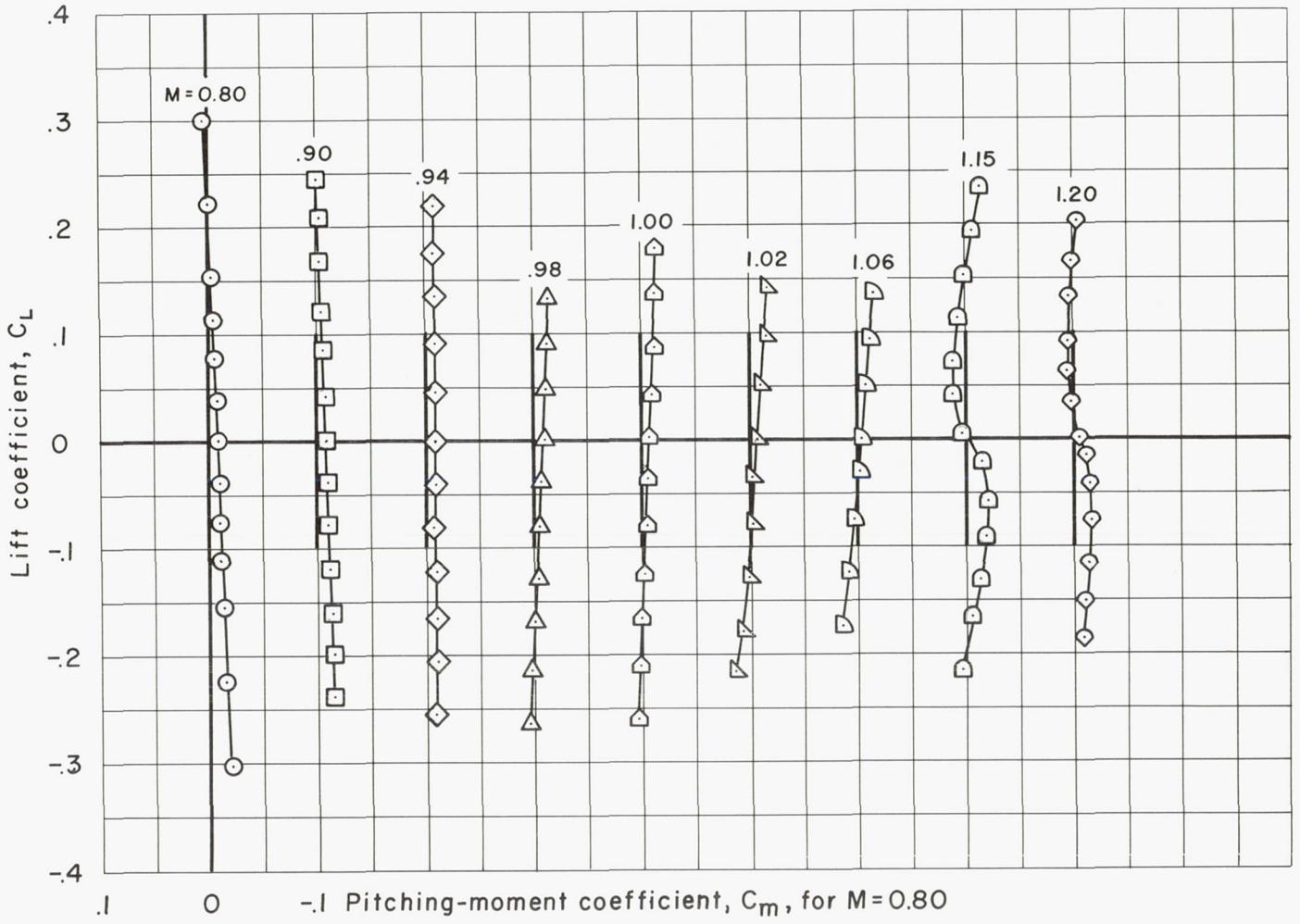

(b) C_L vs. C_m

Figure 10.- Continued.

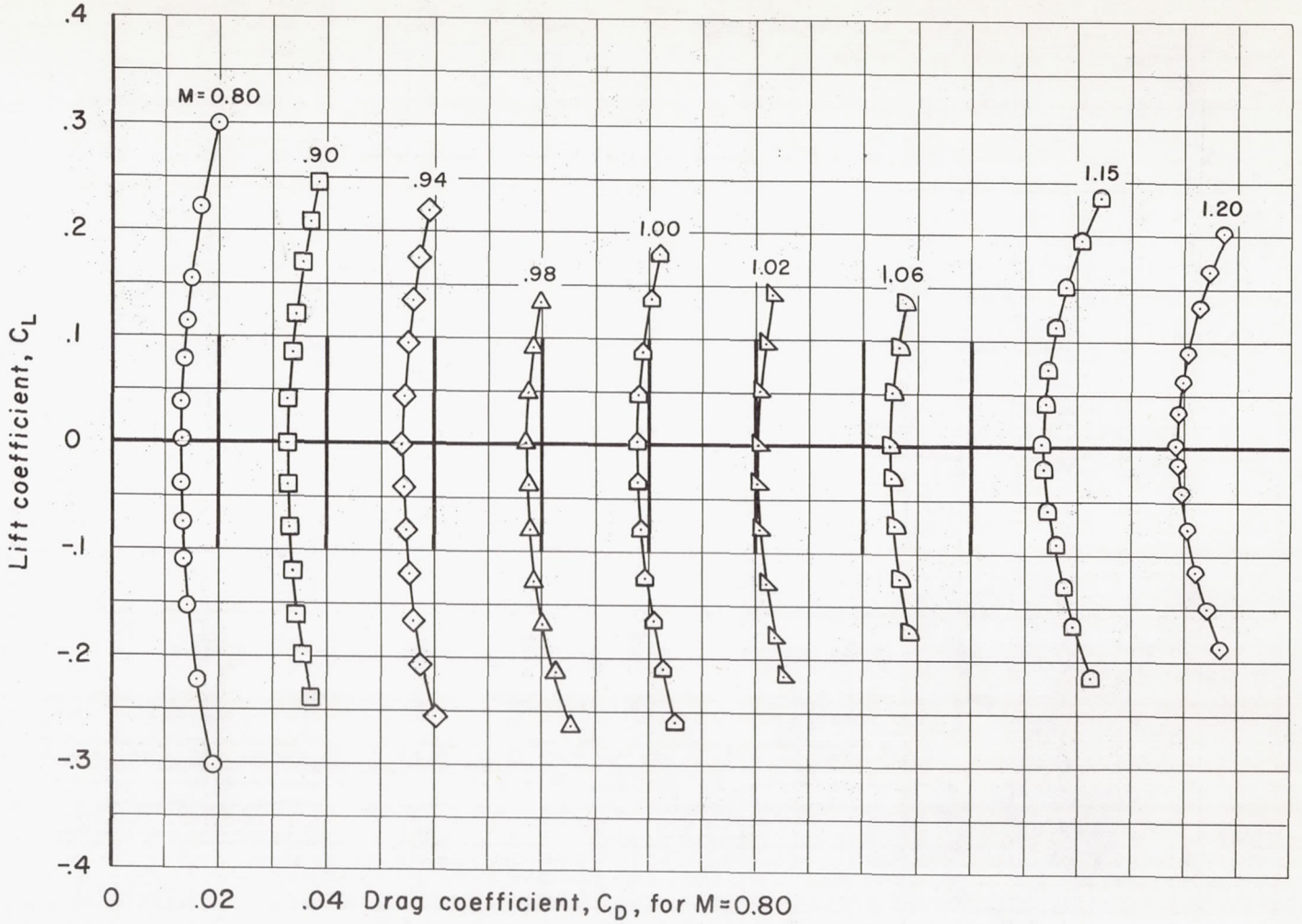

(c) C_L vs. C_D

Figure 10.- Continued.

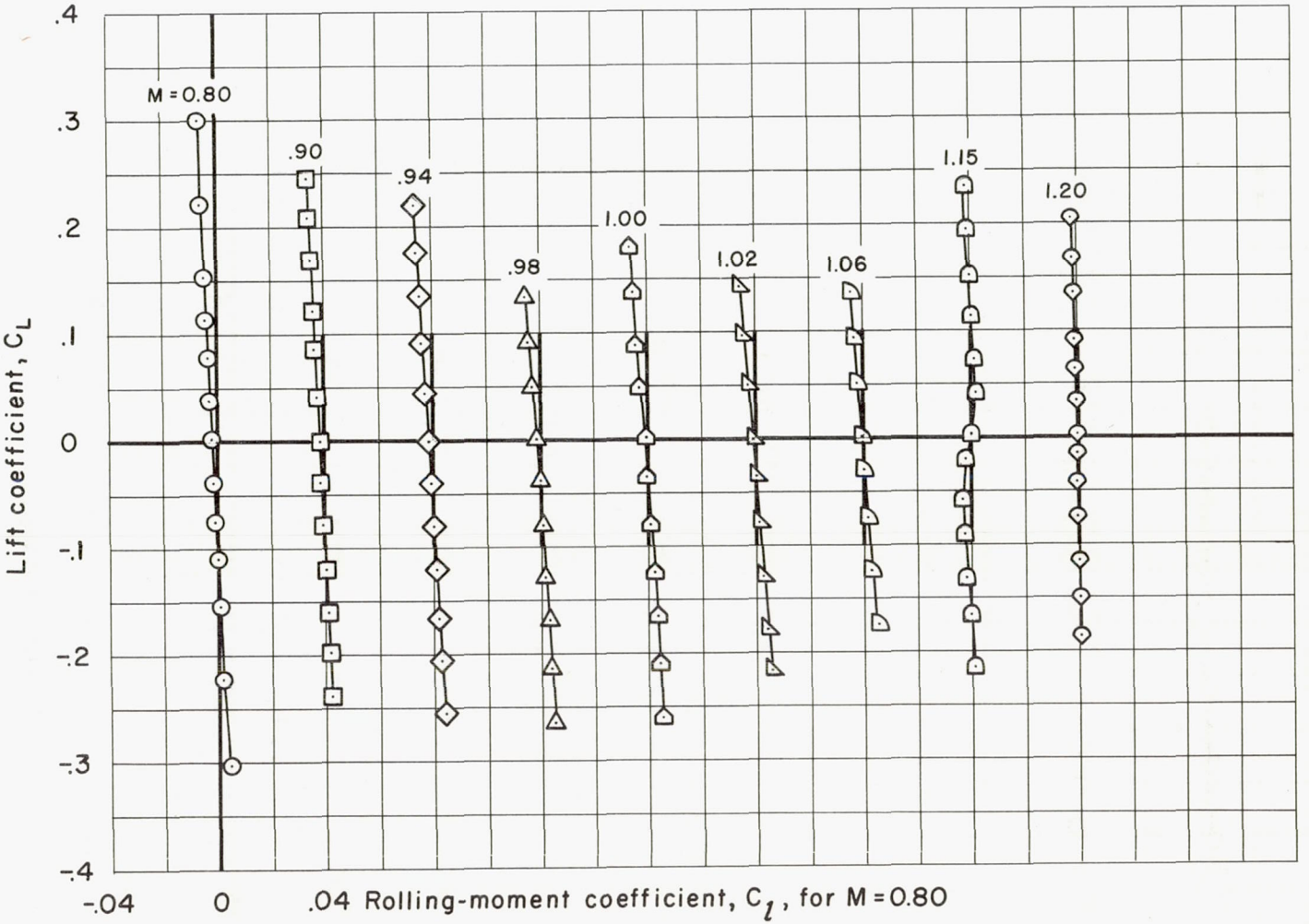

(d) C_L vs. C_l

Figure 10.- Continued.

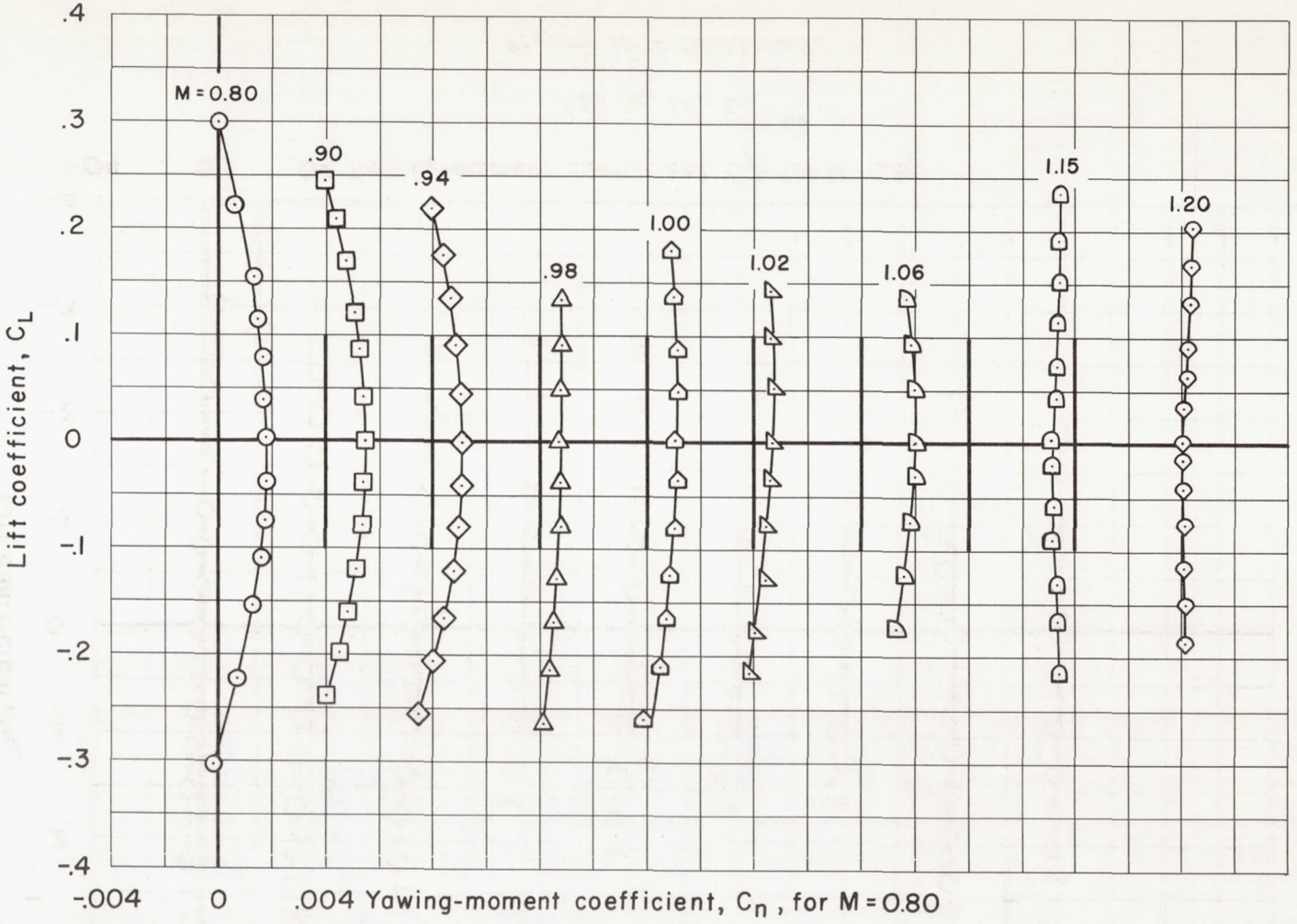

(e) C_L vs. C_n

Figure 10.- Continued.

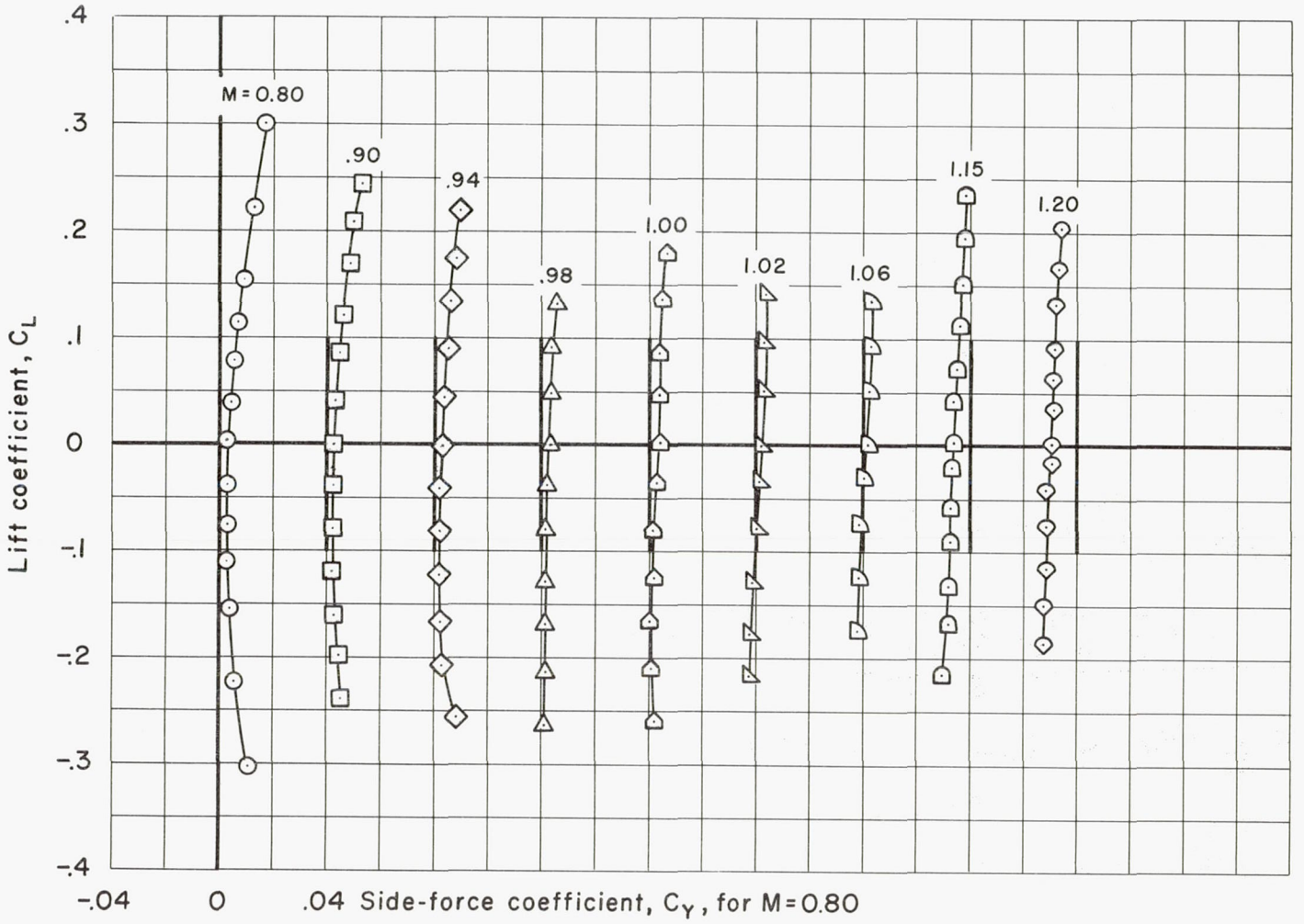

(f) C_L vs. C_Y

Figure 10.- Concluded.

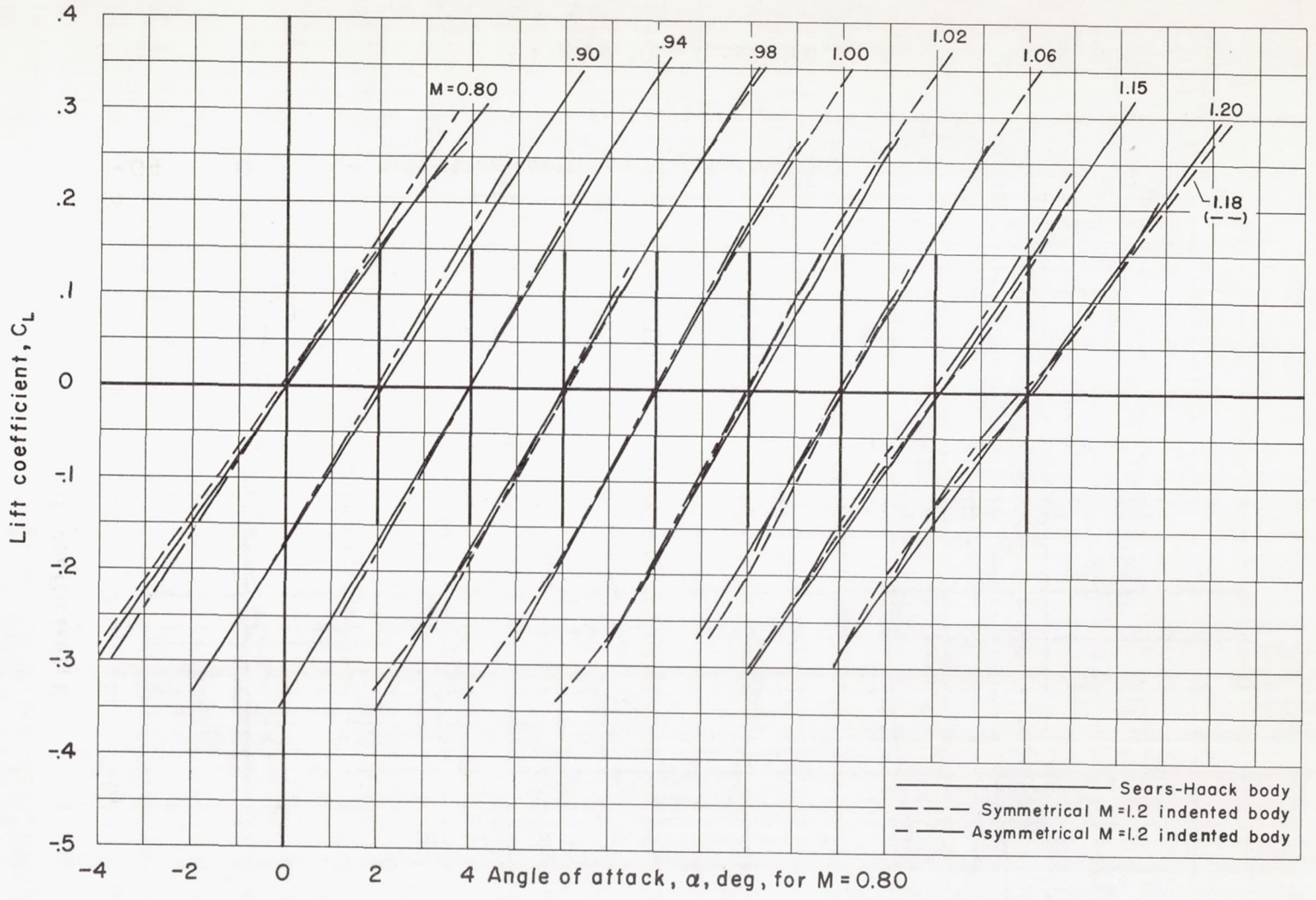

(a) C_L vs. α

Figure 11.- Aerodynamic characteristics of the aspect-ratio-6 yawed wing with various bodies.

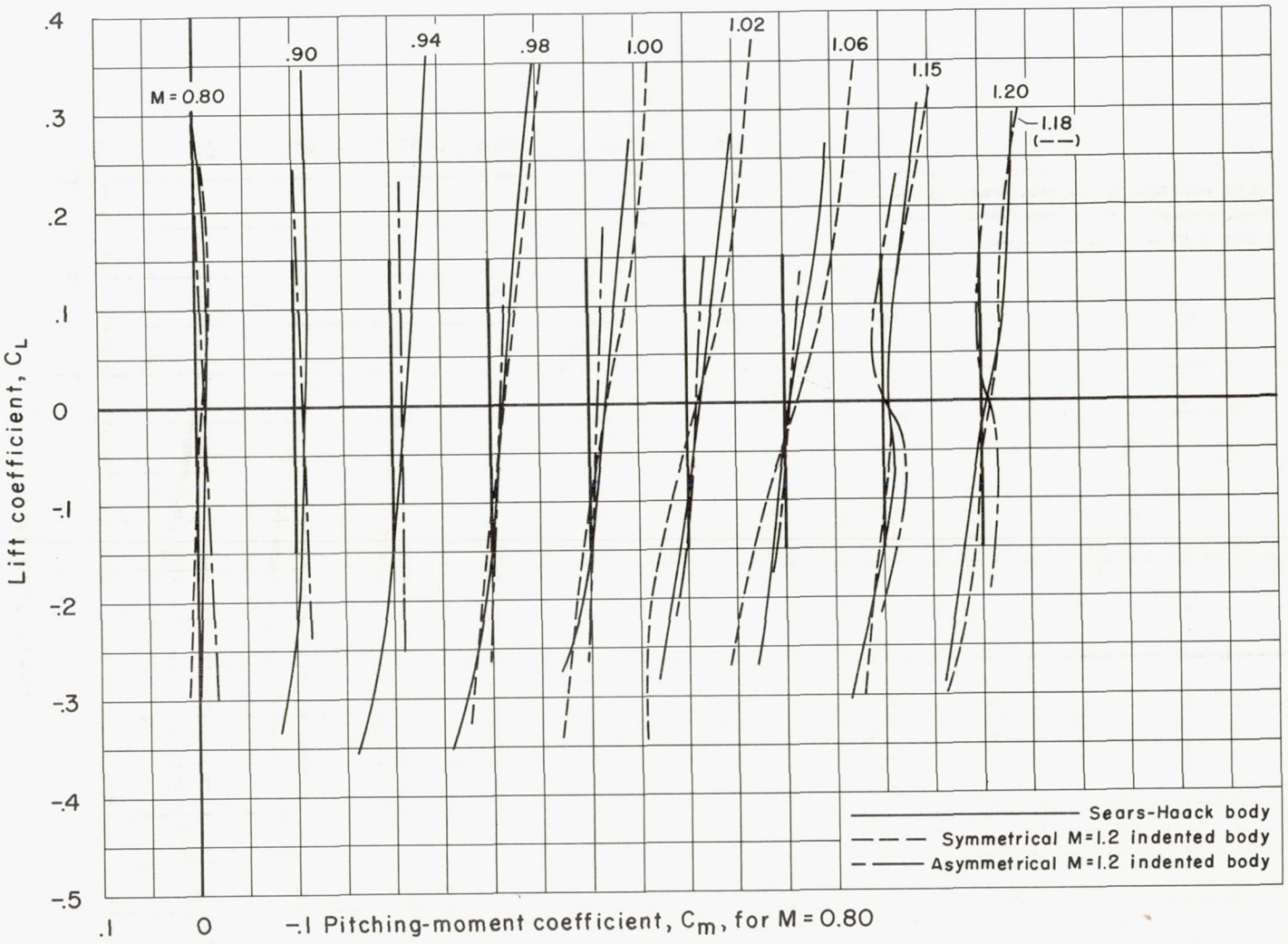

(b) C_L vs. C_m

Figure 11.- Continued.

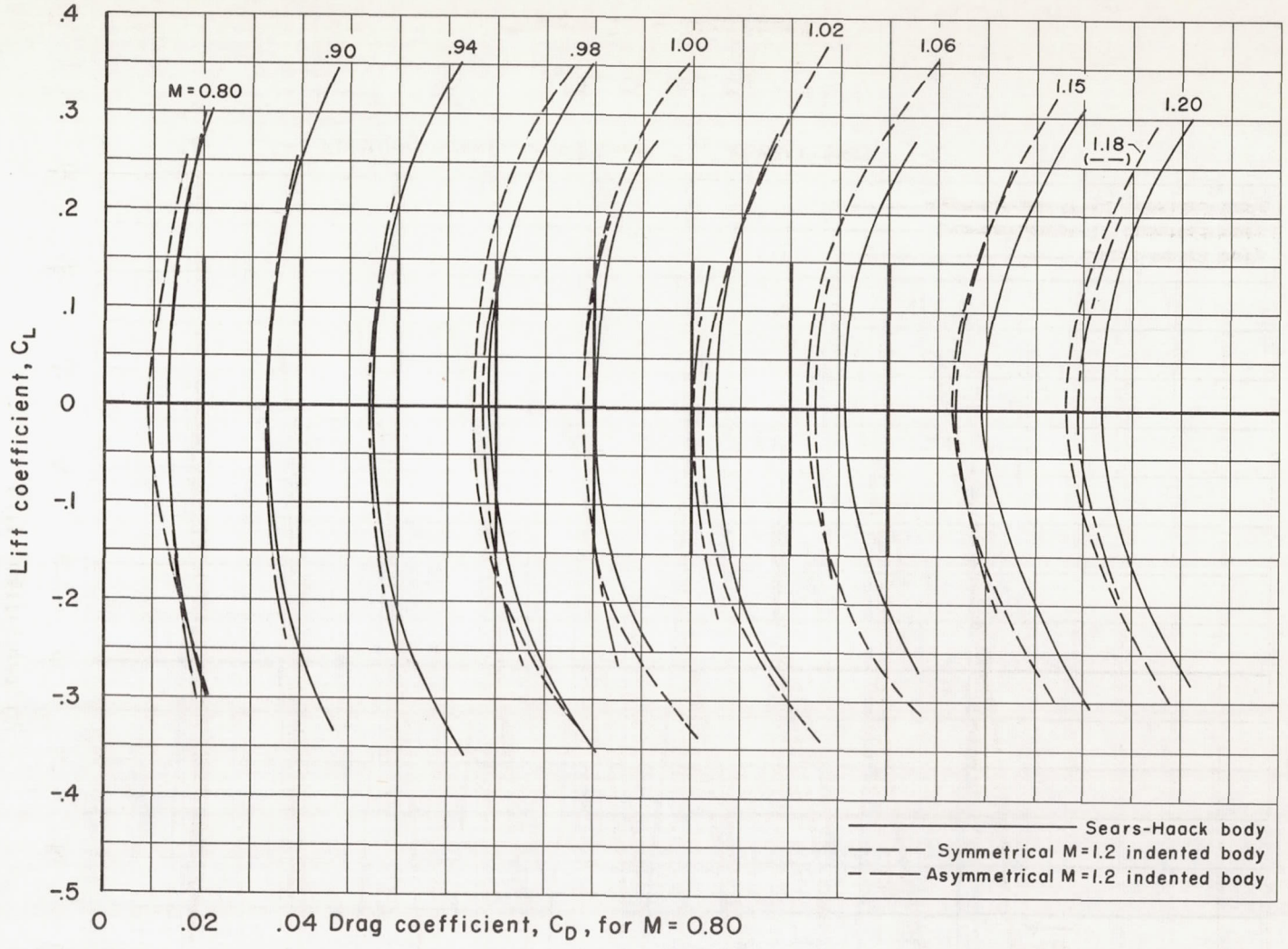

(c) C_L vs. C_D

Figure 11.- Continued.

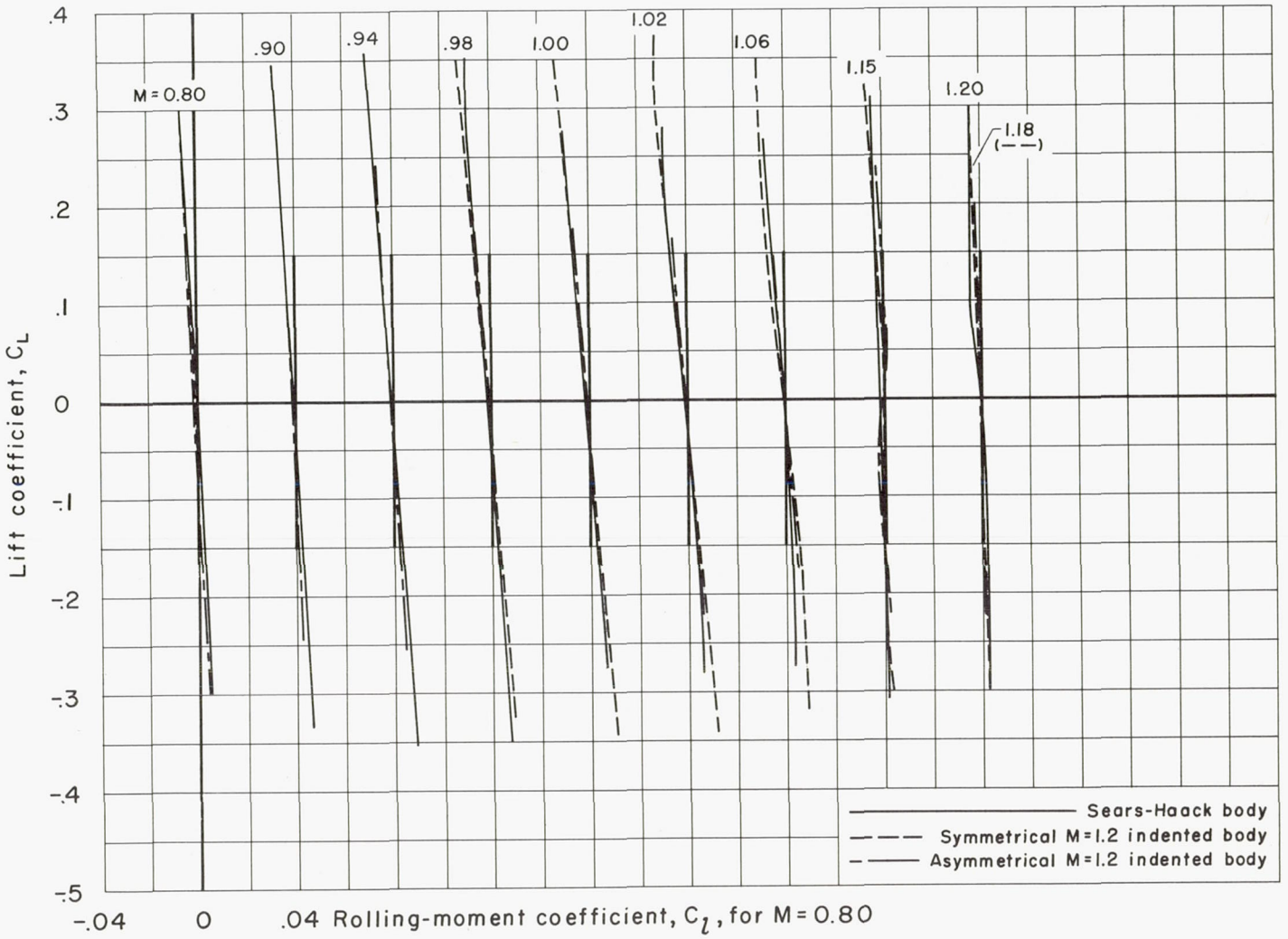

(d) C_L vs. C_l

Figure 11.- Concluded.

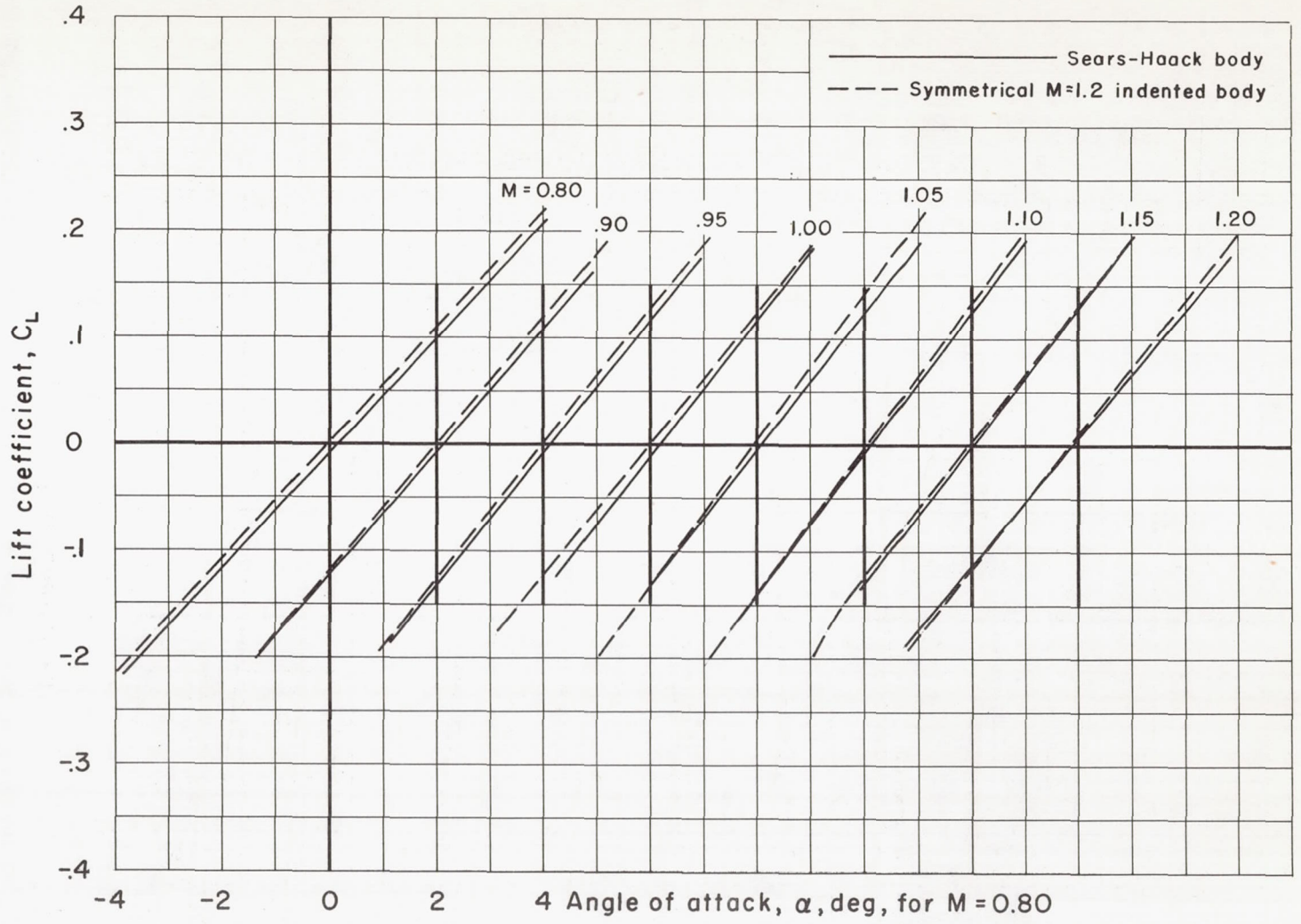

(a) C_L vs. α

Figure 12.- Aerodynamic characteristics of the aspect-ratio-3 yawed wing with two different bodies.

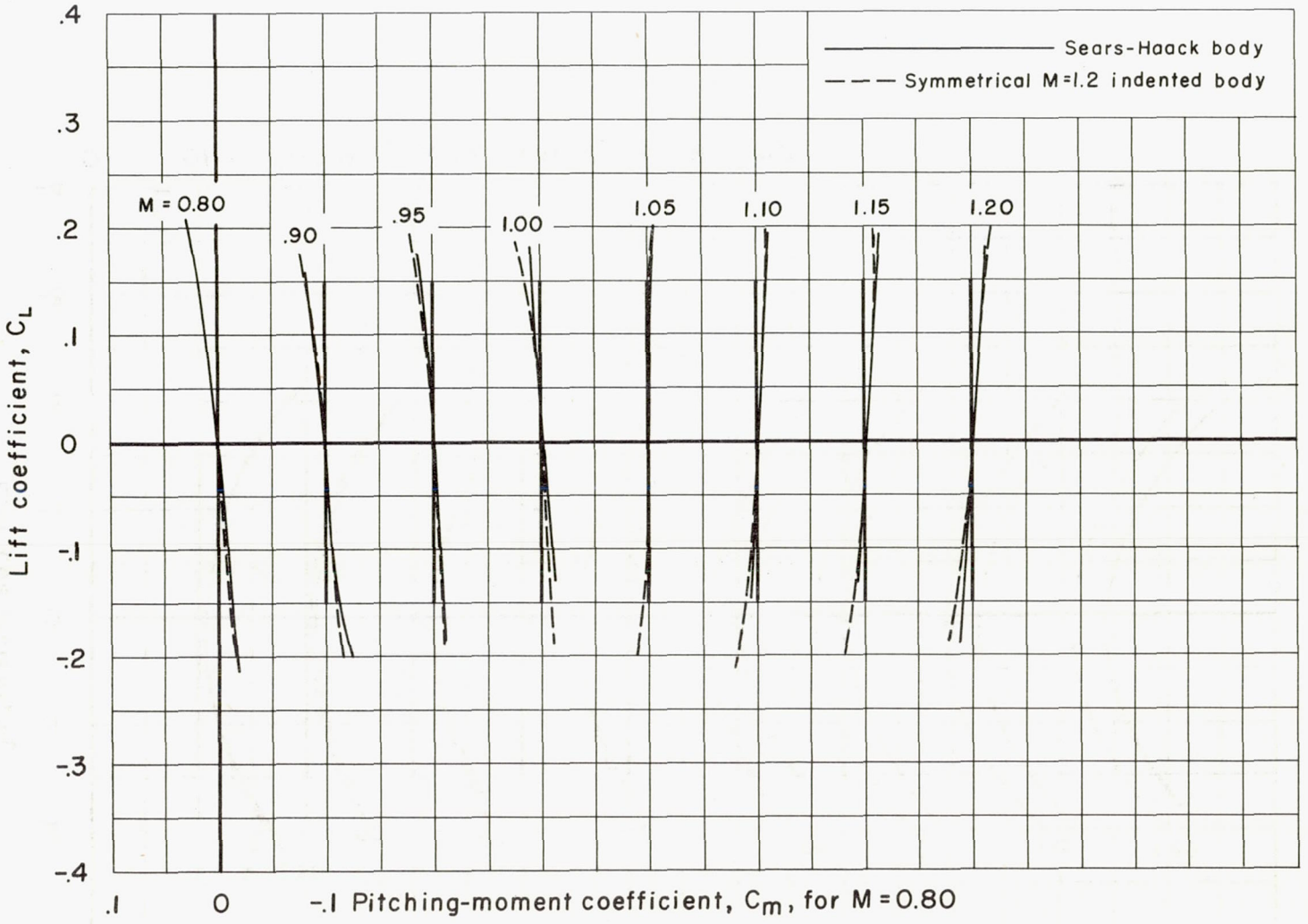

(b) C_L vs. C_m

Figure 12.- Continued.

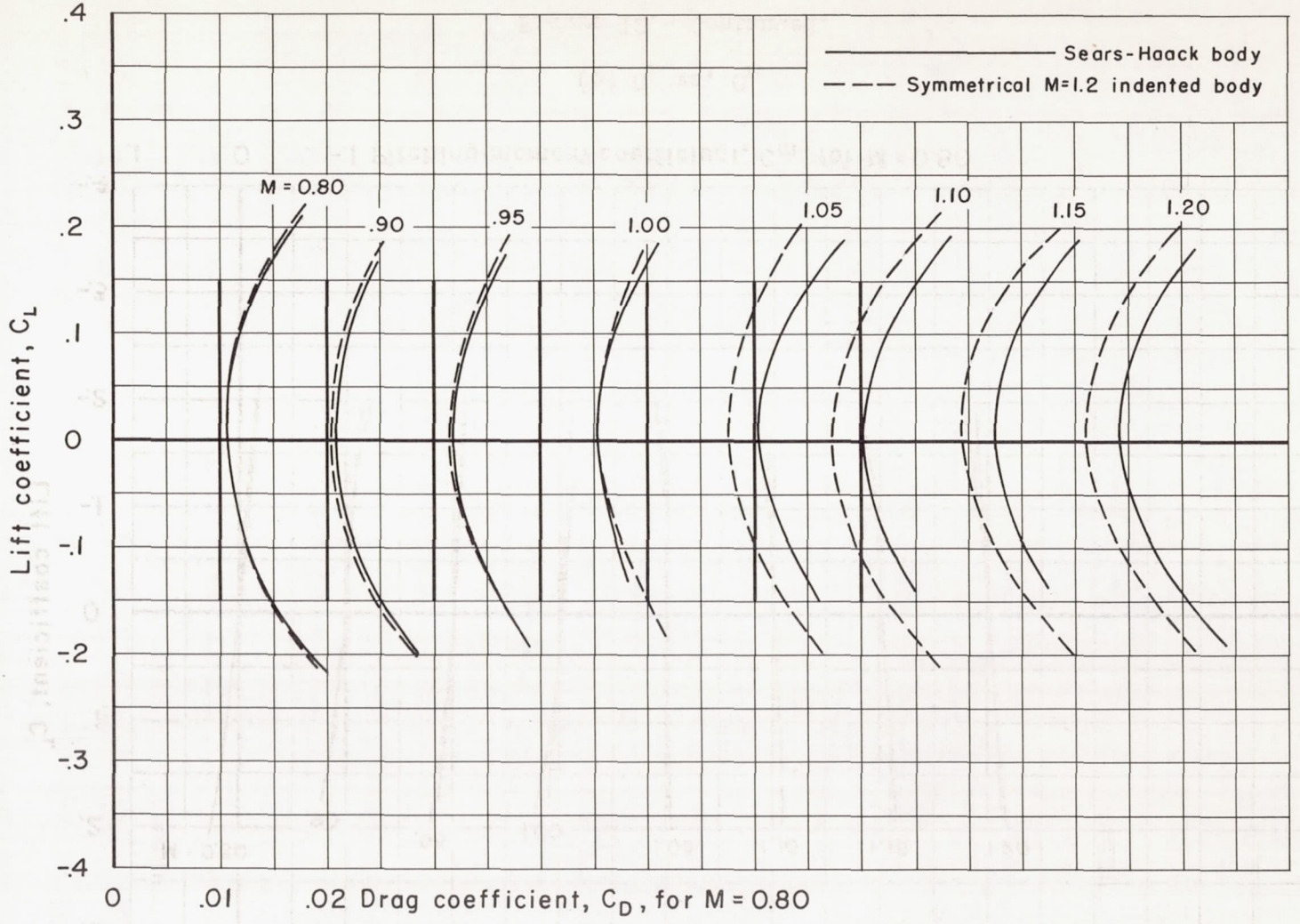

(c) C_L vs. C_D

Figure 12.- Continued.

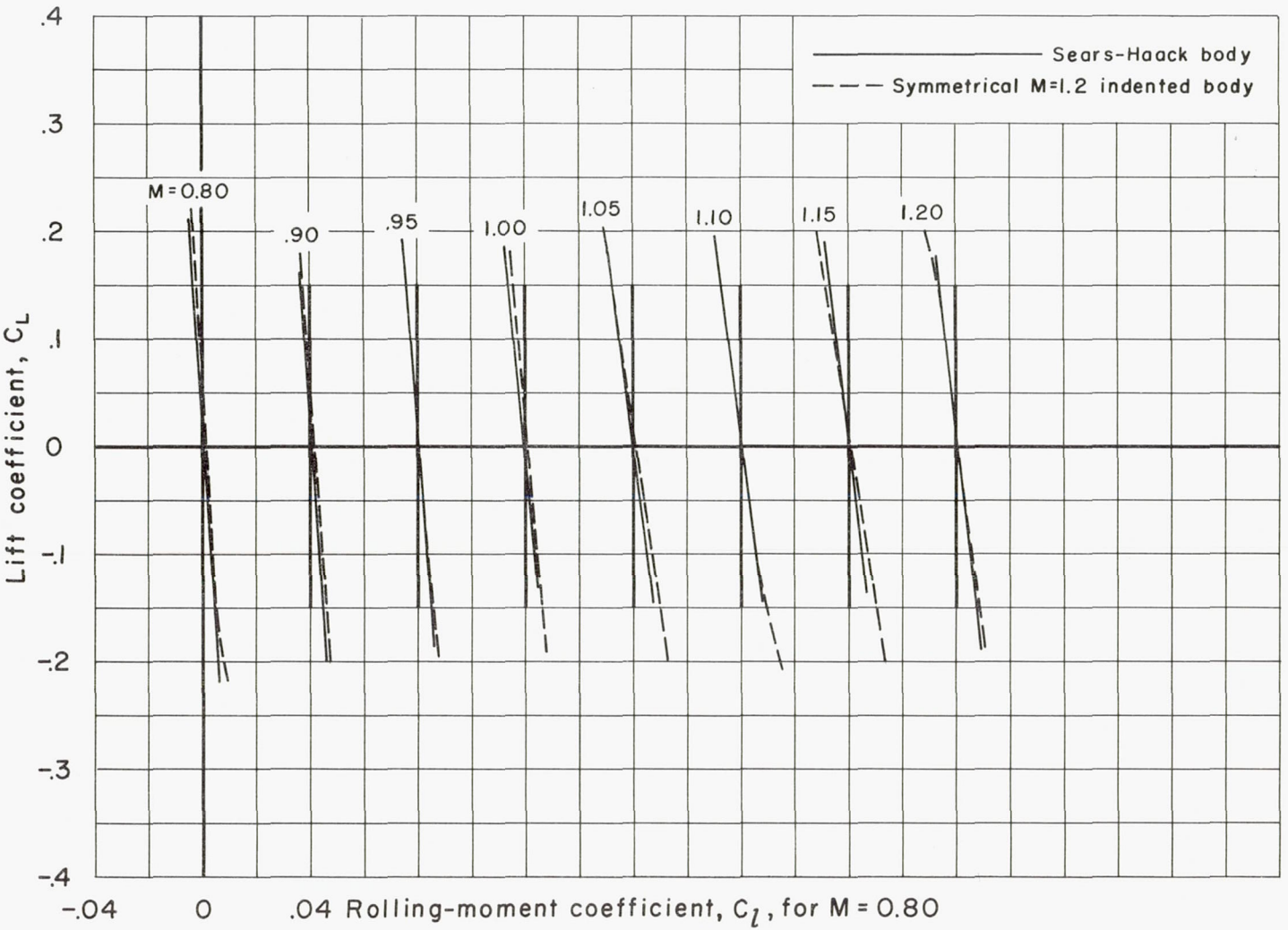

(d) C_L vs. C_l

Figure 12.- Concluded.

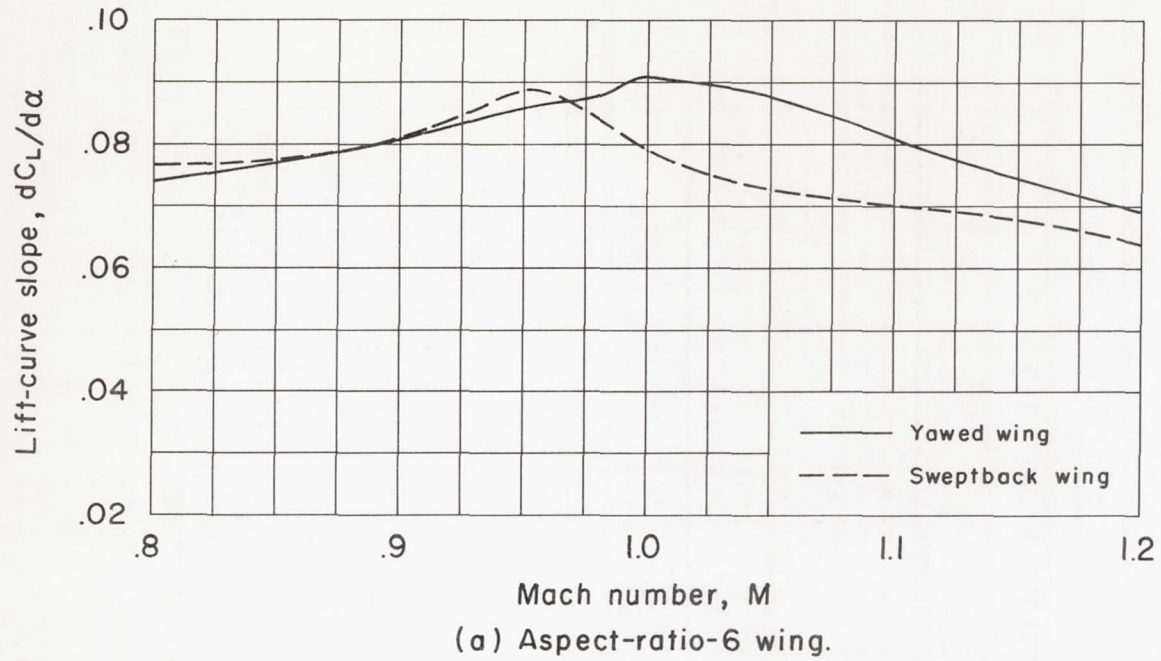

(a) Aspect-ratio-6 wing.

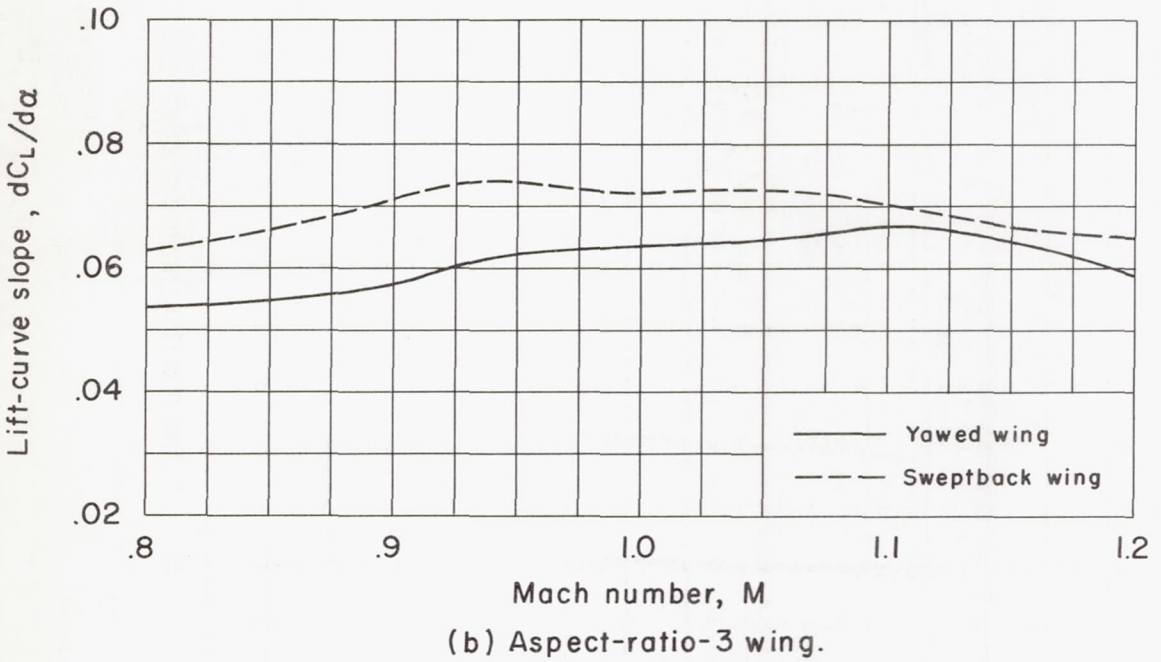

(b) Aspect-ratio-3 wing.

Figure 13.- Lift-curve slopes for the yawed wings and sweptback wings (ref. 7) with Sears-Haack bodies.

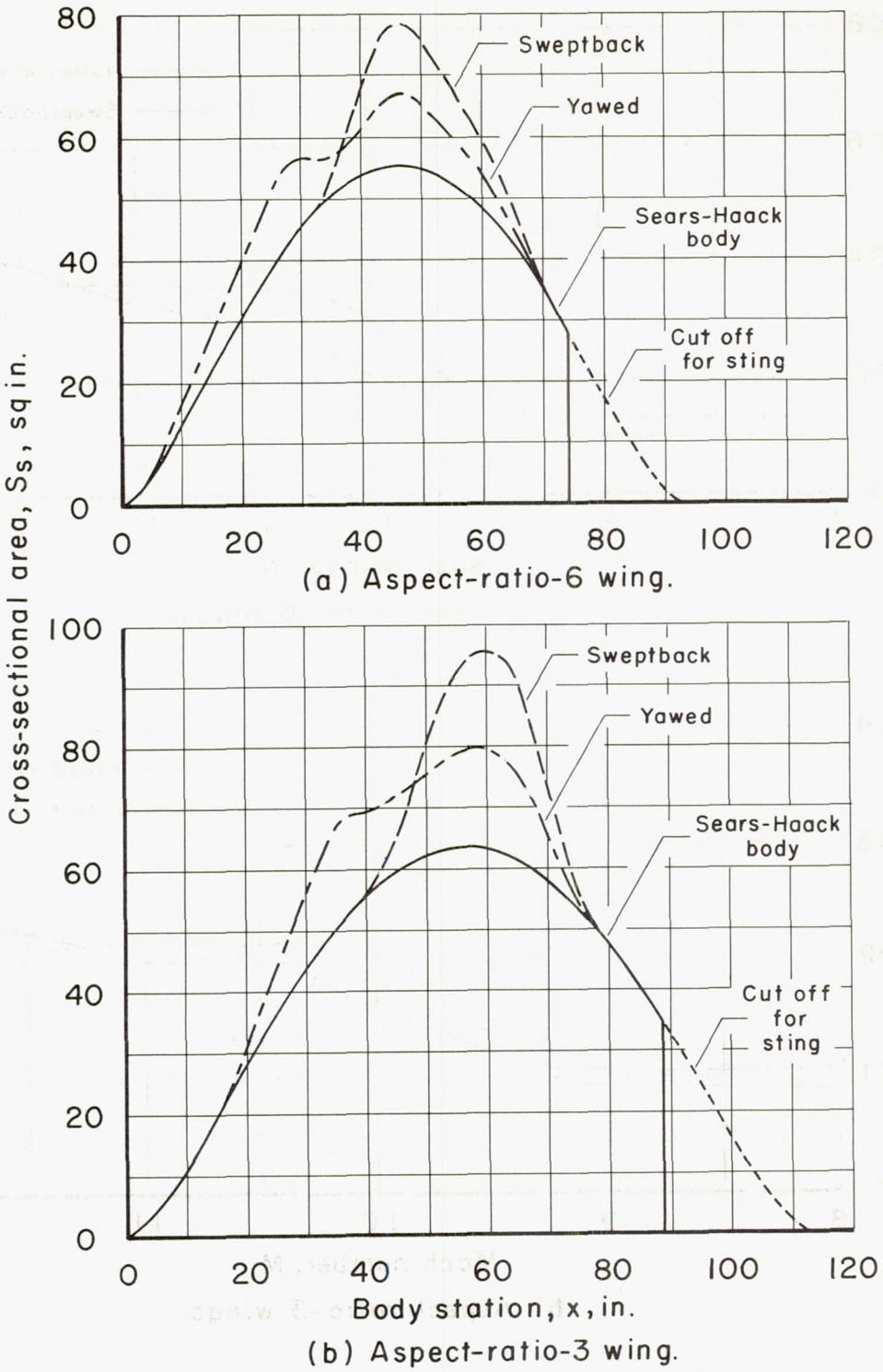

Figure 14.- Cross-sectional area distributions for the yawed and sweptback wings with the Sears-Haack bodies (M = 1.00).

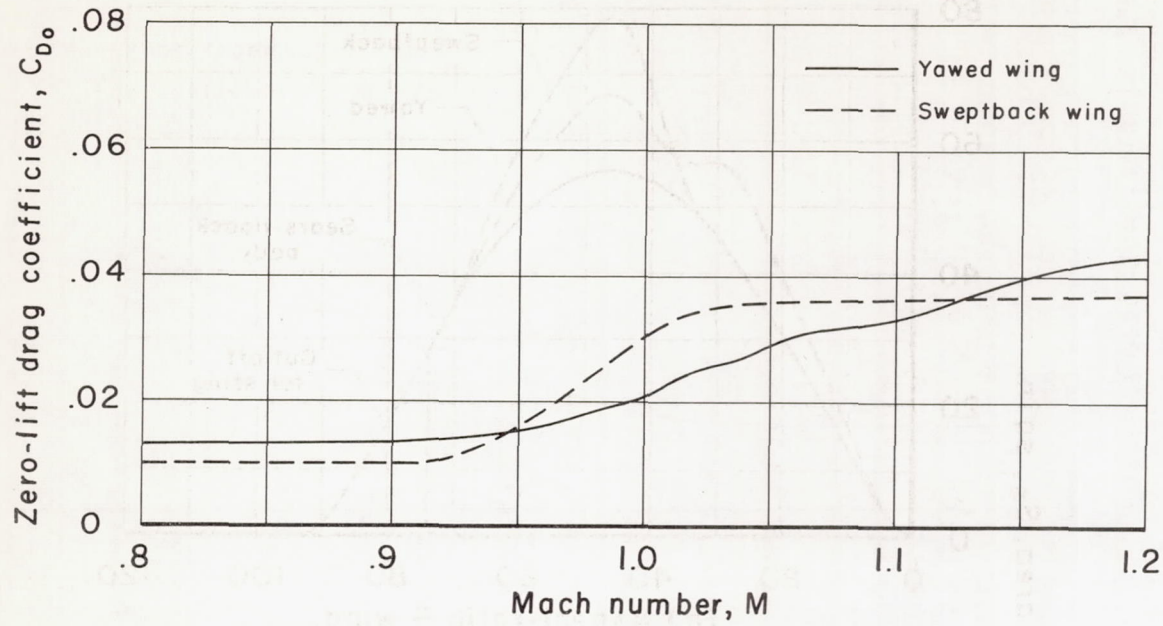

(a) Aspect-ratio-6 wings.

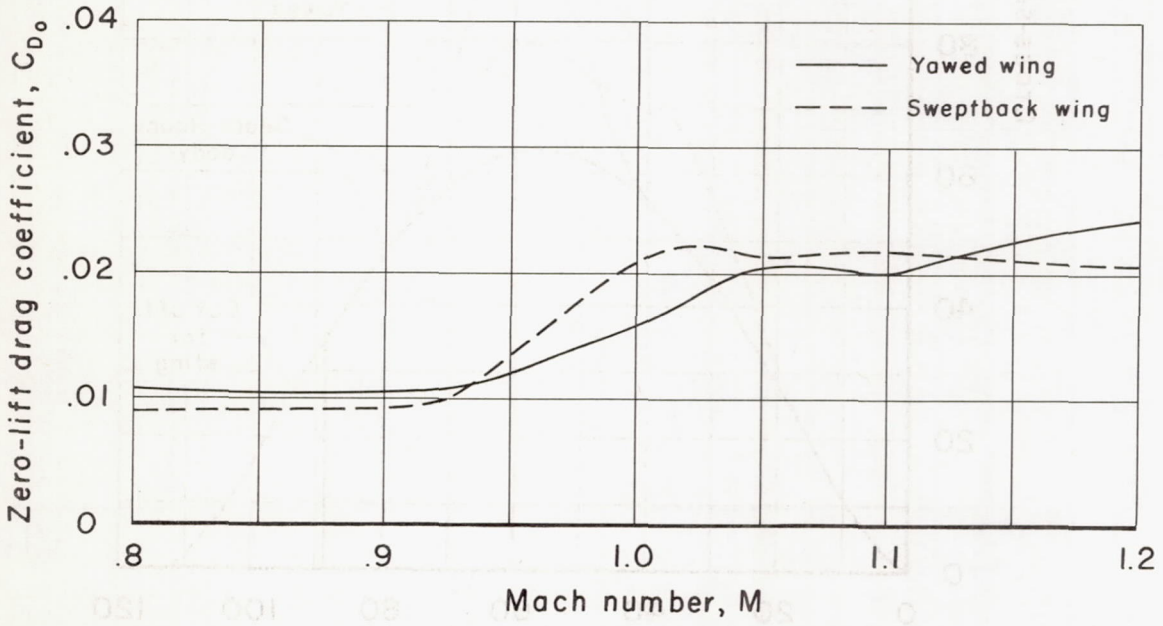

(b) Aspect-ratio-3 wings.

Figure 15.- Zero-lift drag coefficients for the yawed wings and sweptback wings (ref. 7) with Sears-Haack bodies.

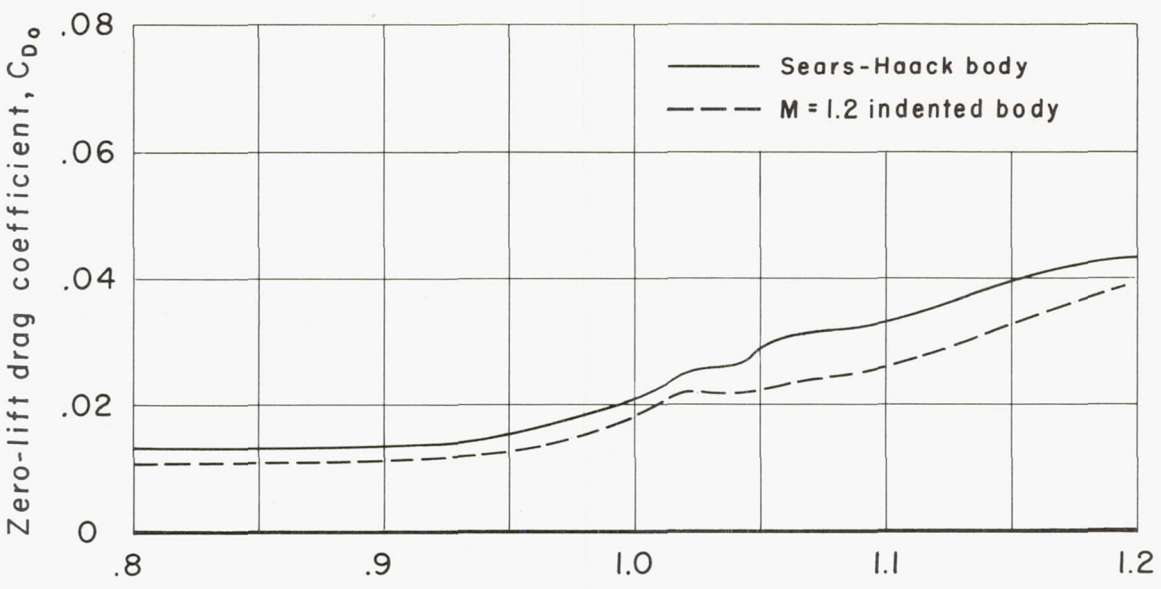

(a) Aspect-ratio-6 yawed wing.

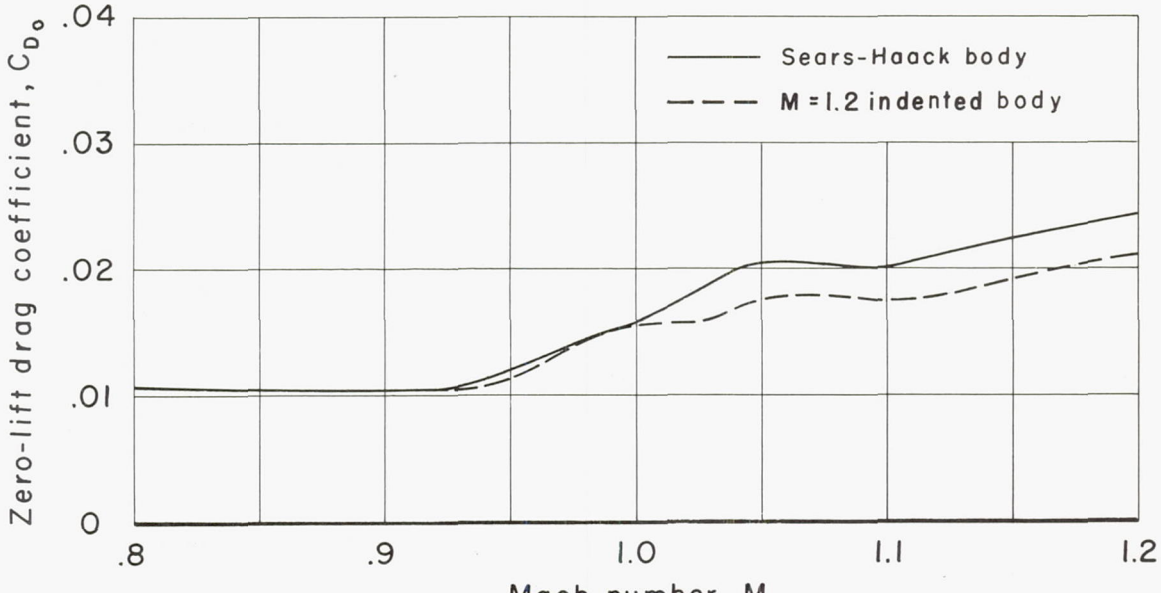

(b) Aspect-ratio-3 yawed wing.

Figure 16.- Zero-lift drag coefficients for the yawed wings with the Sears-Haack and symmetrical M = 1.20 indented bodies.

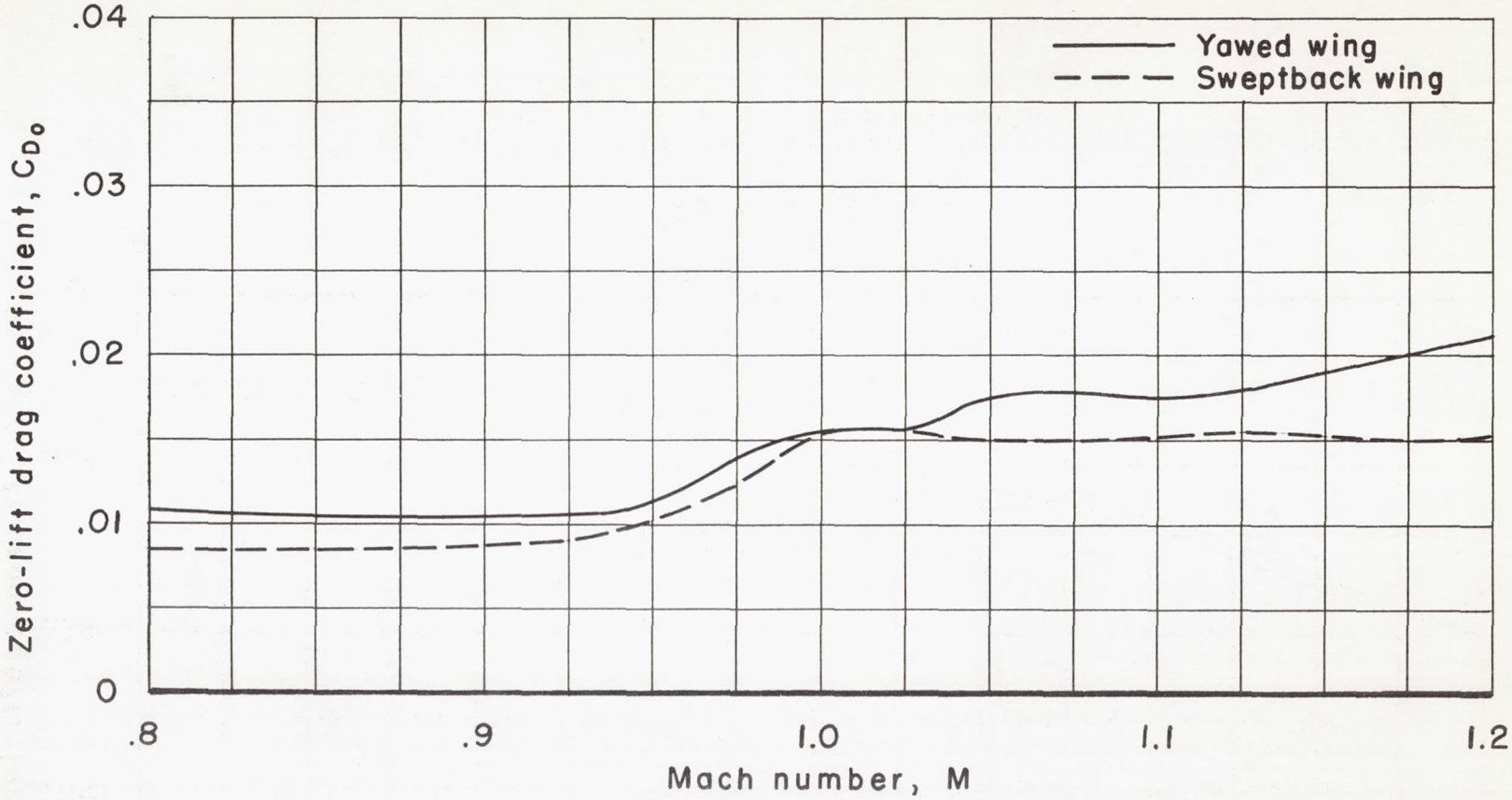

Figure 17.- Zero-lift drag coefficients for the aspect-ratio-3 yawed wing and sweptback wing (ref. 8) with symmetrical M = 1.20 indented bodies.

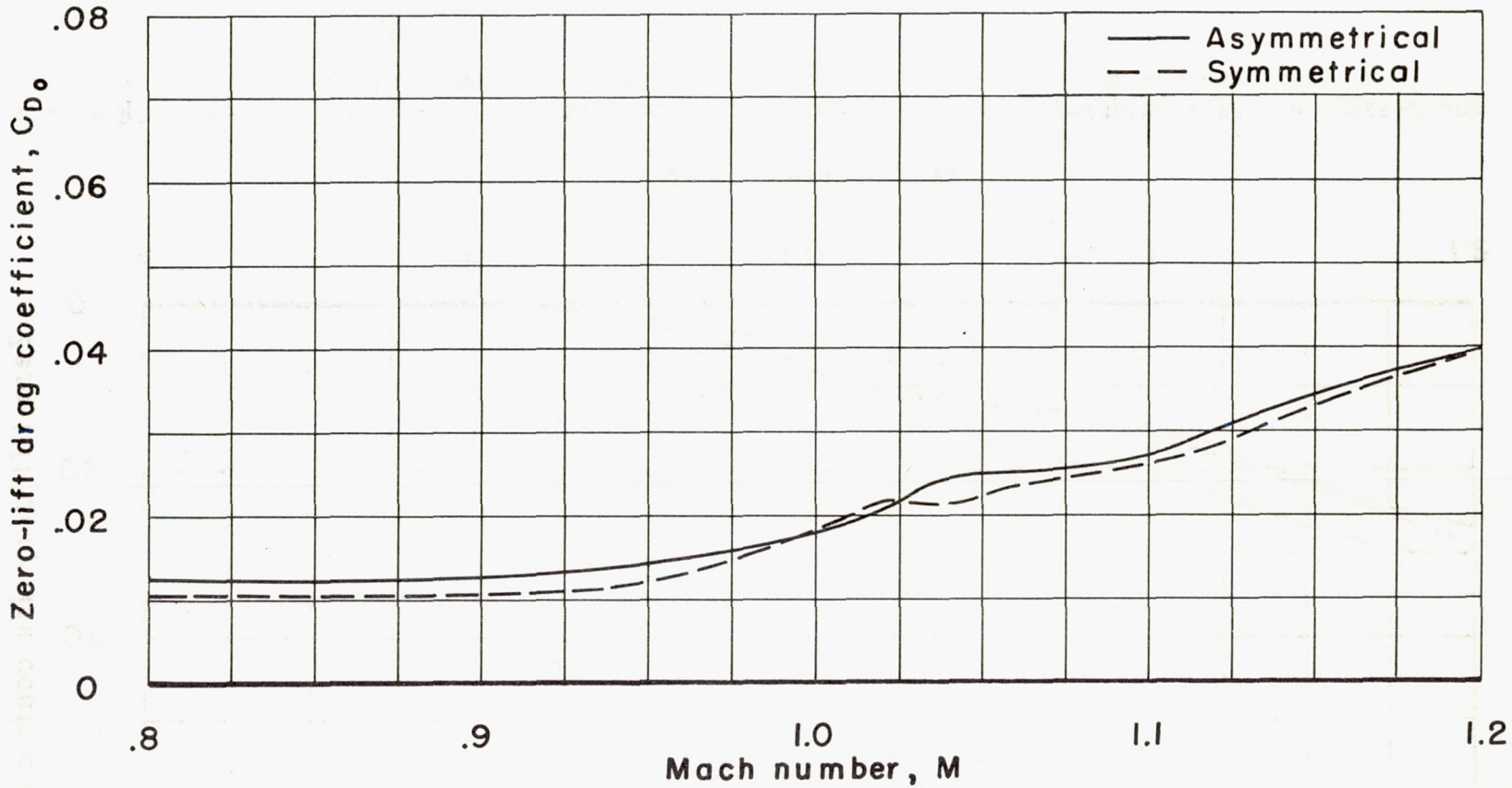

Figure 18.- Zero-lift drag coefficients for the aspect-ratio-6 yawed wing with the symmetrical and asymmetrical M = 1.20 indented bodies.

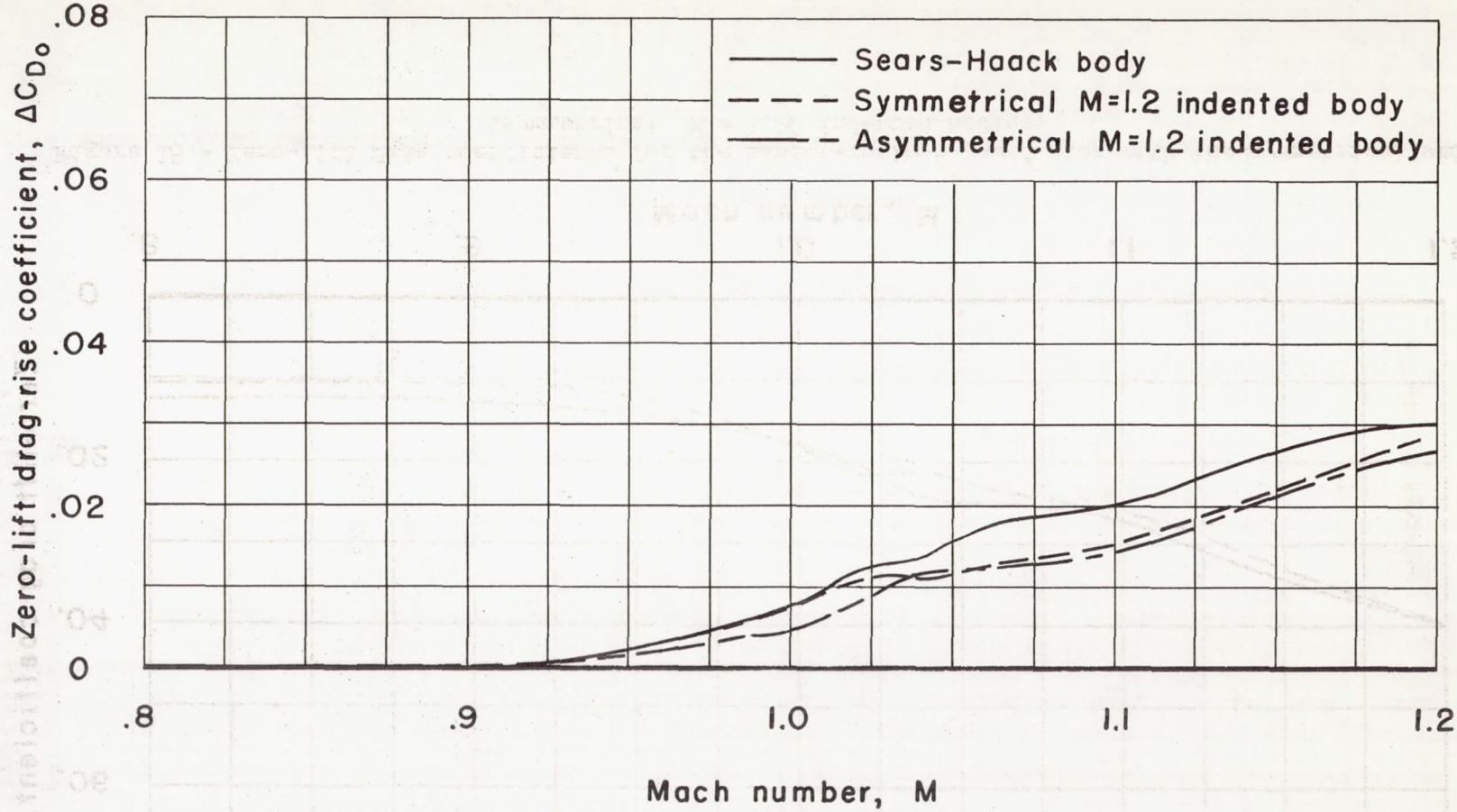

Figure 19.- Zero-lift drag-rise coefficients for the aspect-ratio-6 yawed wing with the Sears-Haack body and the symmetrical and asymmetrical M = 1.20 indented bodies.

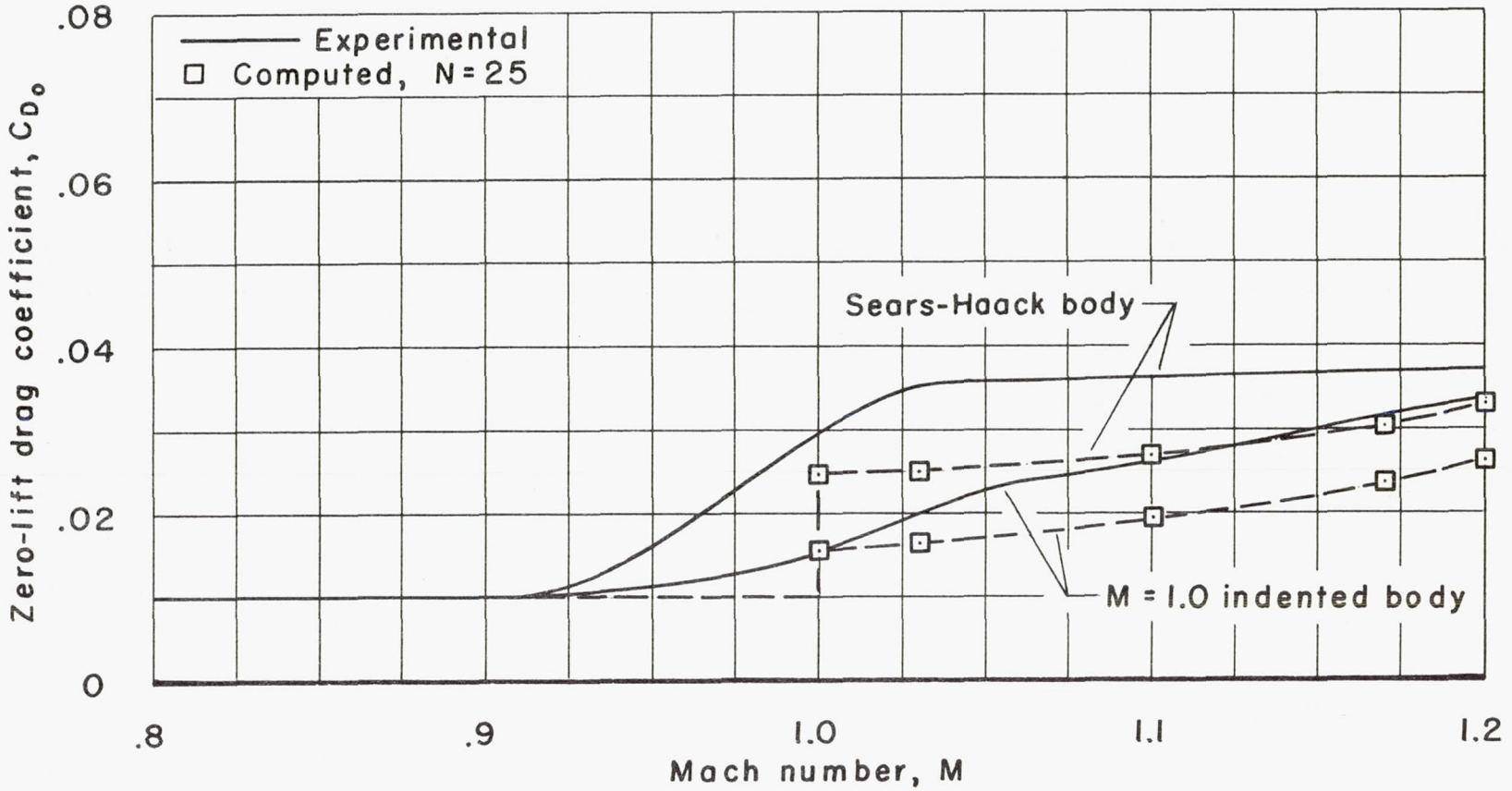

Figure 20.- Experimental (ref. 7) and computed zero-lift drag coefficients for the aspect-ratio-6 sweptback wing with a Sears-Haack body and an M = 1.00 indented body.

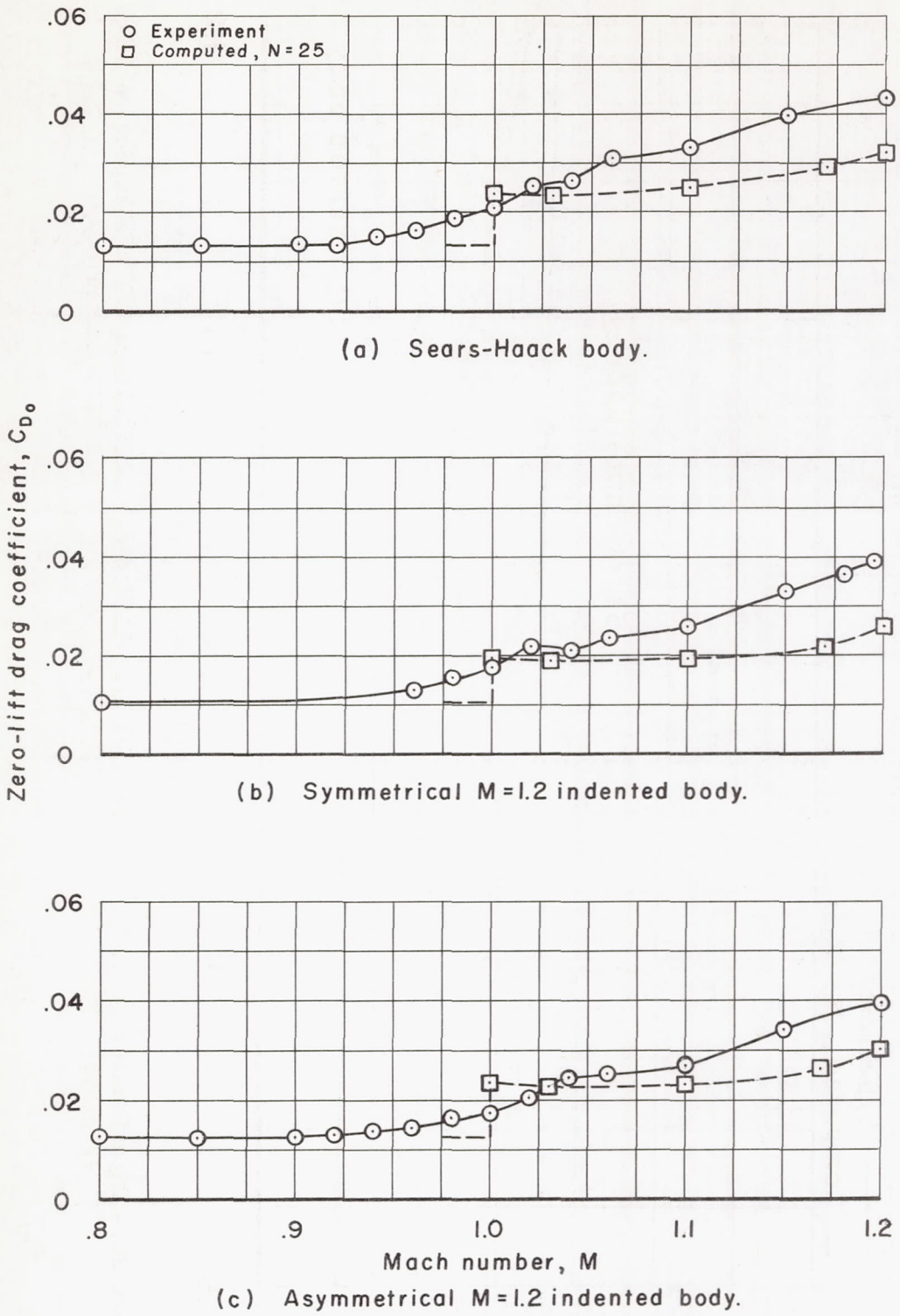

Figure 21.- Experimental and computed zero-lift drag coefficients for the aspect-ratio-6 yawed wing with the various bodies.

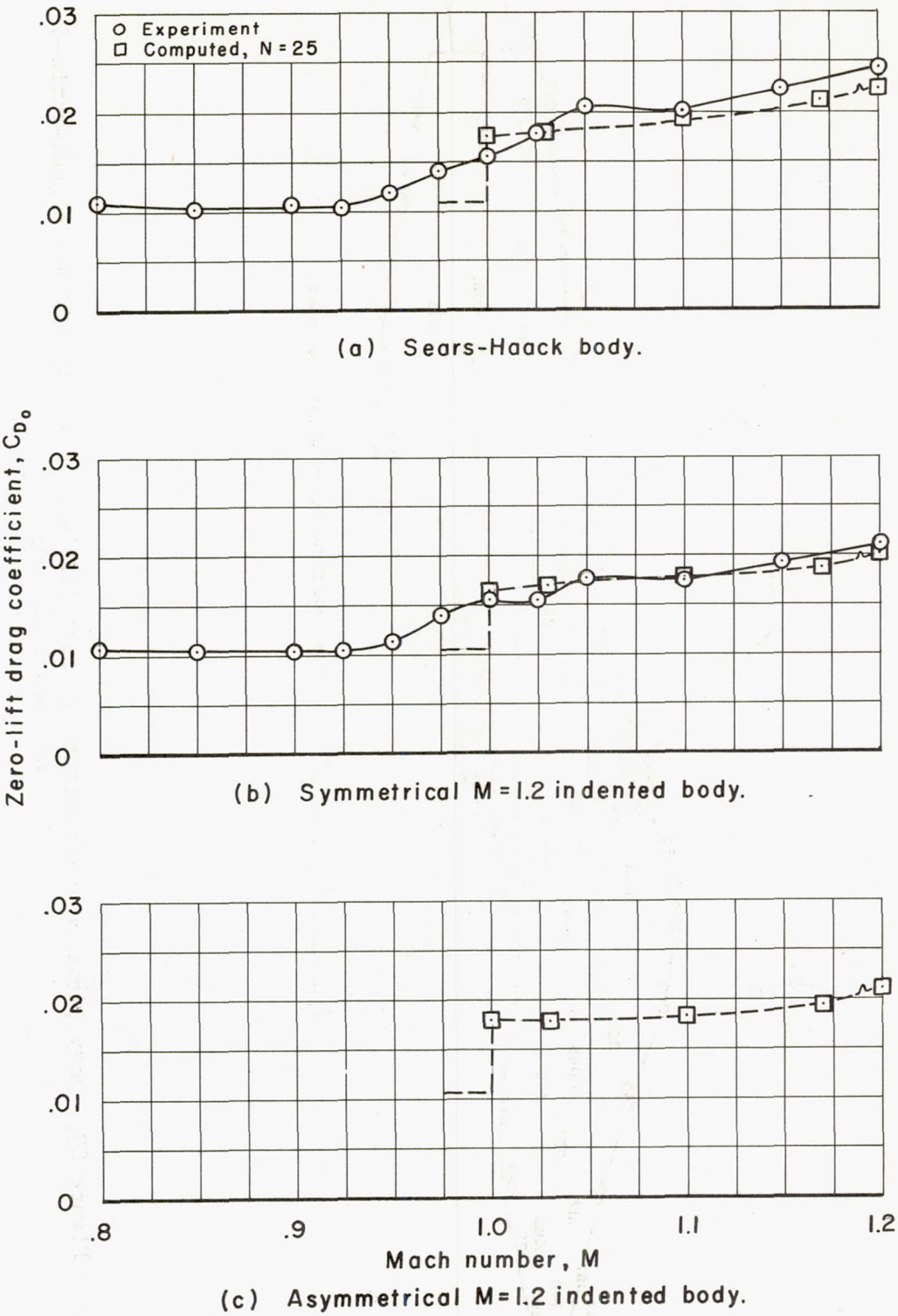

Figure 22.- Experimental and computed zero-lift drag coefficients for the aspect-ratio-3 yawed wing with the various bodies.

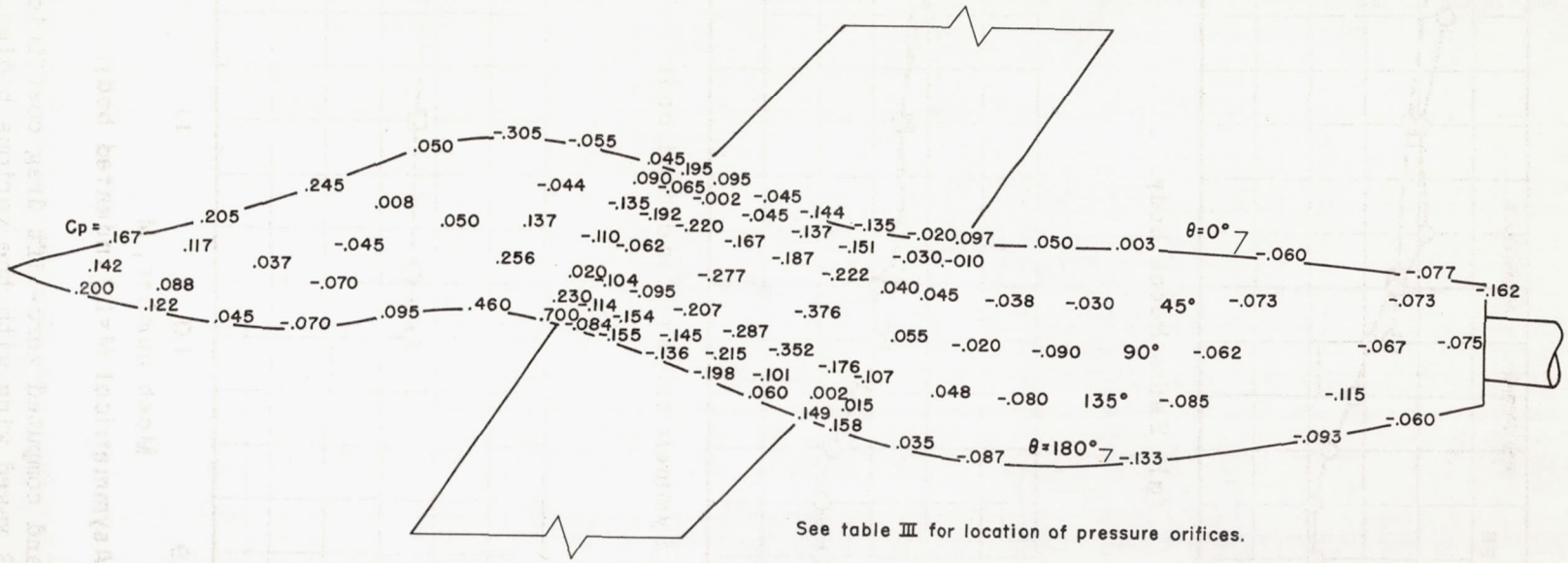

See table III for location of pressure orifices.

Figure 23.- Body pressure coefficients at zero lift and M = 1.20 for the aspect-ratio-6 asymmetrical body.

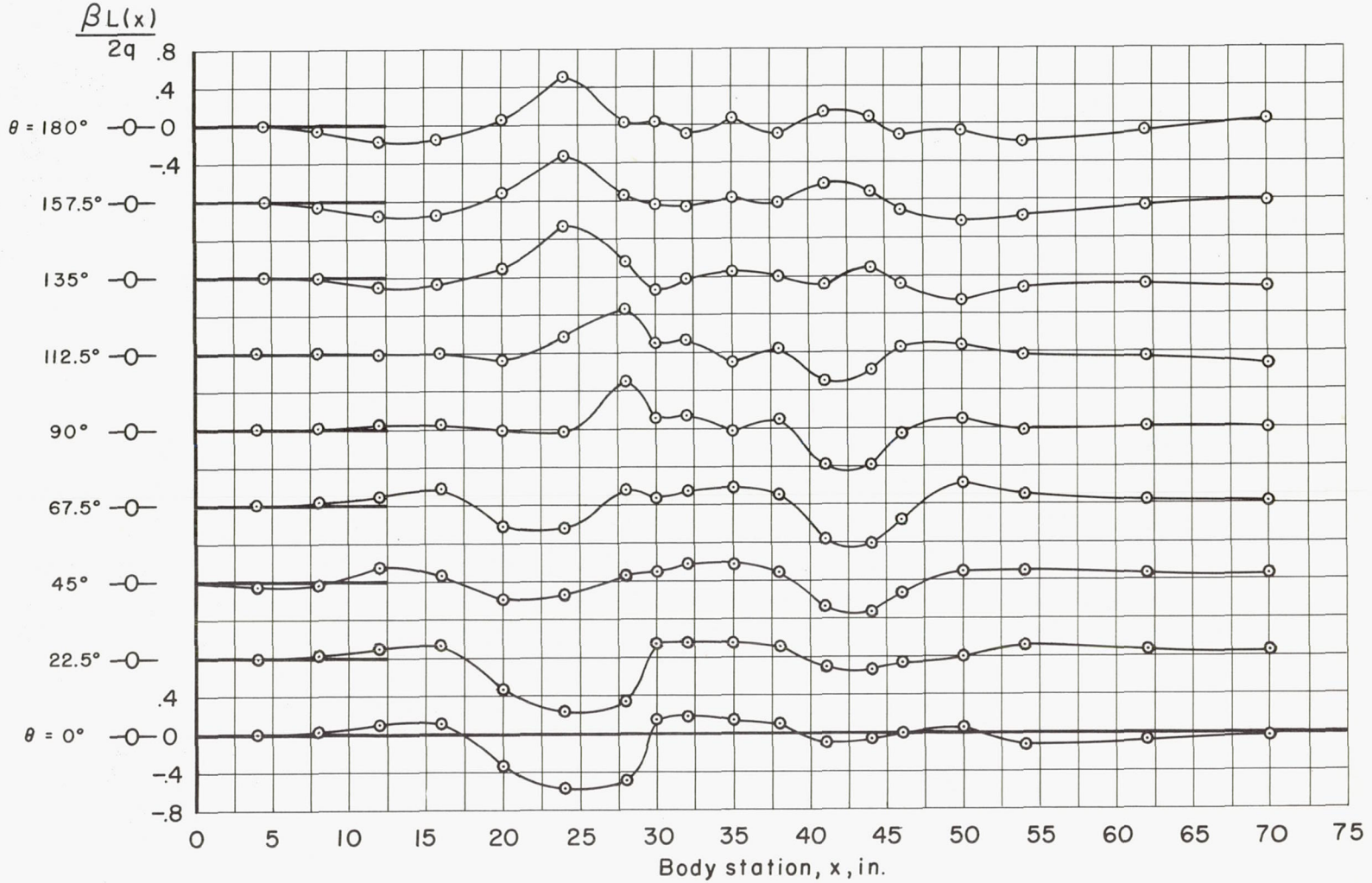

Figure 24.- Oblique-force term (ref. 4) for various cutting angles, θ, at M = 1.20 for the aspect-ratio-6 yawed wing with the asymmetrical M = 1.20 indented body.

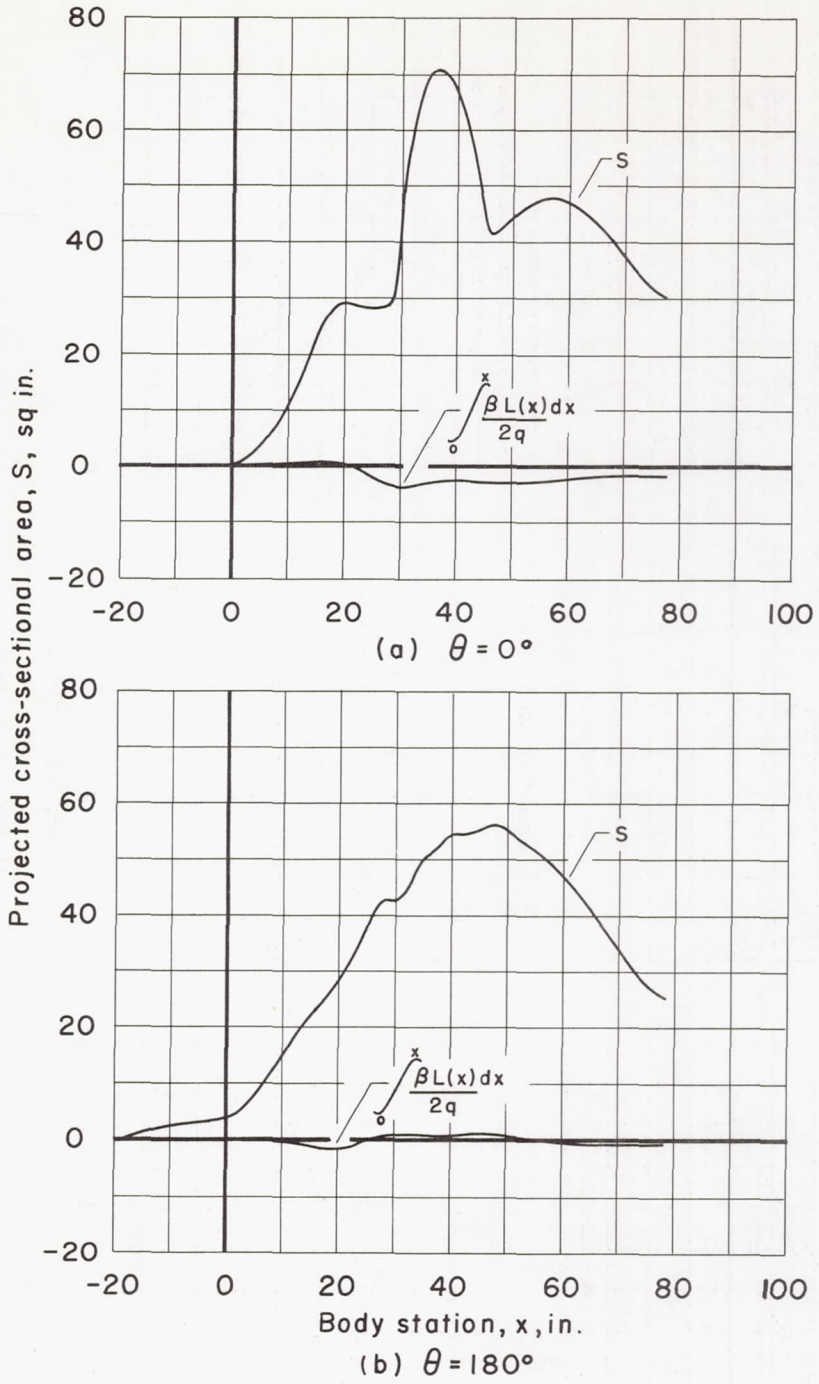

Figure 25.- Equivalent areas of the oblique-force term $\int_0^x \frac{\beta L(x)dx}{2q}$ (ref. 4) and the total projected areas, each at M = 1.20 and at representative cutting angles of $\theta = 0°$ and $180°$ for the aspect-ratio-6 yawed wing with the asymmetrical M = 1.20 indented body.

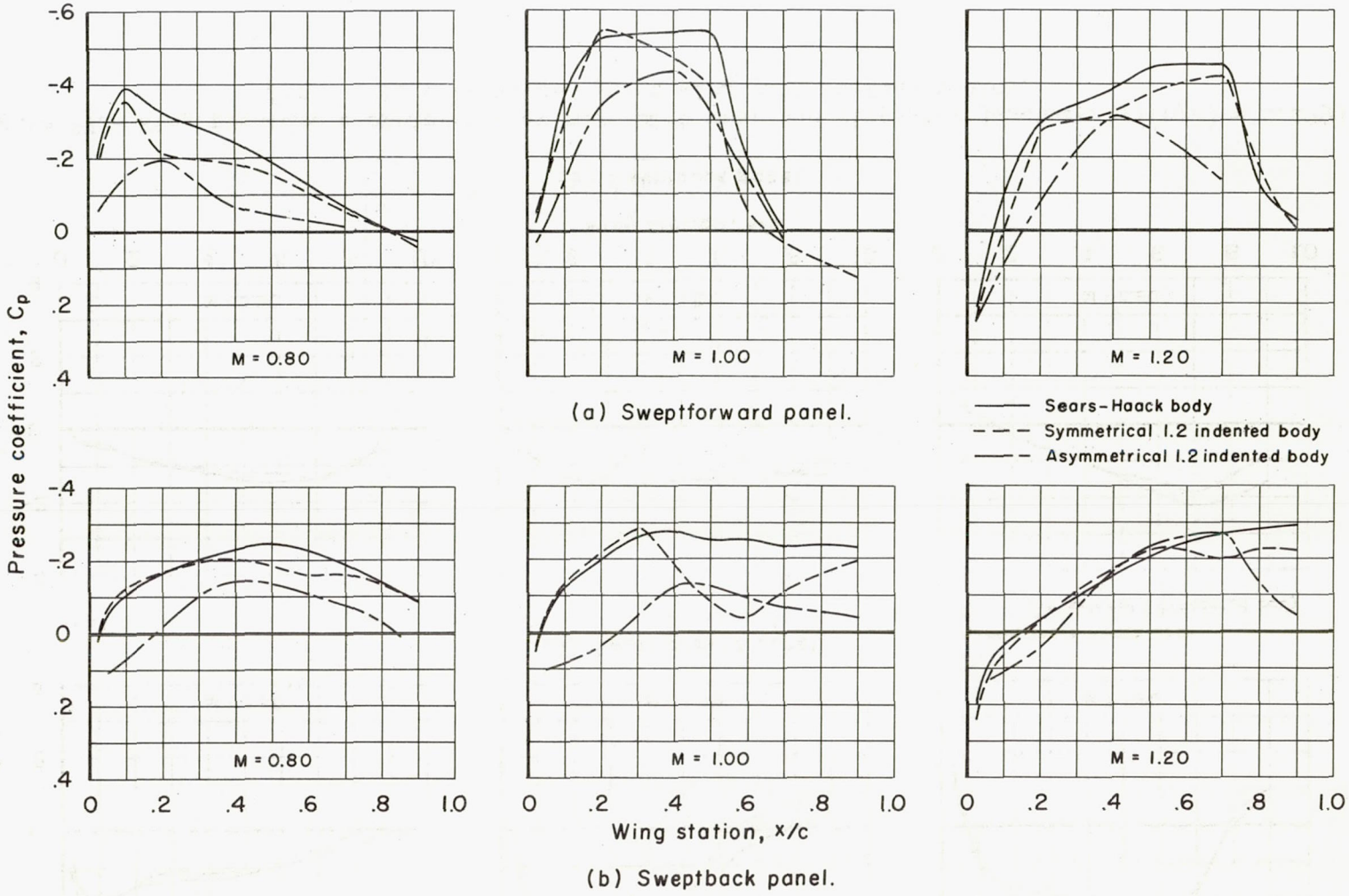

Figure 26.- Wing pressure coefficients at zero lift near the wing-body juncture (y/(b/2) = 0.139) for the aspect-ratio-6 yawed wing with various bodies.

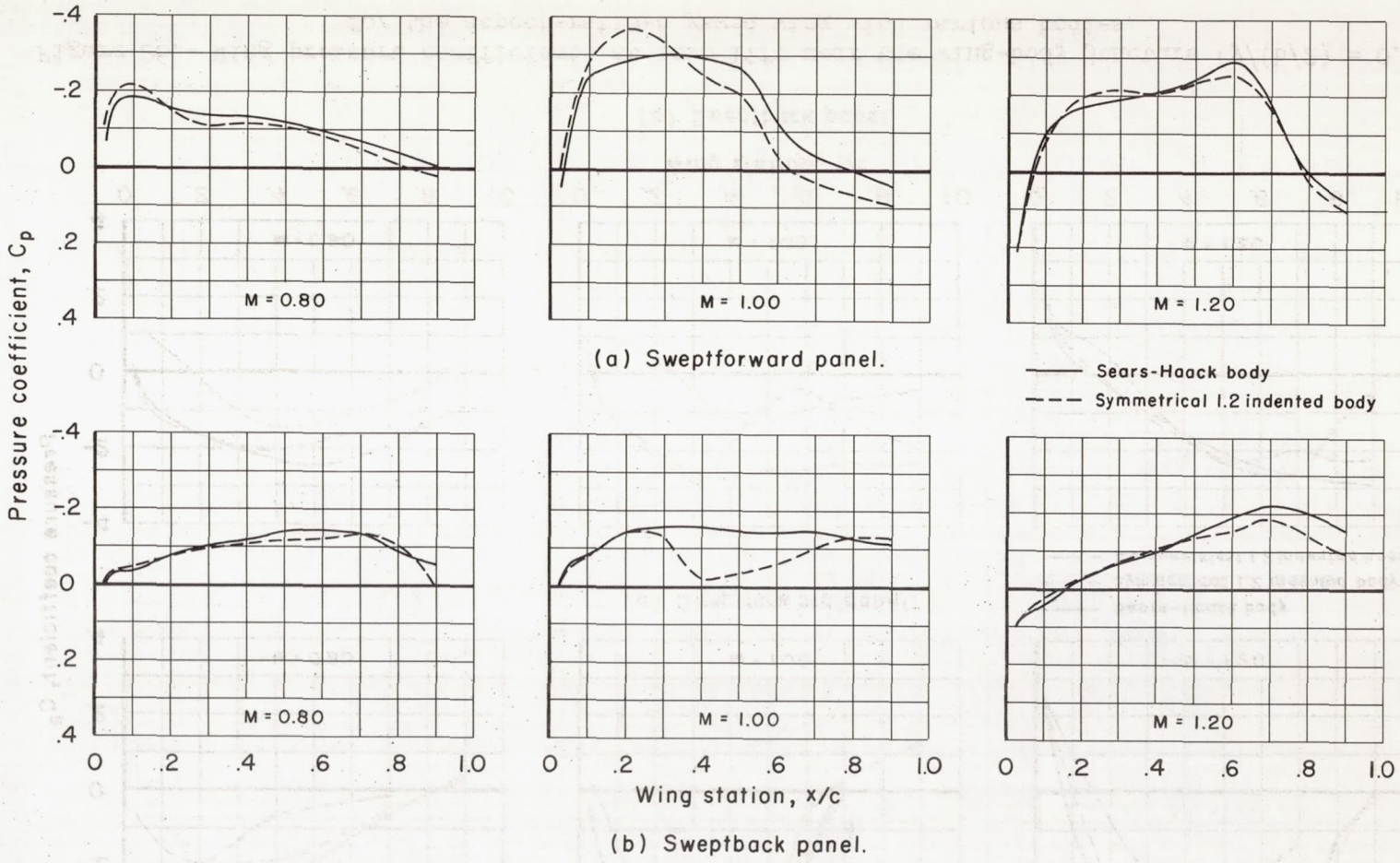

Figure 27.- Wing pressure coefficients at zero lift near the wing-body juncture (y/(b/2) = 0.179) for the aspect-ratio-3 yawed wing with various bodies.

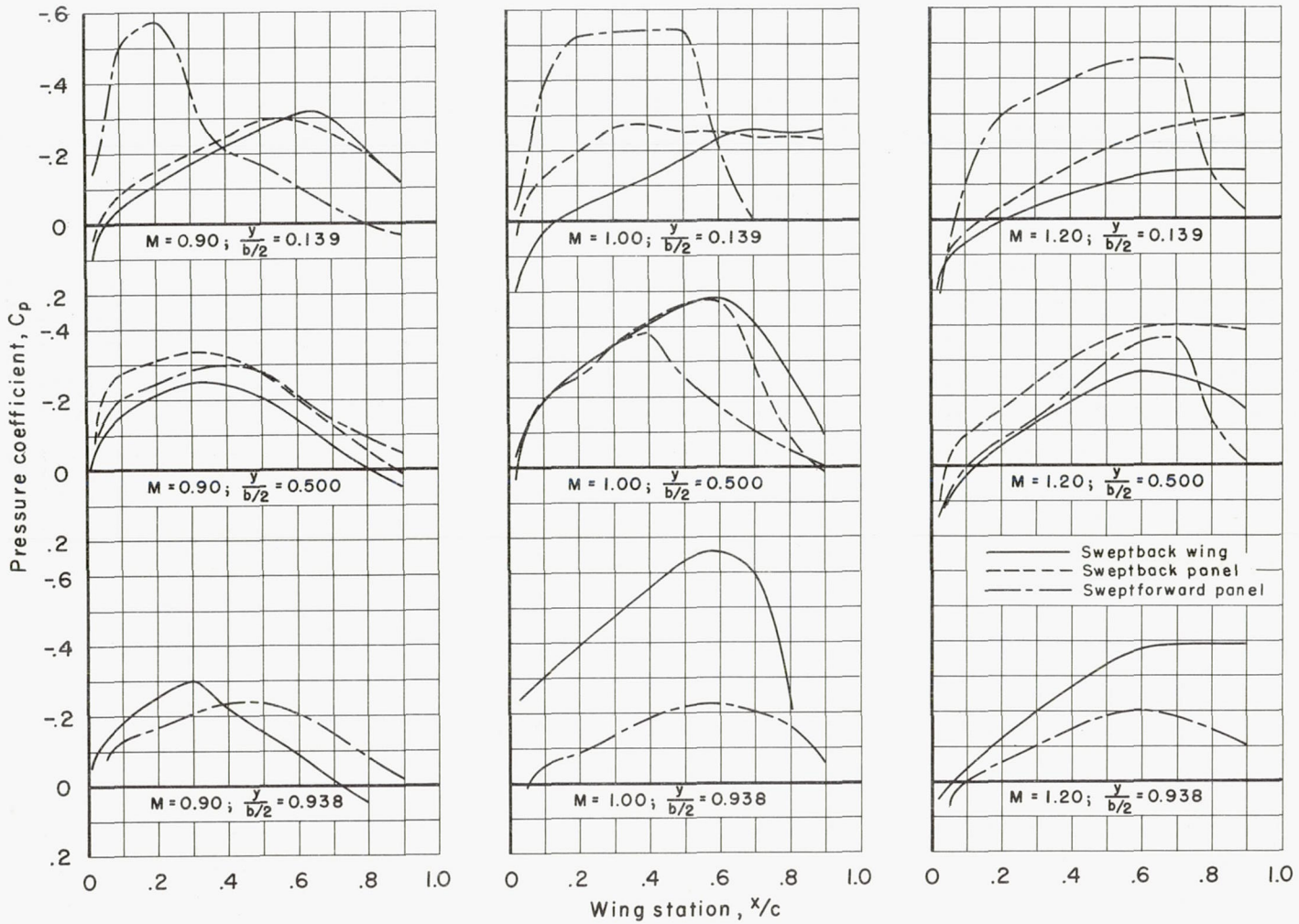

Figure 28.- Wing pressure coefficients at zero lift for the aspect-ratio-6 wing at three spanwise stations for the sweptforward panel, the sweptback panel, and the sweptback wing (ref. 7) with the Sears-Haack body.

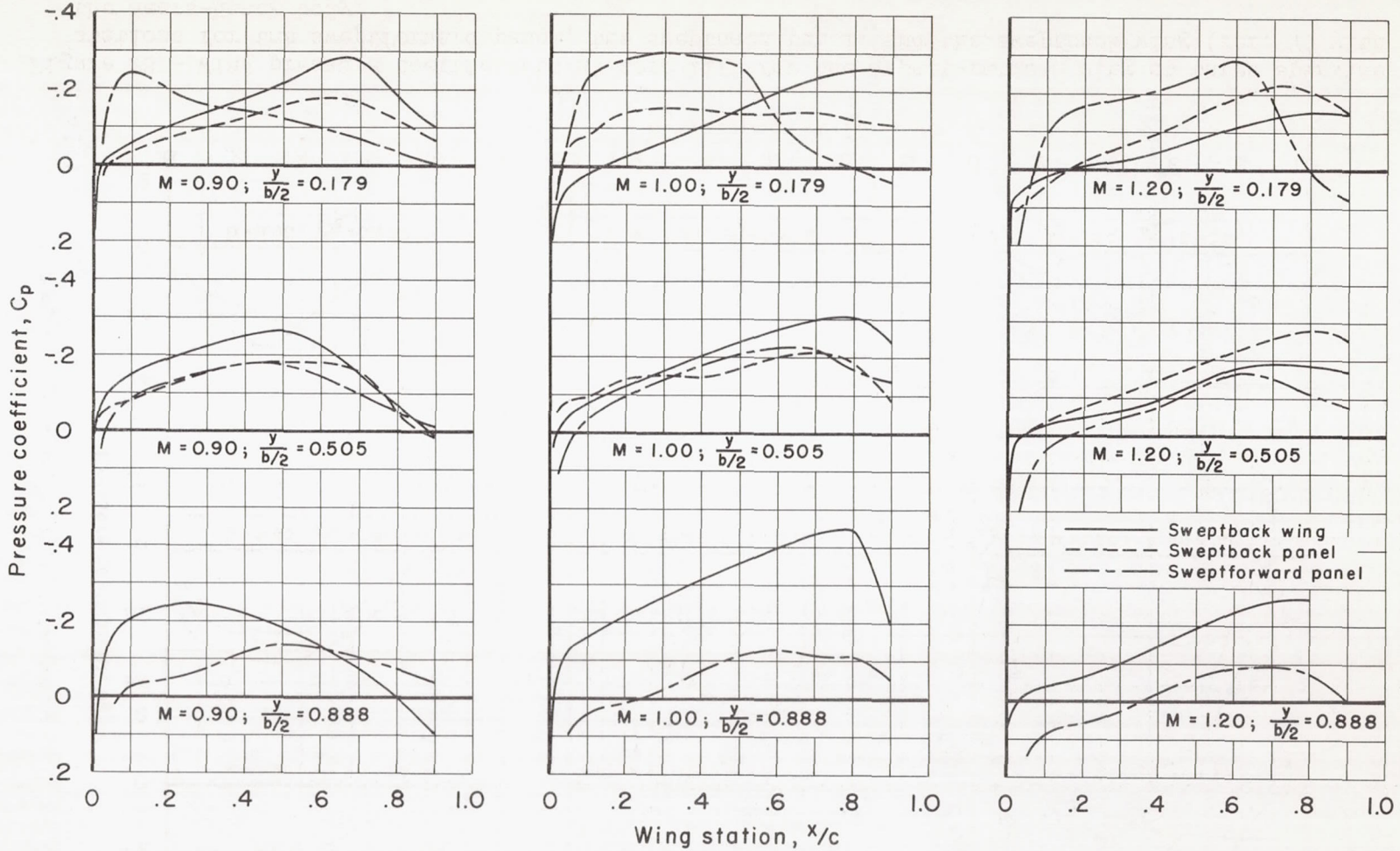

Figure 29.- Wing pressure coefficients at zero lift for the aspect-ratio-3 wing at three spanwise stations for the sweptforward panel, the sweptback panel, and the sweptback wing (refs. 7 and 8) with the Sears-Haack body.

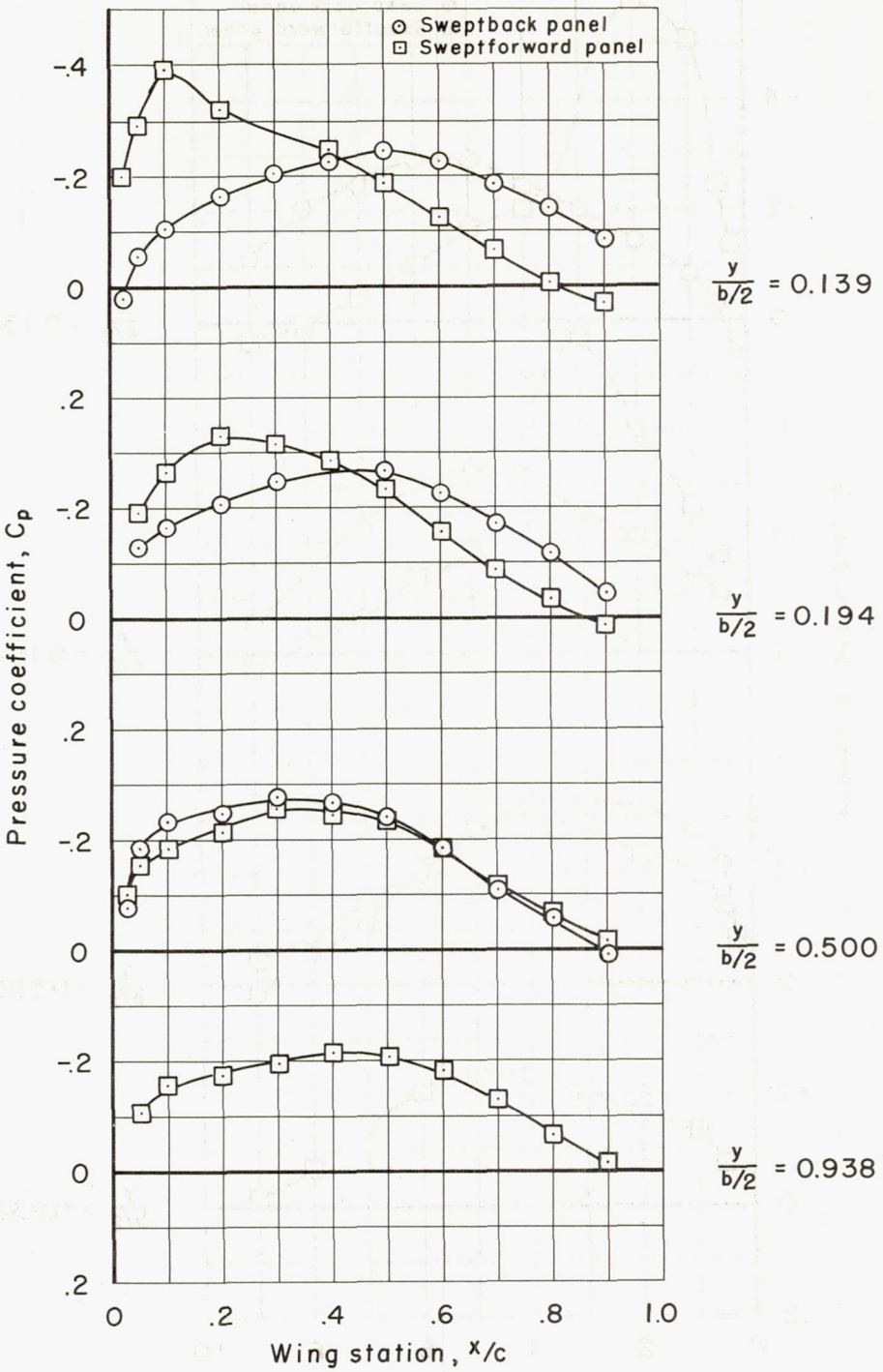

(a) M = 0.80; Sears-Haack body

Figure 30.- Wing pressure coefficients at zero lift for the aspect-ratio-6 yawed wing with a Sears-Haack body.

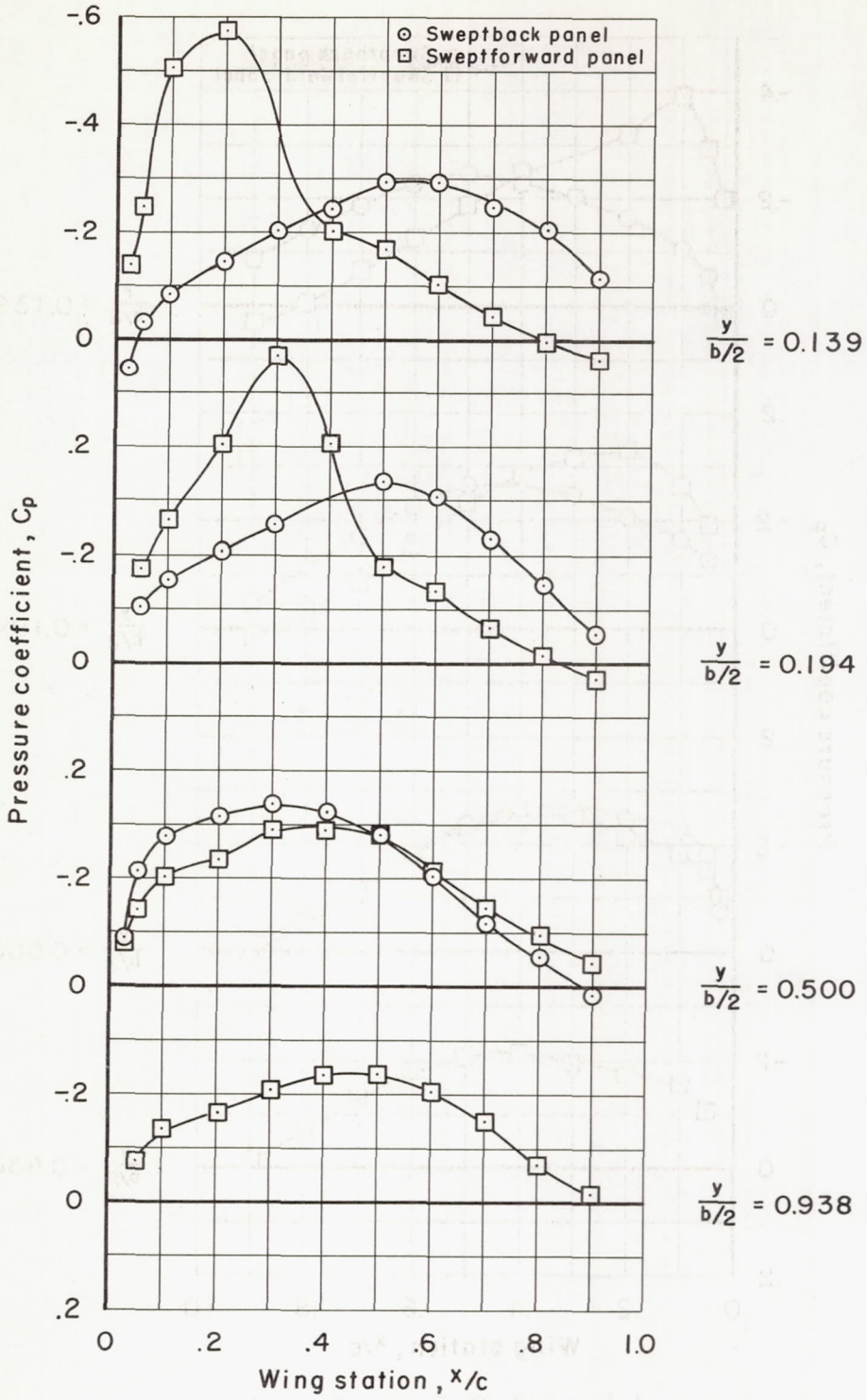

(b) M = 0.90; Sears-Haack body

Figure 30.- Continued.

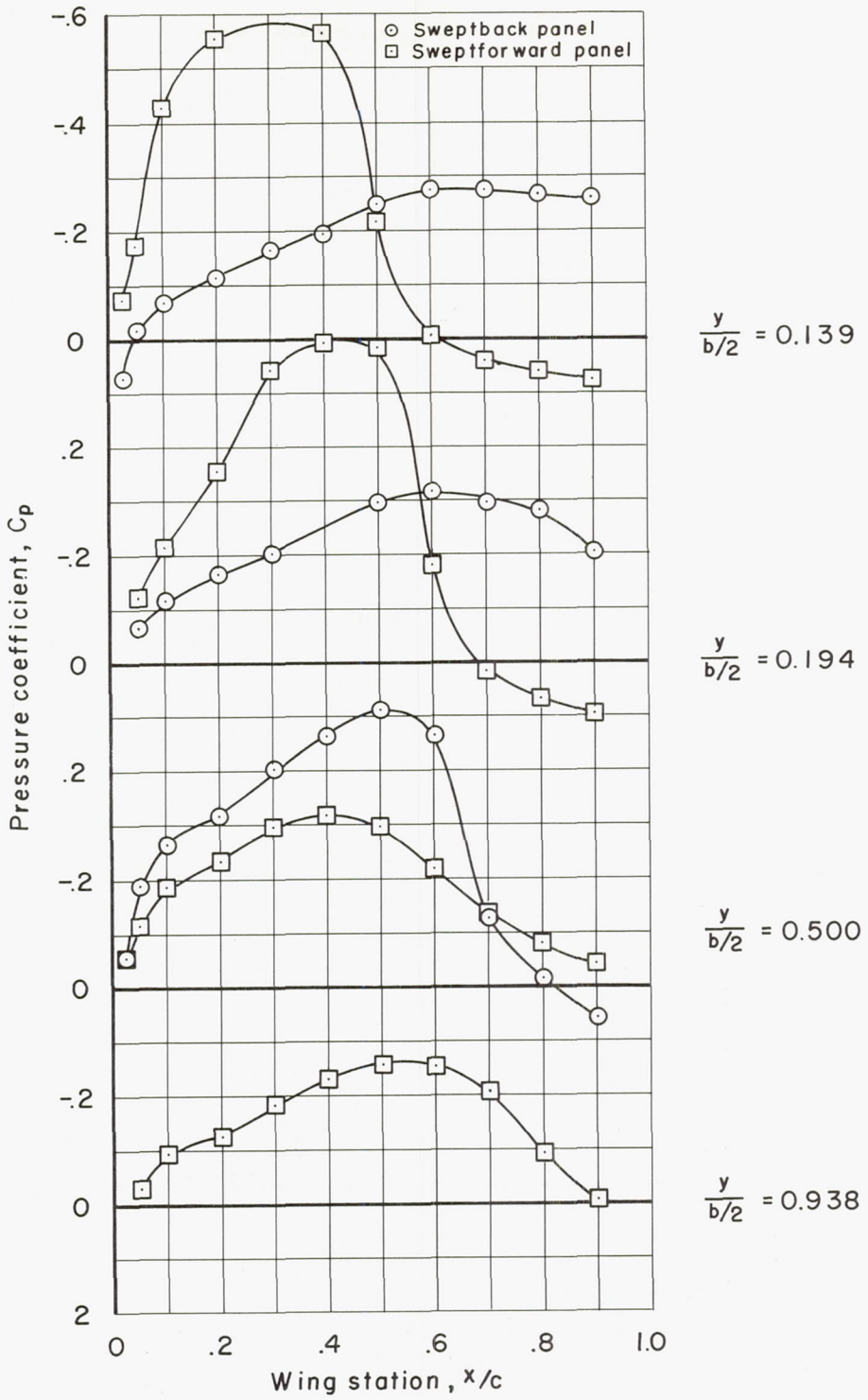

(c) M = 0.96; Sears-Haack body

Figure 30.- Continued.

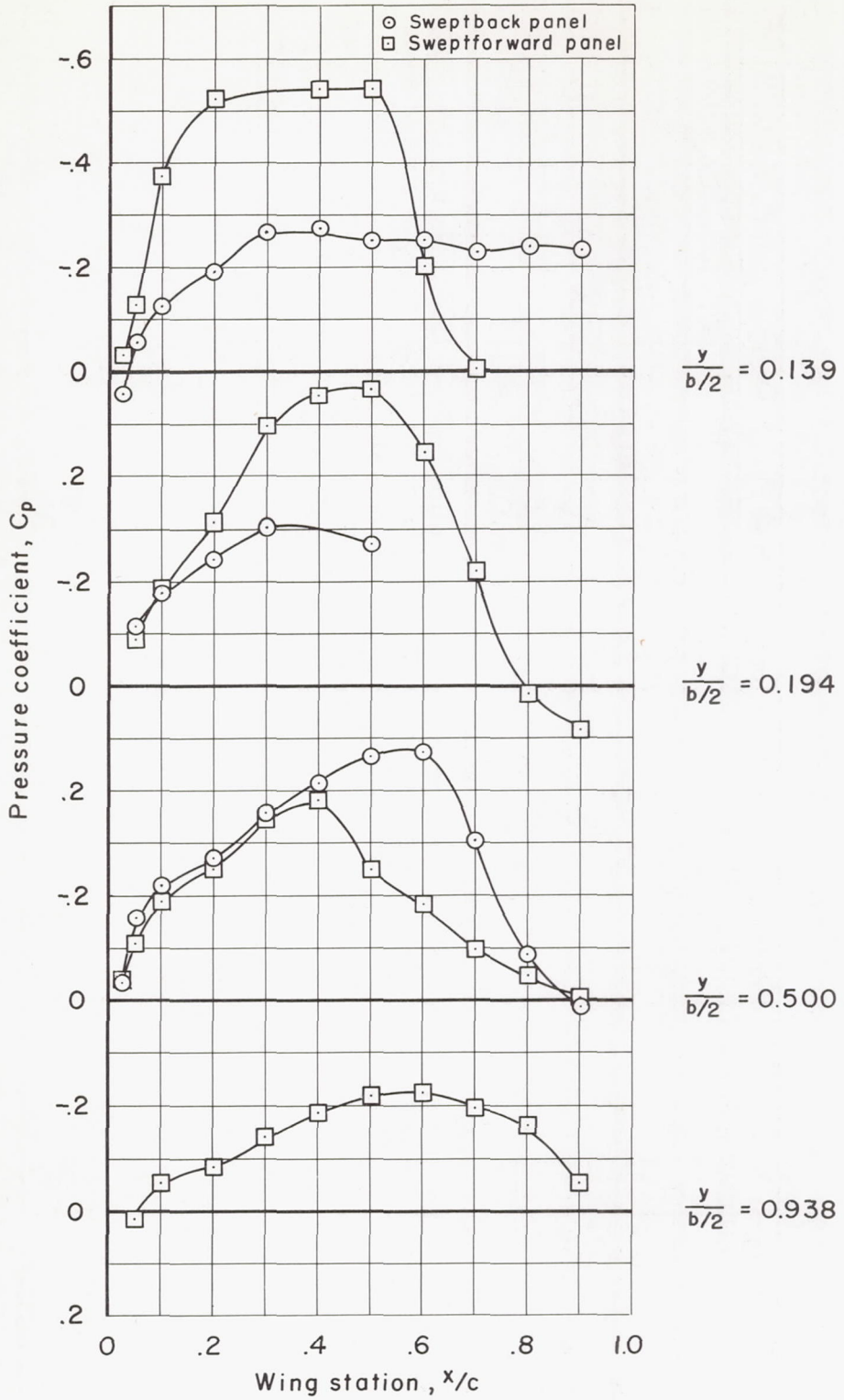

(d) M = 1.00; Sears-Haack body

Figure 30.- Continued.

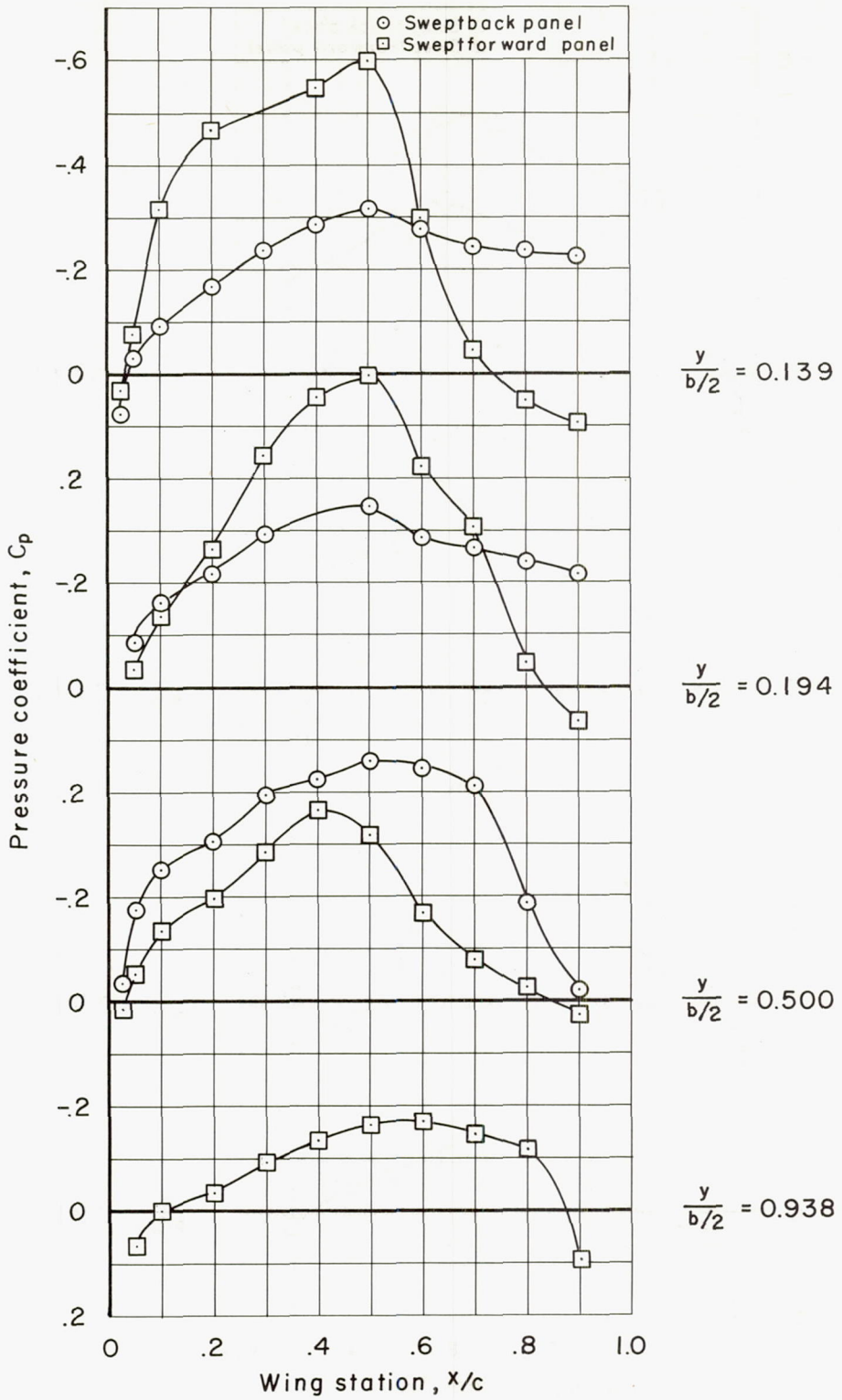

(e) M = 1.04; Sears-Haack body

Figure 30.- Continued.

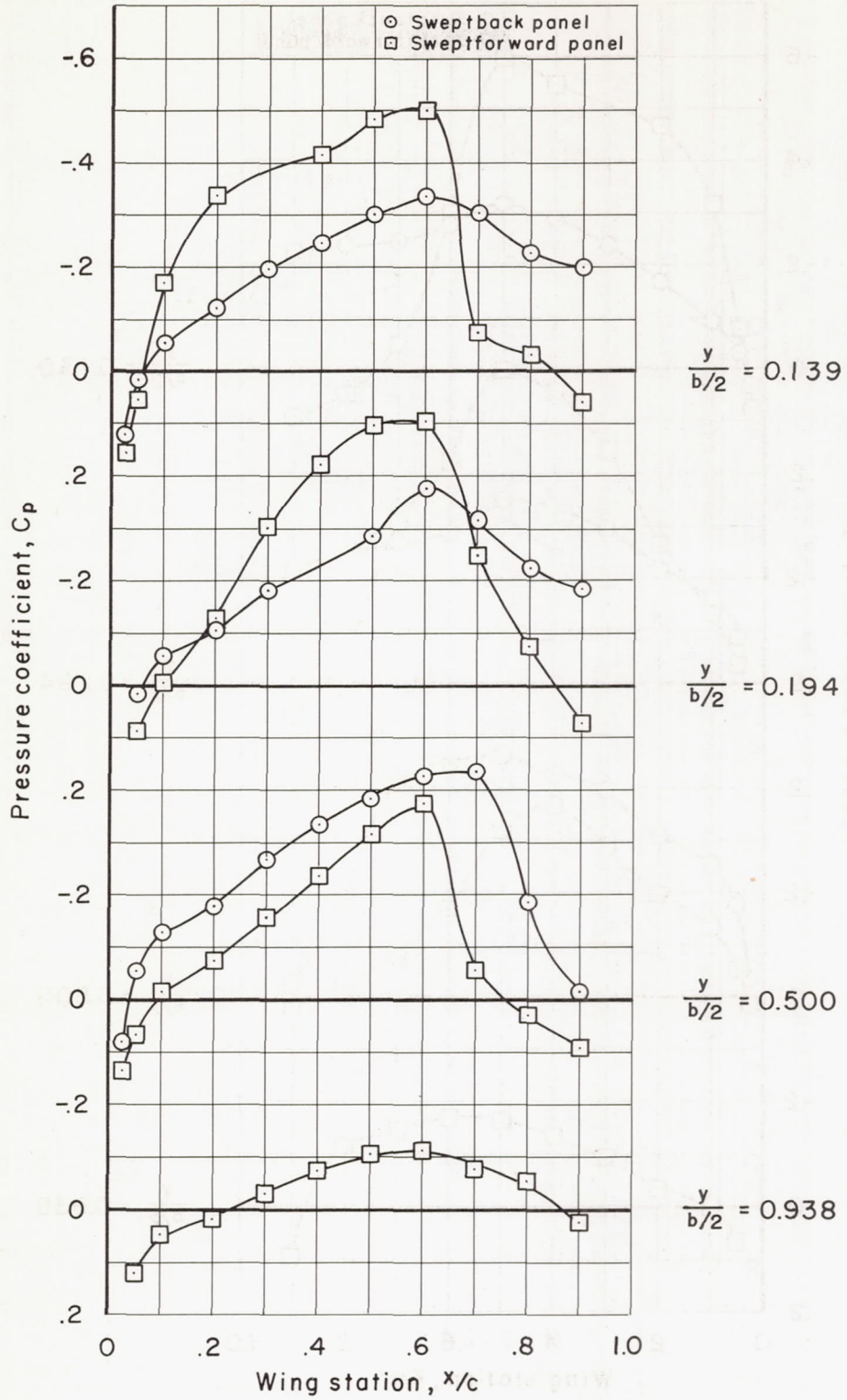

(f) M = 1.10; Sears-Haack body

Figure 30.- Continued.

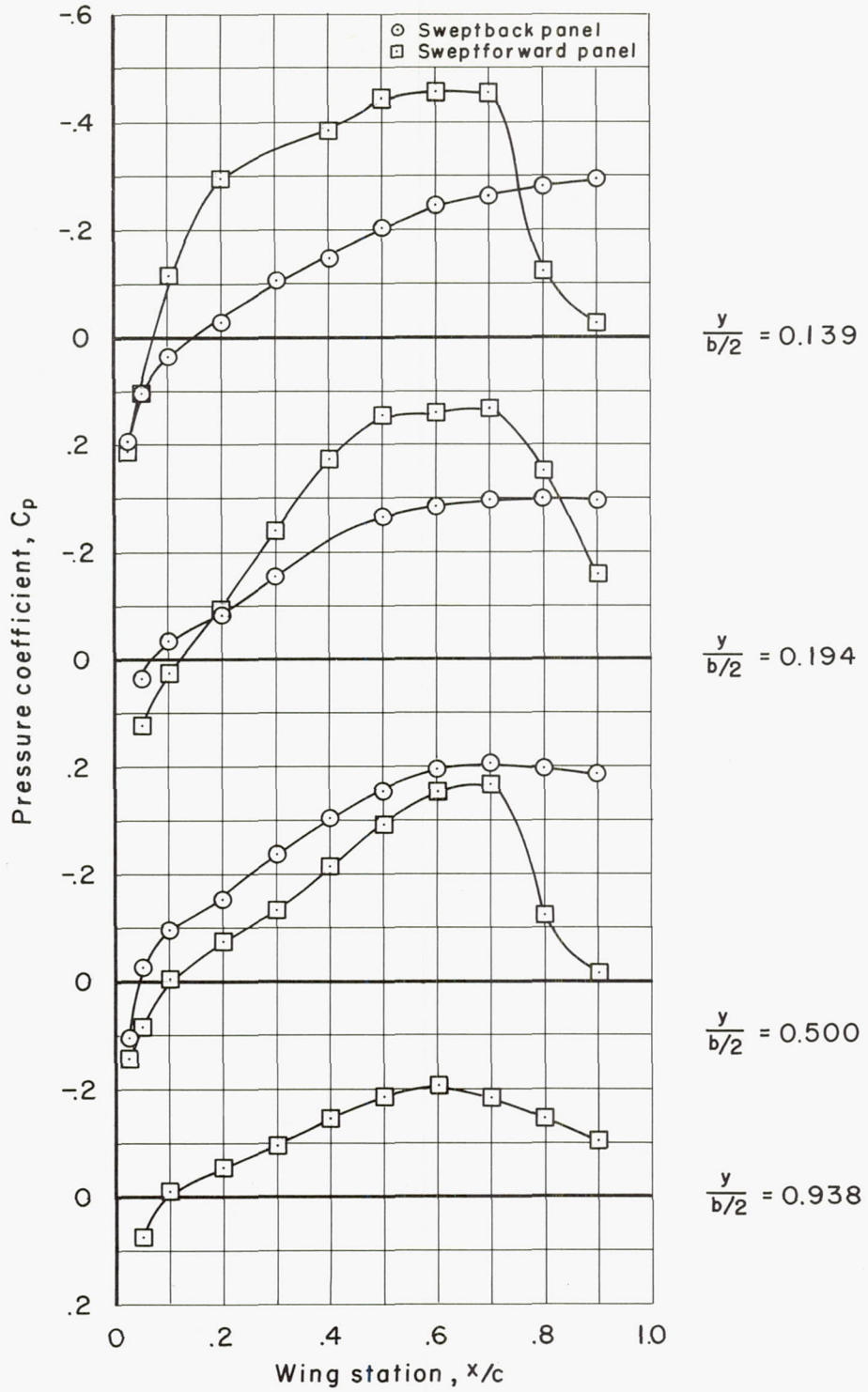

(g) M = 1.20; Sears-Haack body

Figure 30.- Concluded.

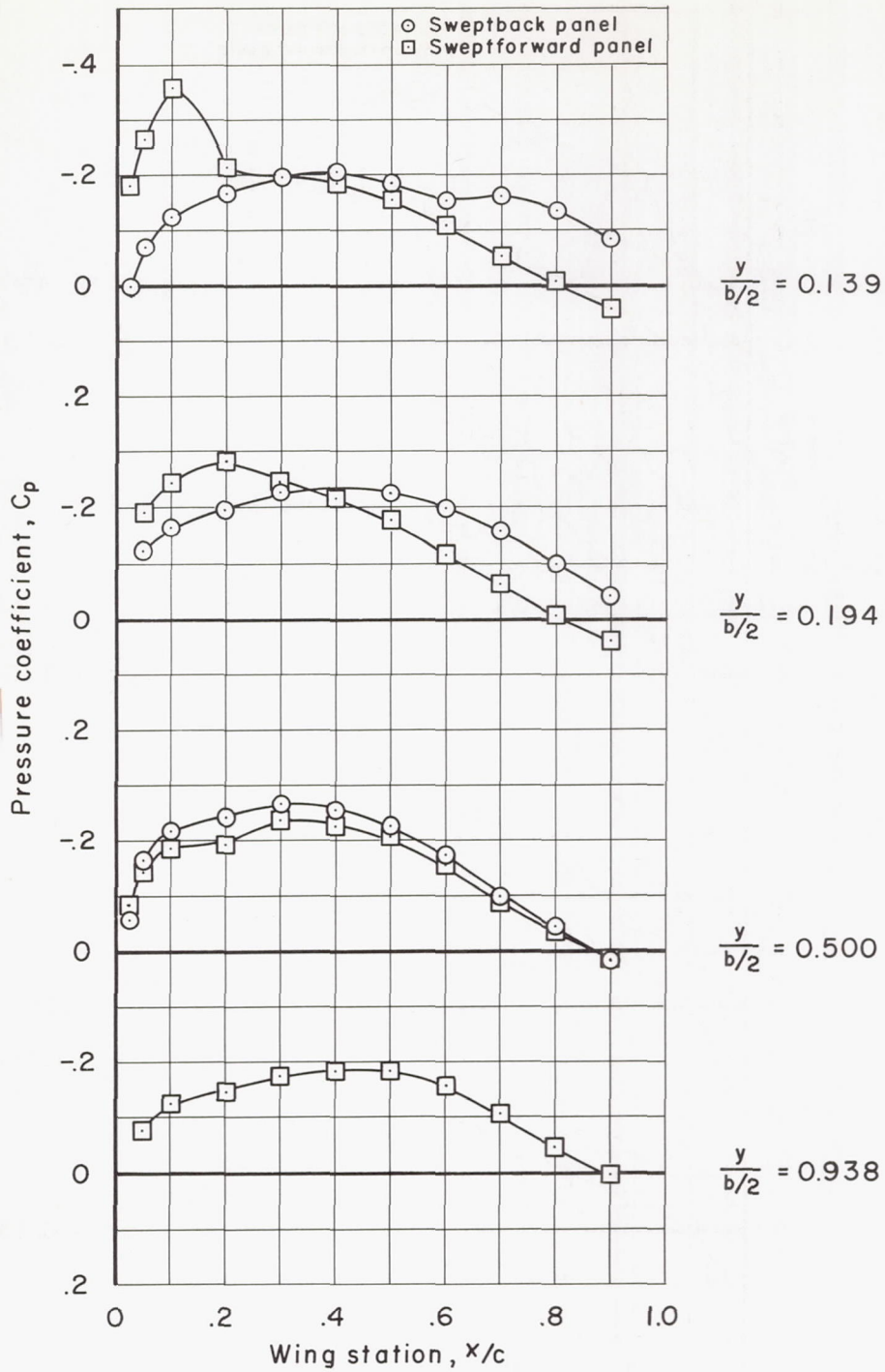

(a) M = 0.80; symmetrical M = 1.20 indented body

Figure 31.- Wing pressure coefficients at zero lift for the aspect-ratio-6 yawed wing with a symmetrical M = 1.20 indented body.

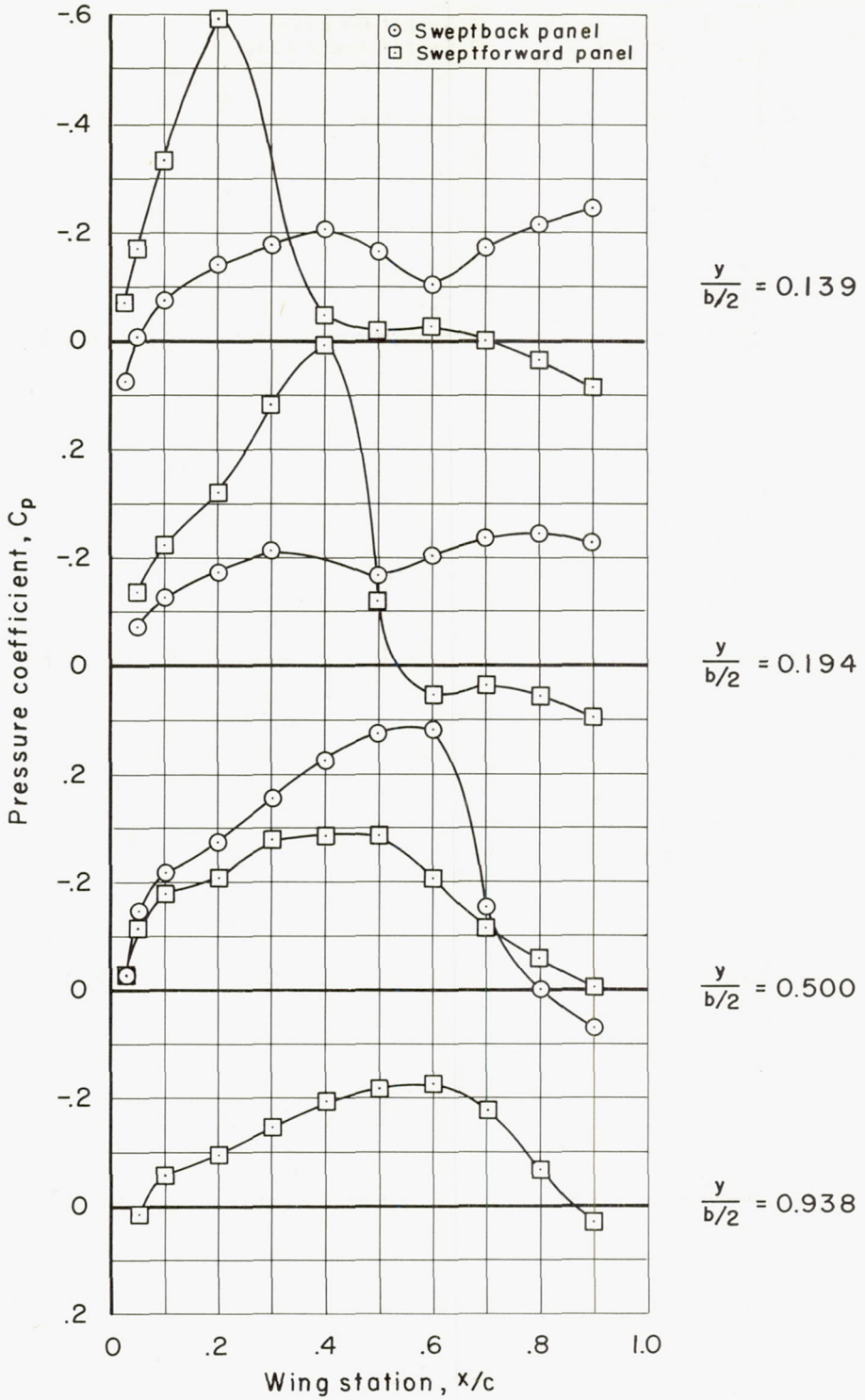

(b) M = 0.96; symmetrical M = 1.20 indented body

Figure 31.- Continued.

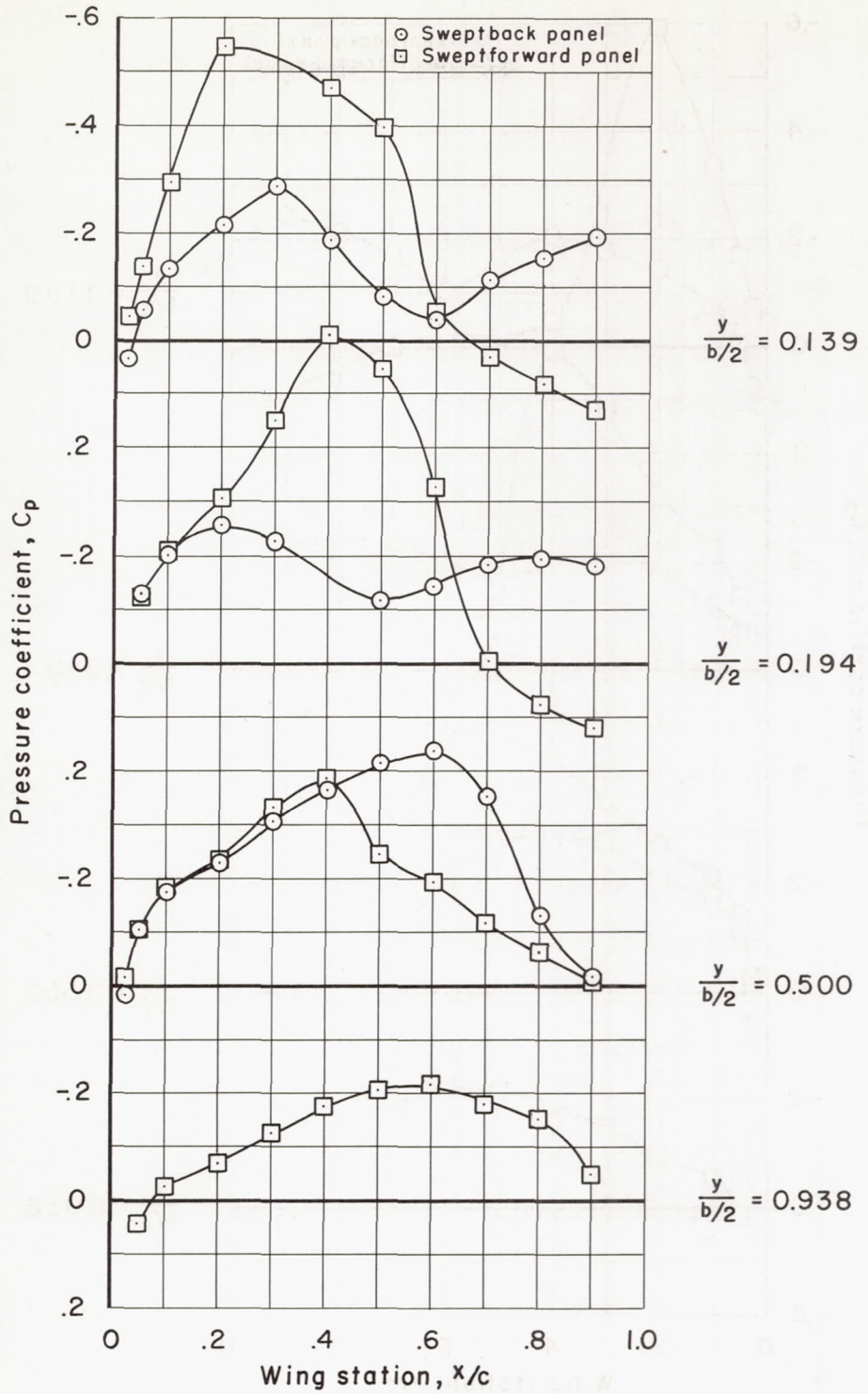

(c) M = 1.00; symmetrical M = 1.20 indented body

Figure 31.- Continued.

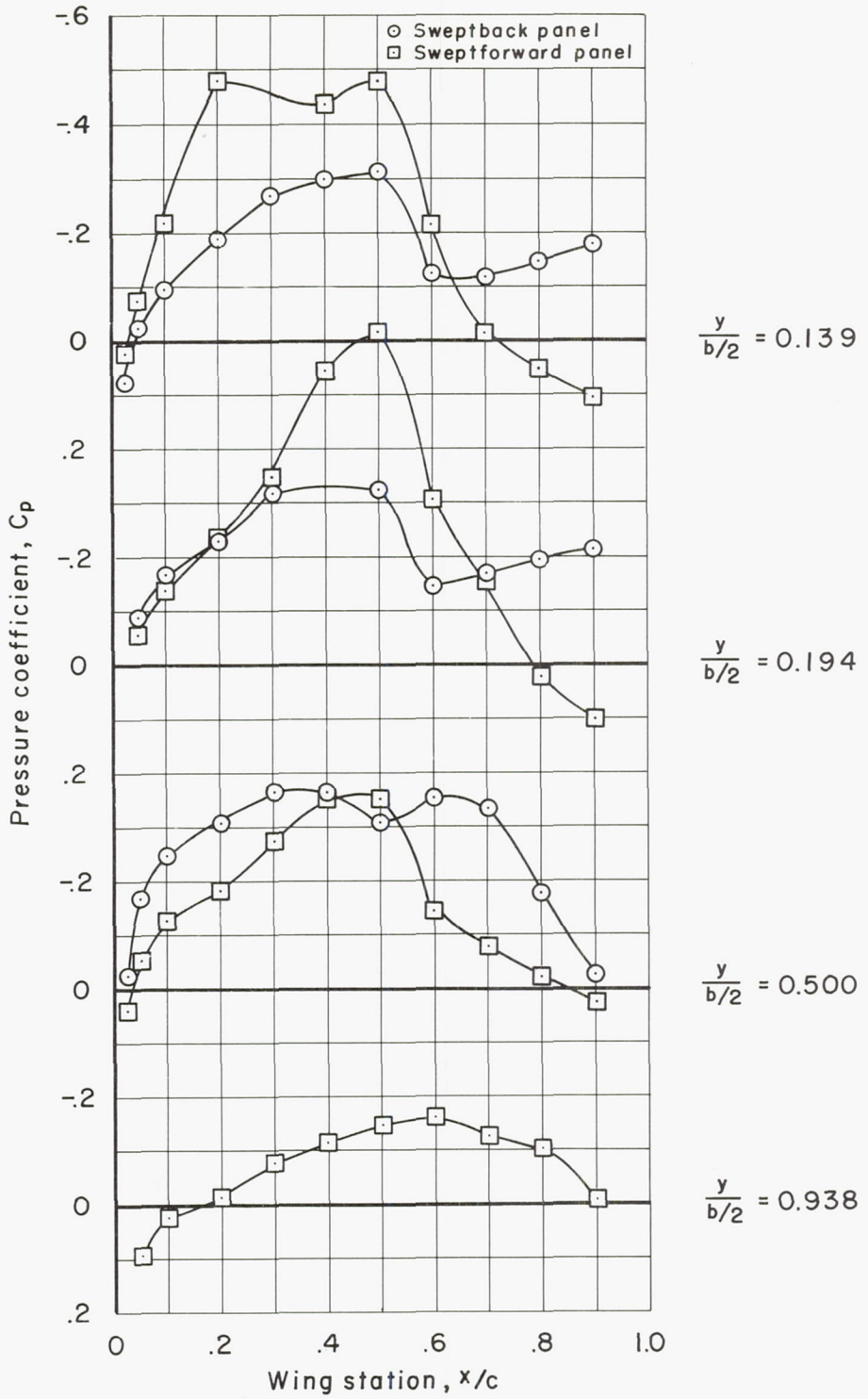

(d) M = 1.04; symmetrical M = 1.20 indented body

Figure 31.- Continued.

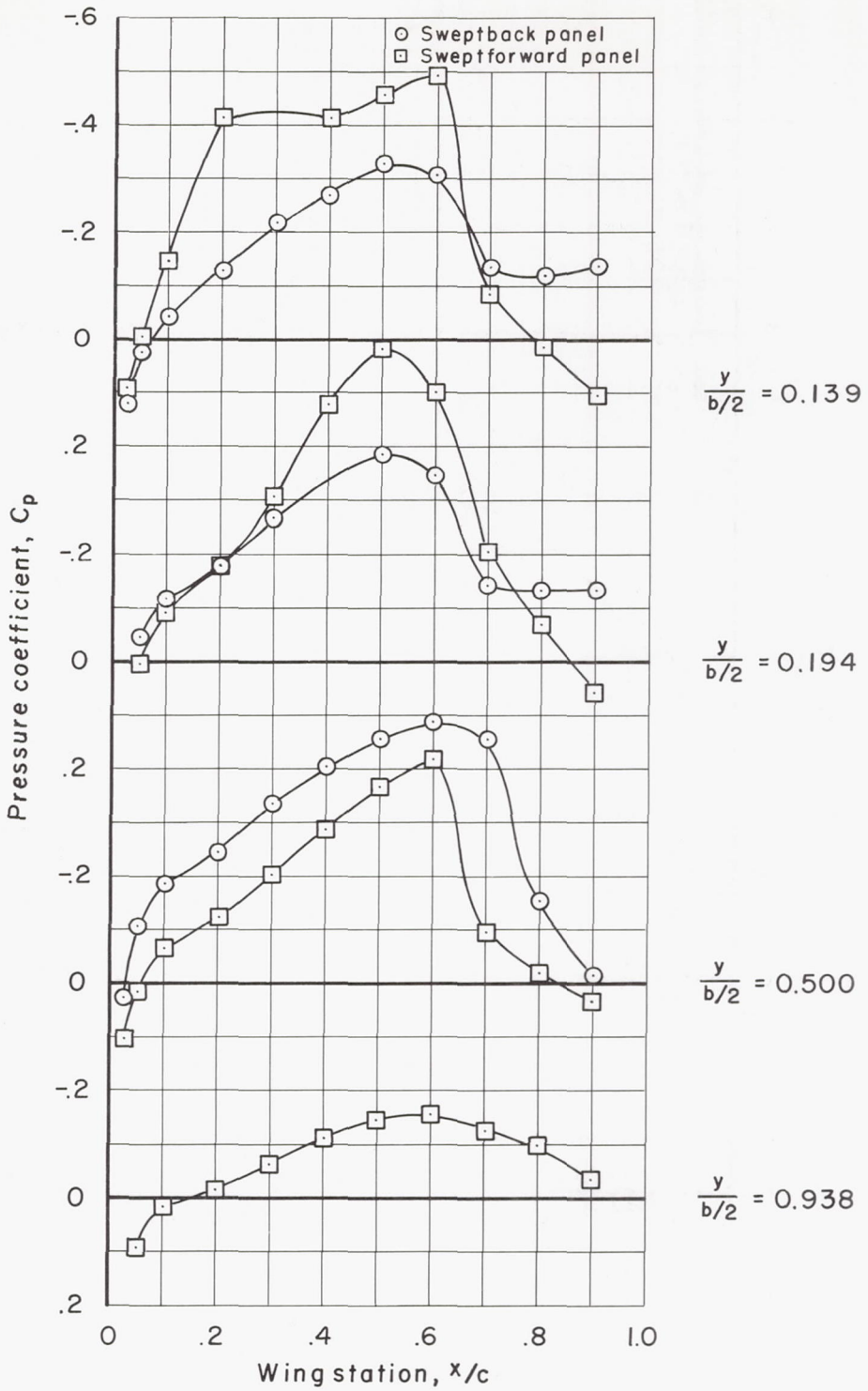

(e) M = 1.10; symmetrical M = 1.20 indented body

Figure 31.- Continued.

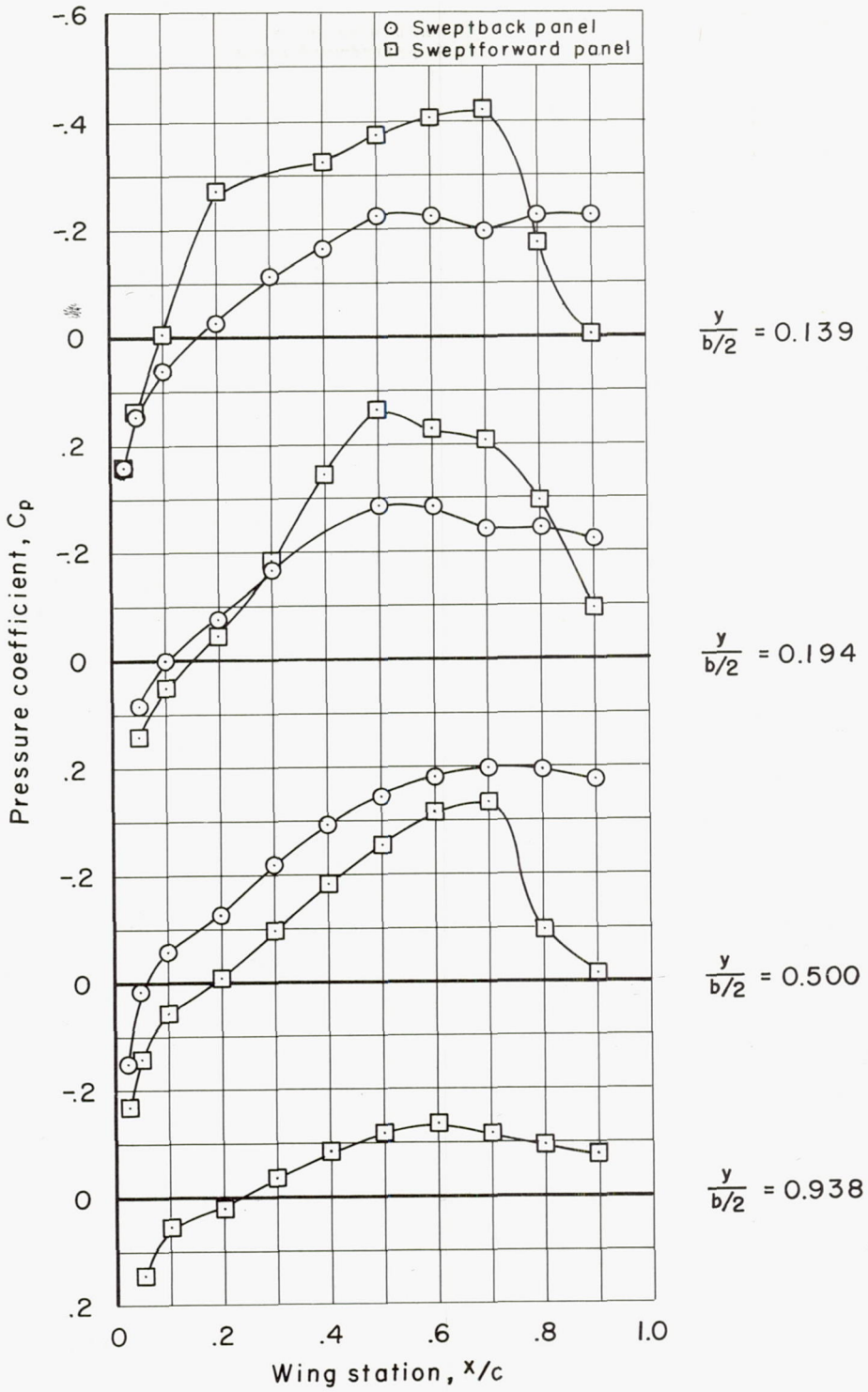

(f) M = 1.20; symmetrical M = 1.20 indented body

Figure 31.- Concluded.

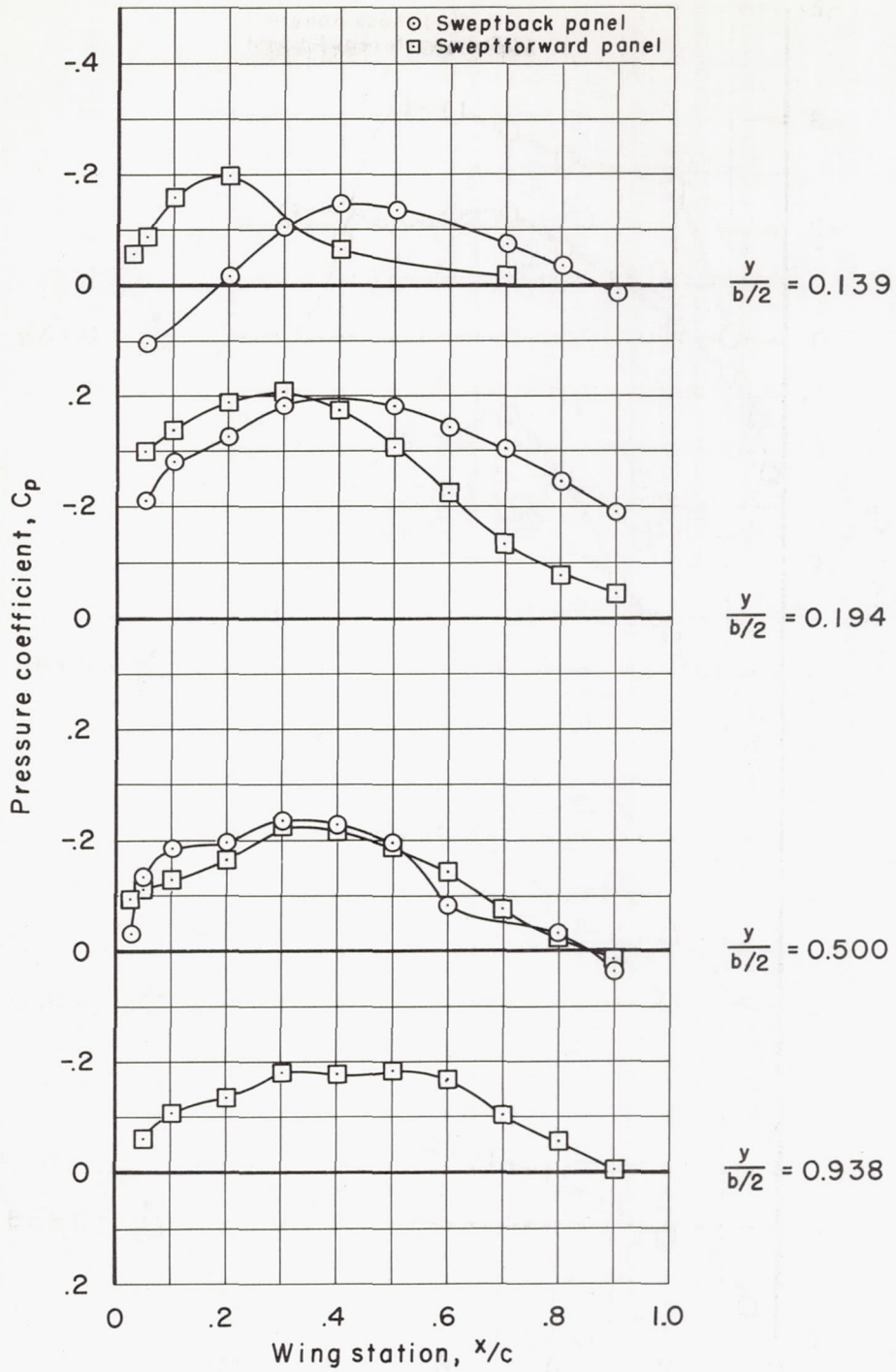

(a) M = 0.80; asymmetrical M = 1.20 indented body

Figure 32.- Wing pressure coefficients at zero lift for the aspect-ratio-6 yawed wing with an asymmetrical M = 1.20 indented body.

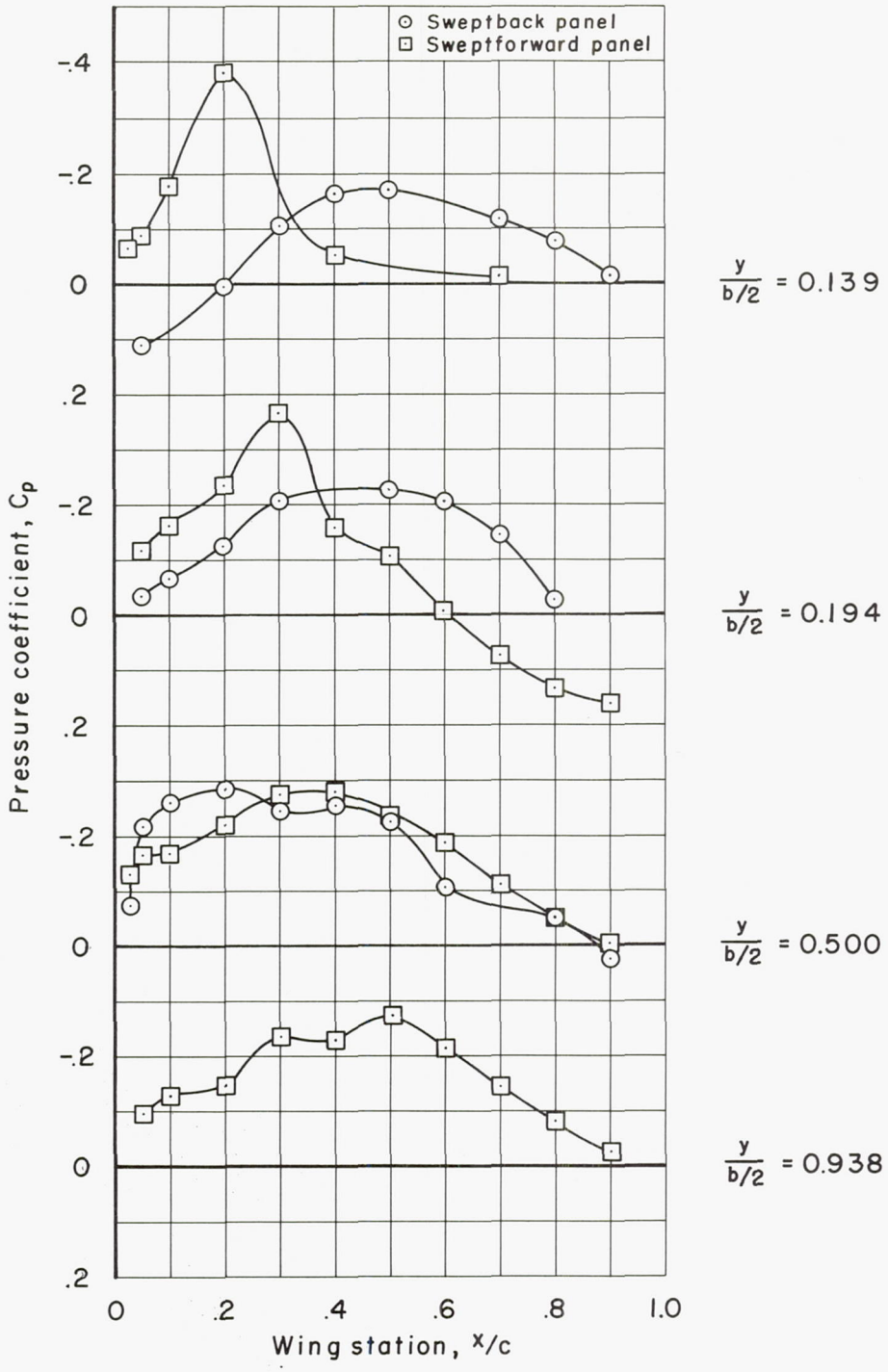

(b) M = 0.90; asymmetrical M = 1.20 indented body

Figure 32.- Continued.

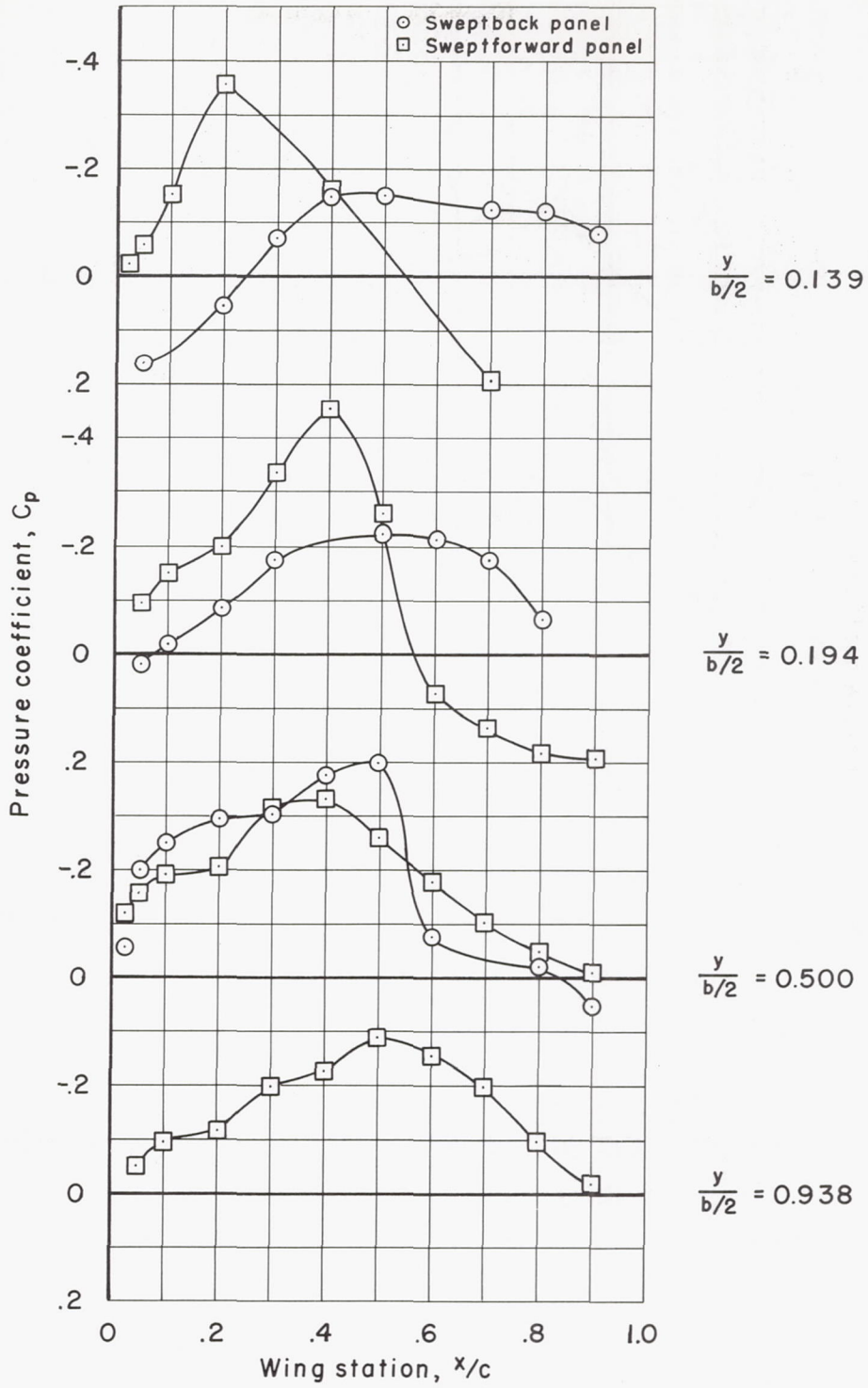

(c) M = 0.96; asymmetrical M = 1.20 indented body

Figure 32.- Continued.

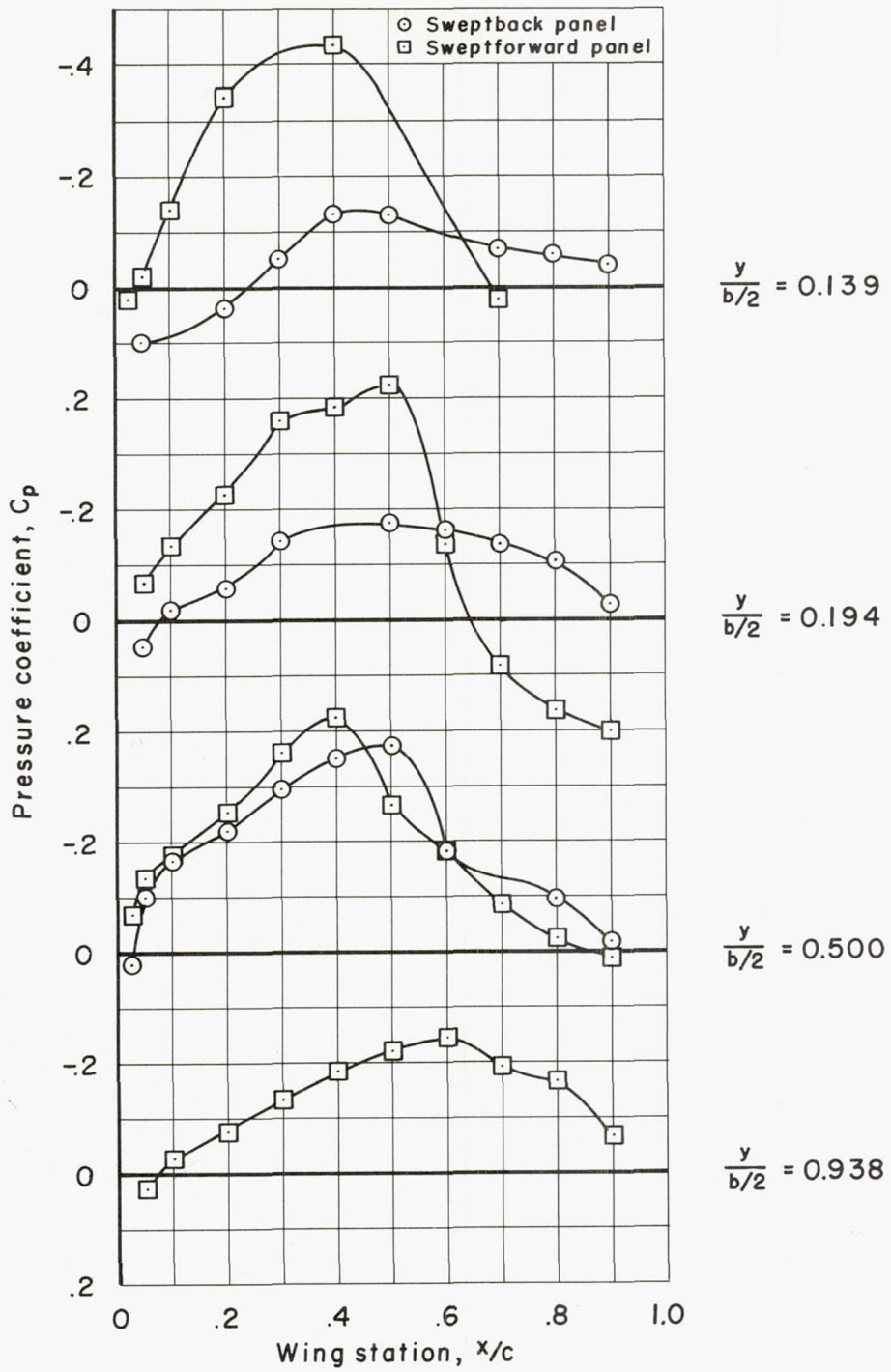

(d) M = 1.00; asymmetrical M = 1.20 indented body

Figure 32.- Continued.

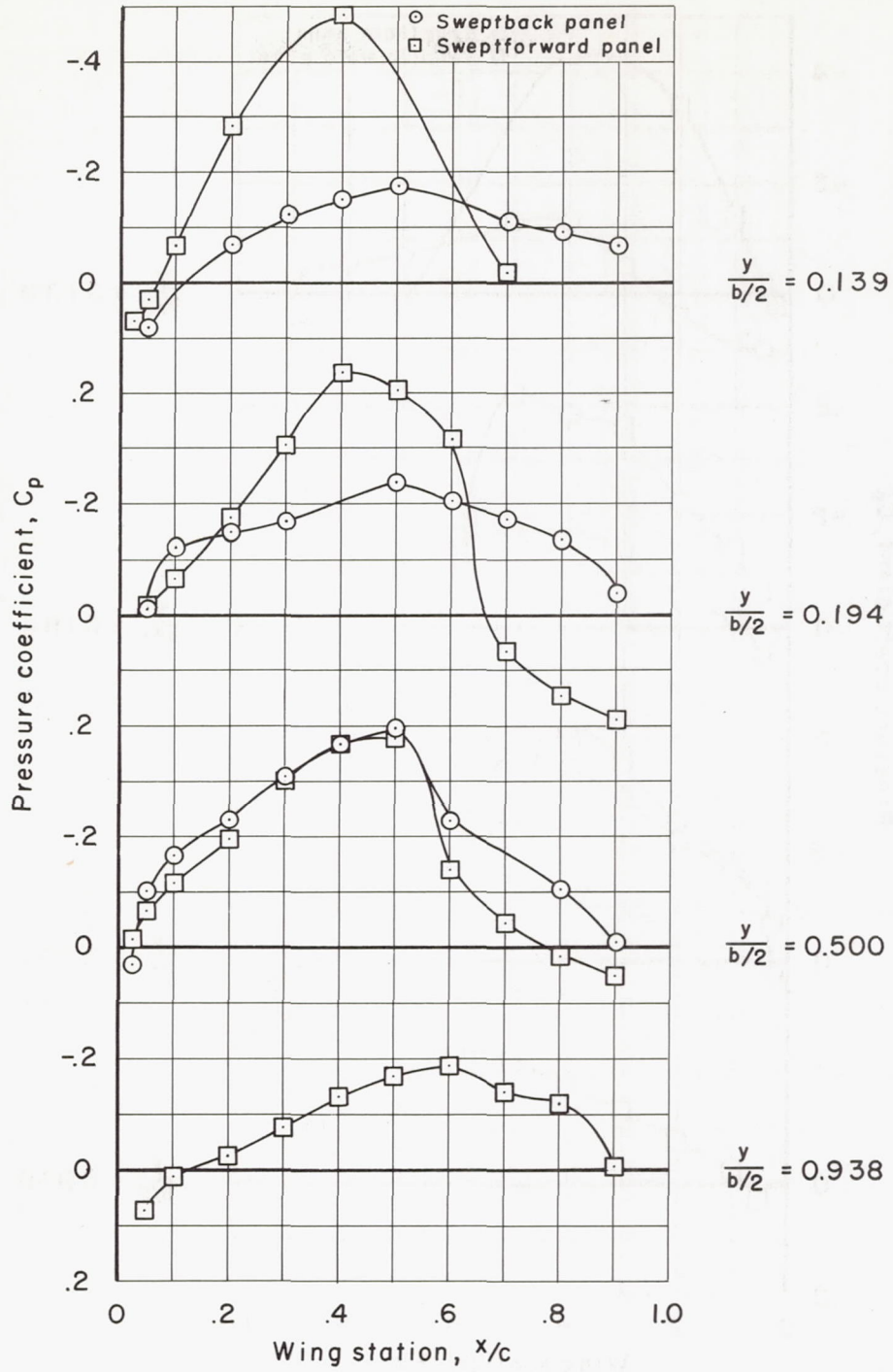

(e) M = 1.04; asymmetrical M = 1.20 indented body

Figure 32.- Continued.

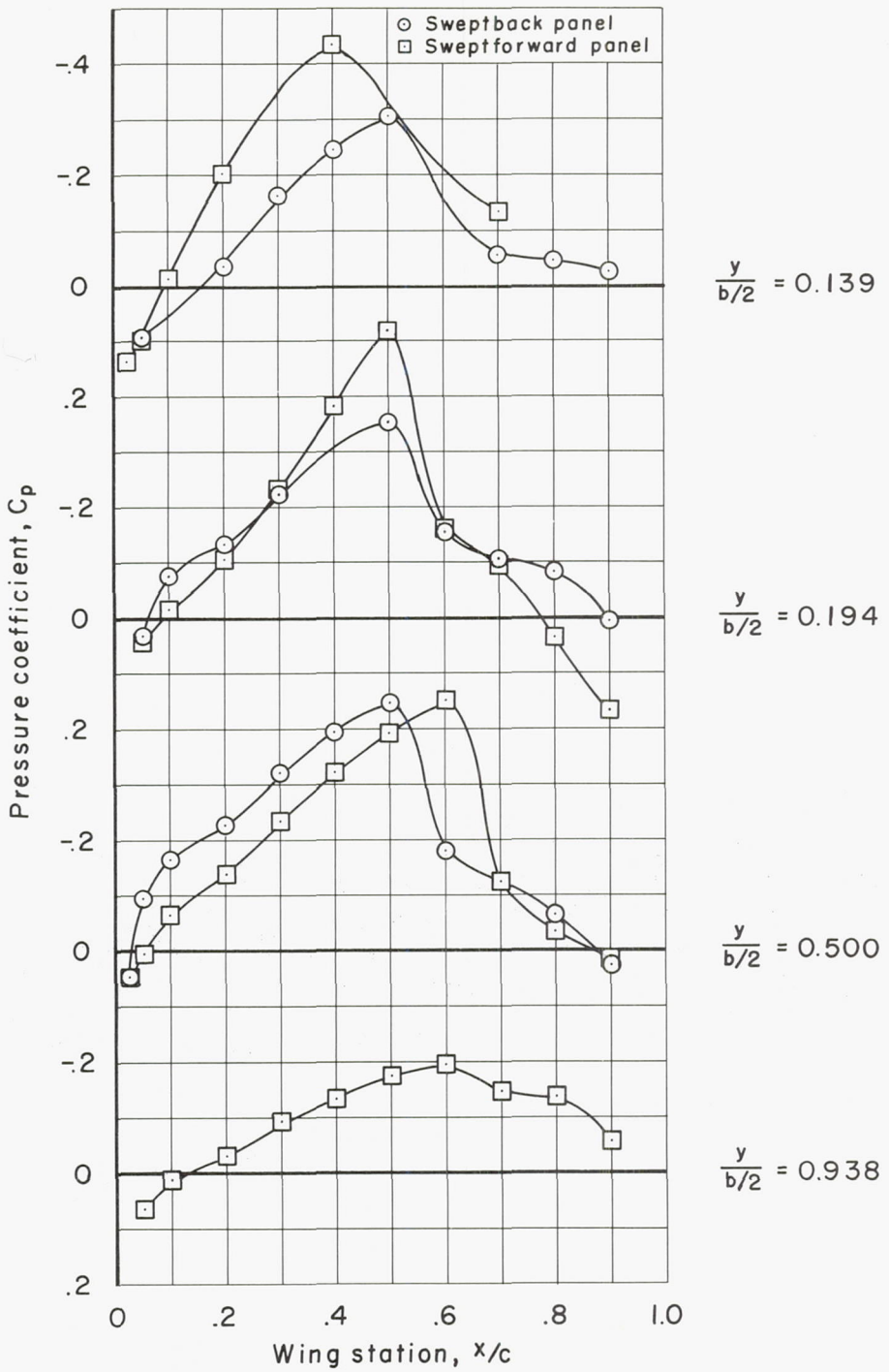

(f) M = 1.10; asymmetrical M = 1.20 indented body

Figure 32.- Continued.

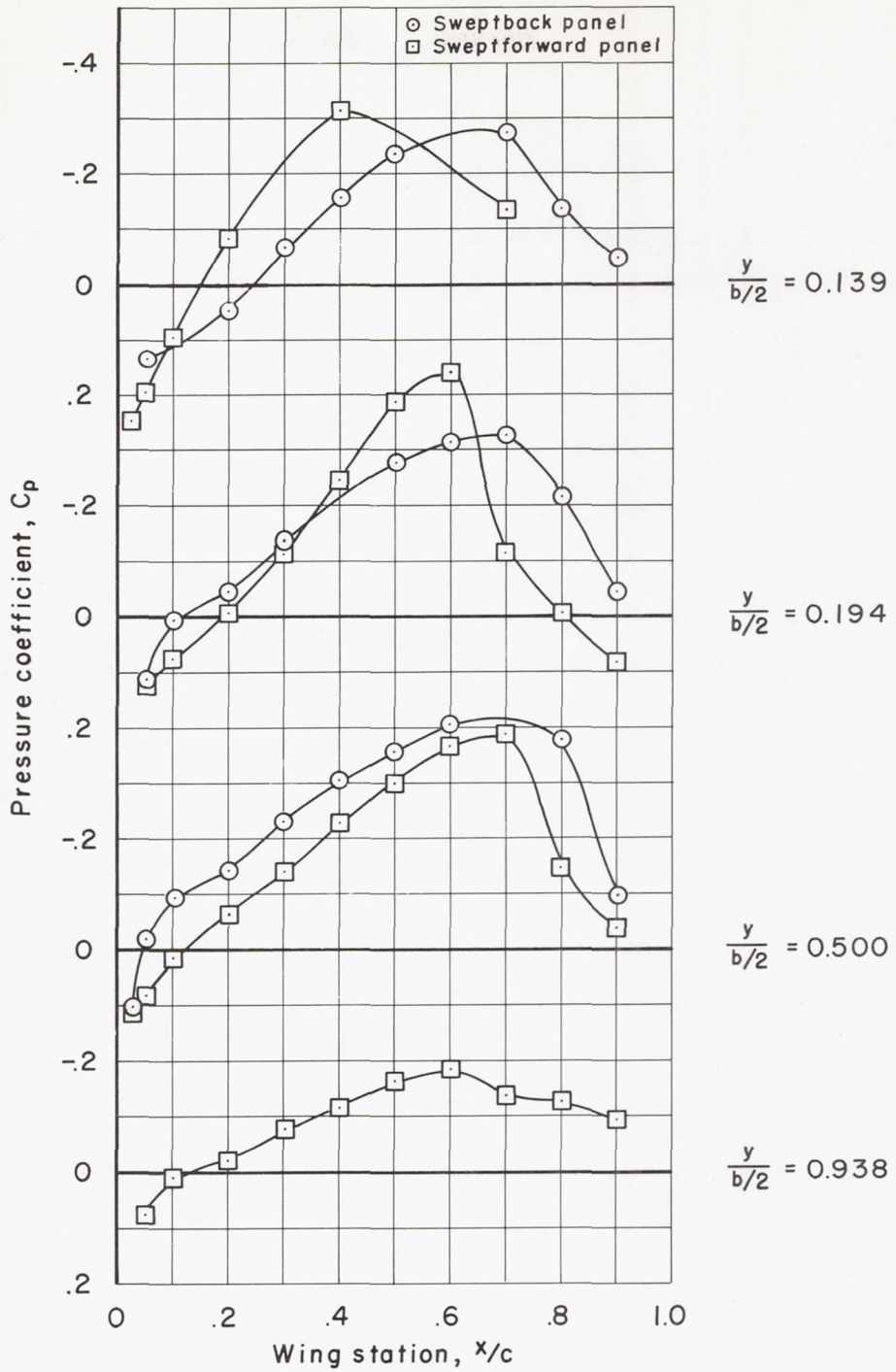

(g) M = 1.20; asymmetrical M = 1.20 indented body

Figure 32.- Concluded.

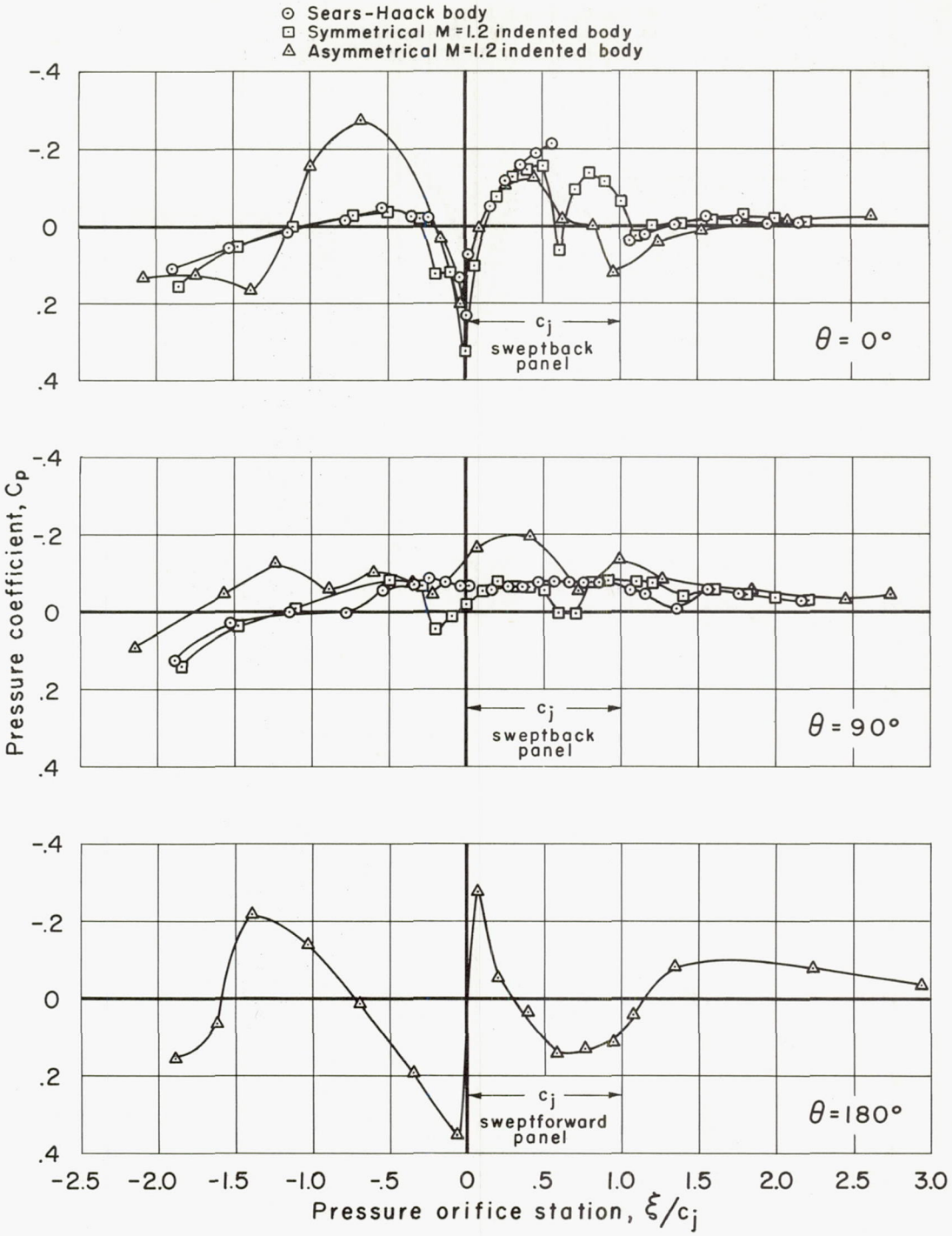

(a) M = 0.80

Figure 33.- Body pressure coefficients at zero lift for the aspect-ratio-6 yawed wing with various bodies.

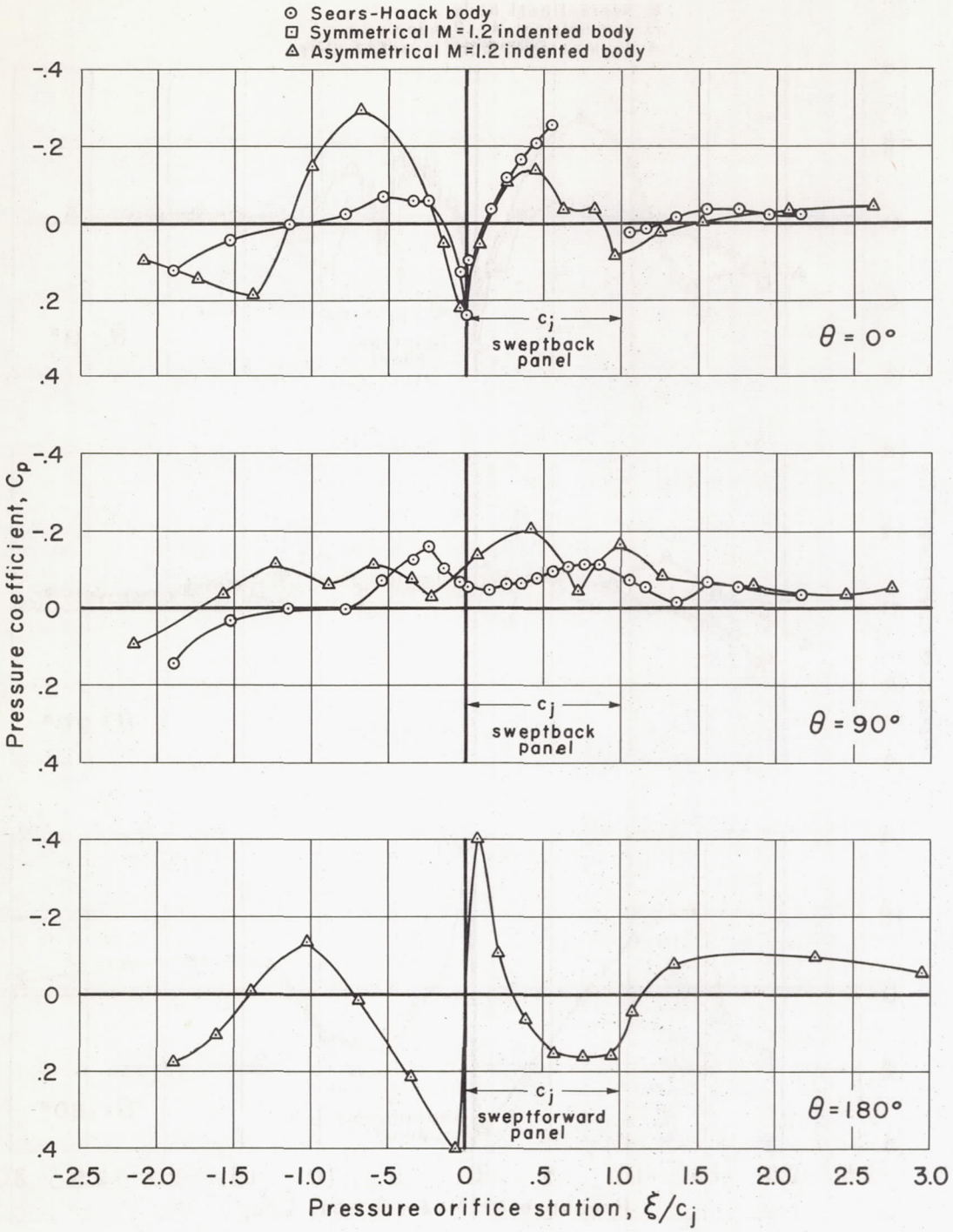

(b) M = 0.90

Figure 33.- Continued.

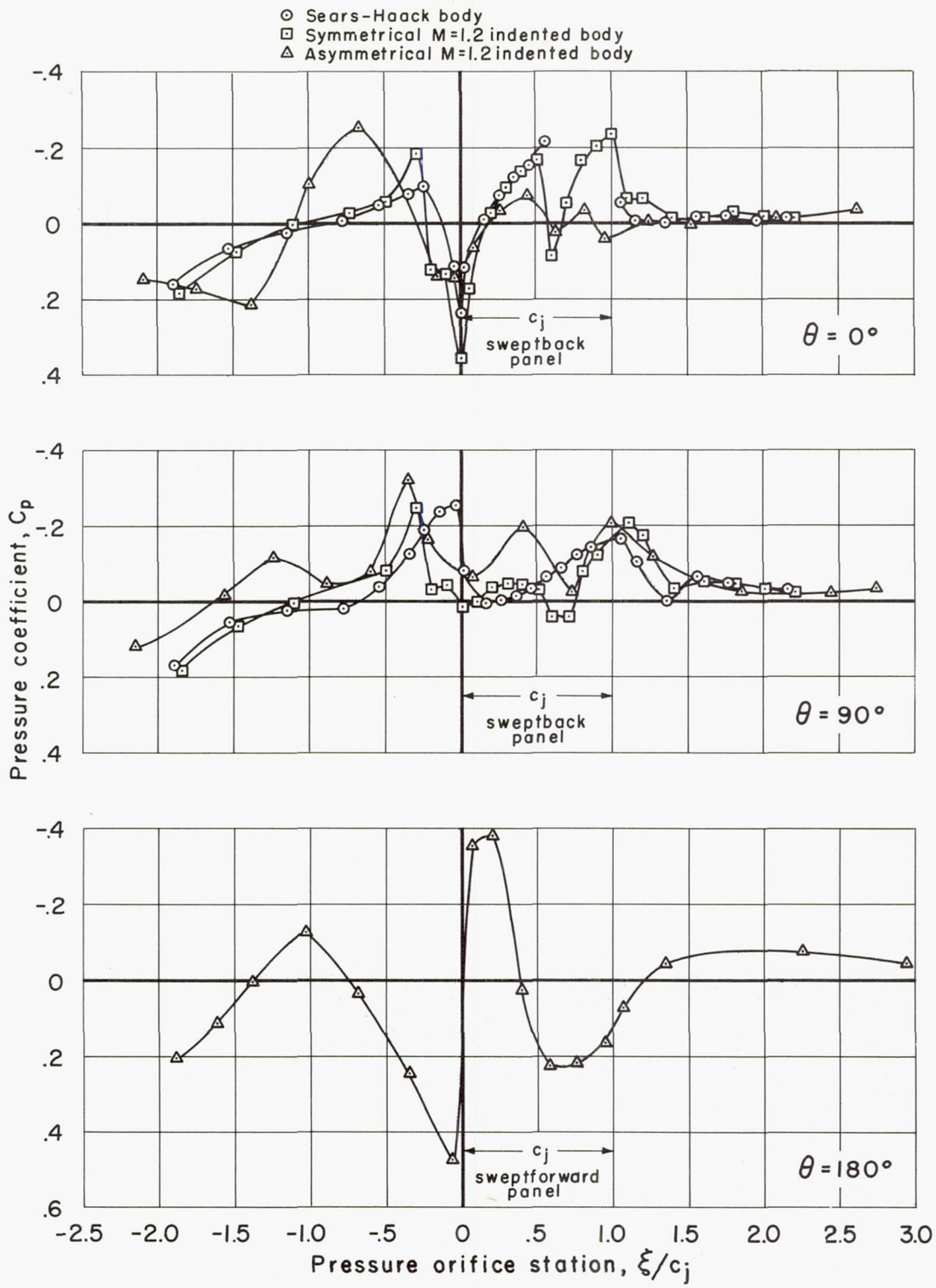

(c) M = 0.96

Figure 33.- Continued.

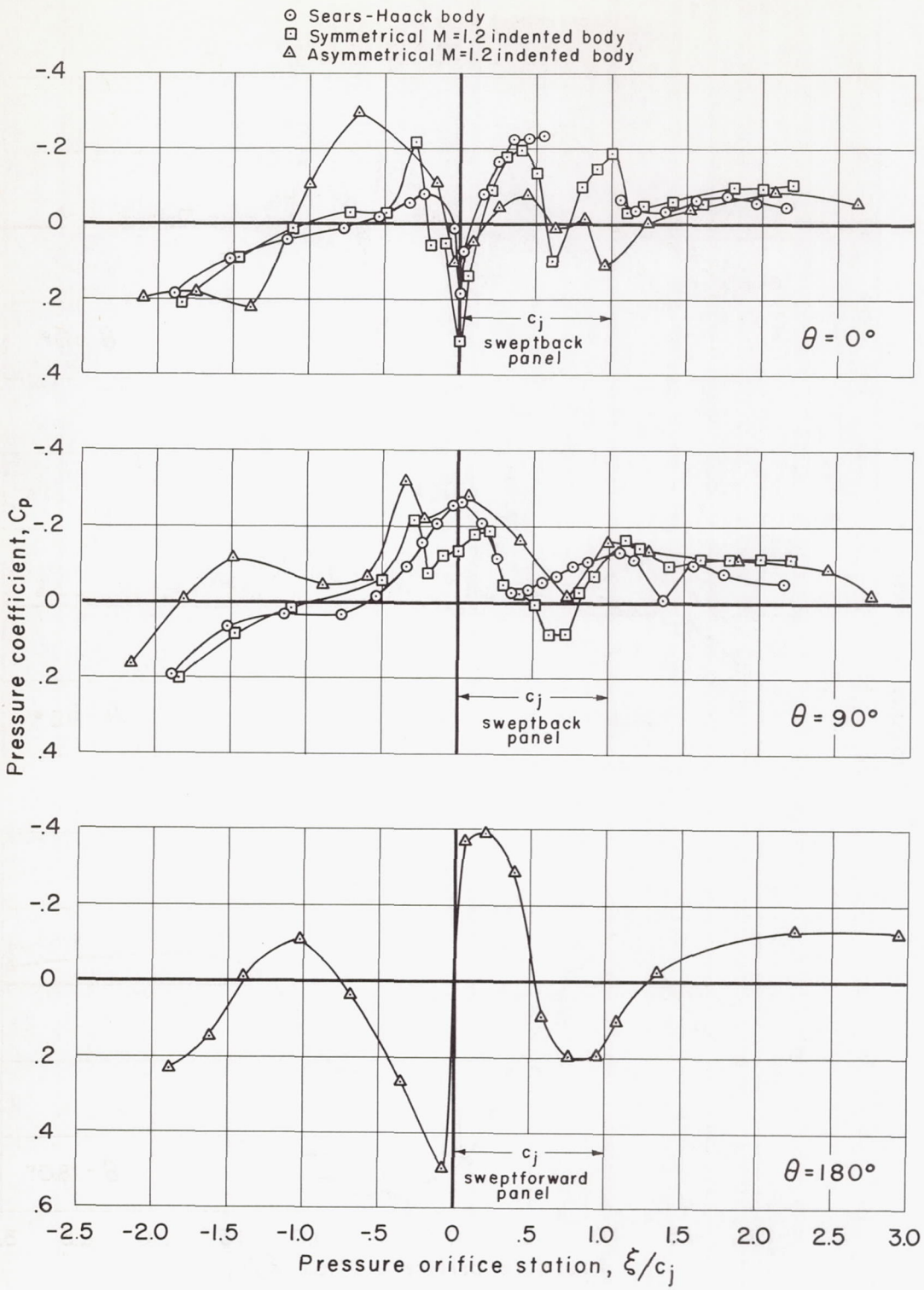

(d) M = 1.00

Figure 33.- Continued.

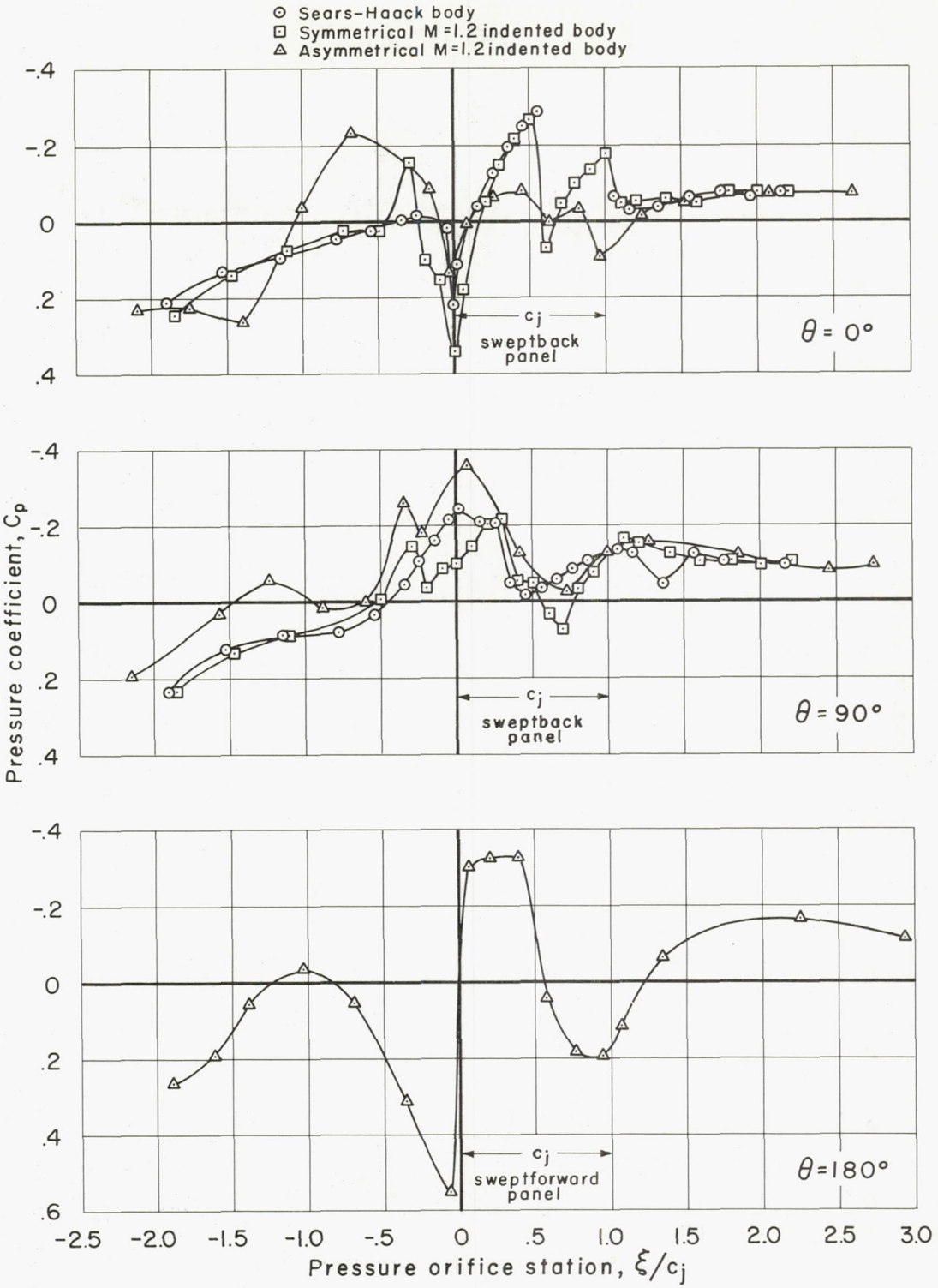

(e) M = 1.04

Figure 33.- Continued.

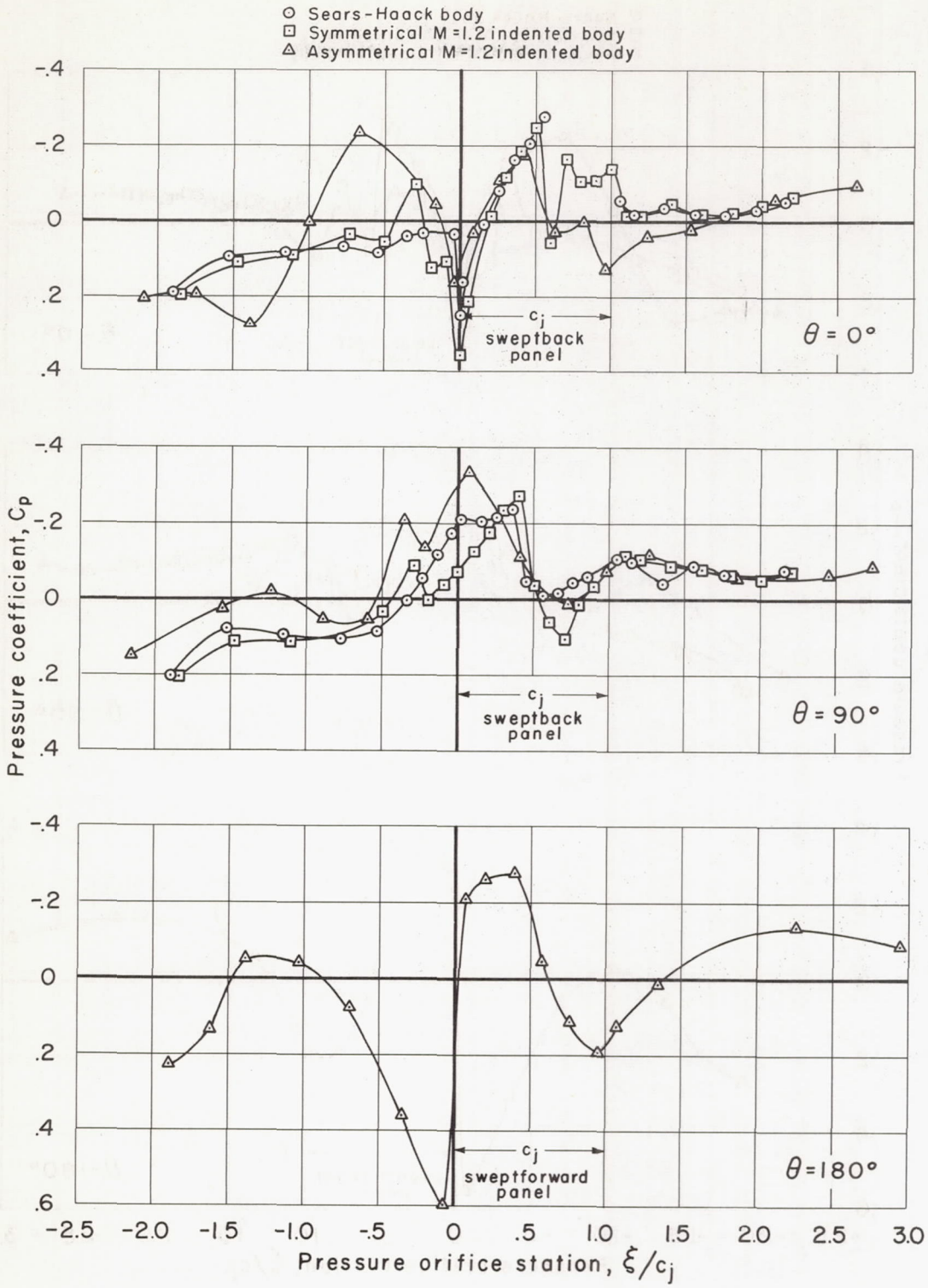

(f) M = 1.10

Figure 33.- Continued.

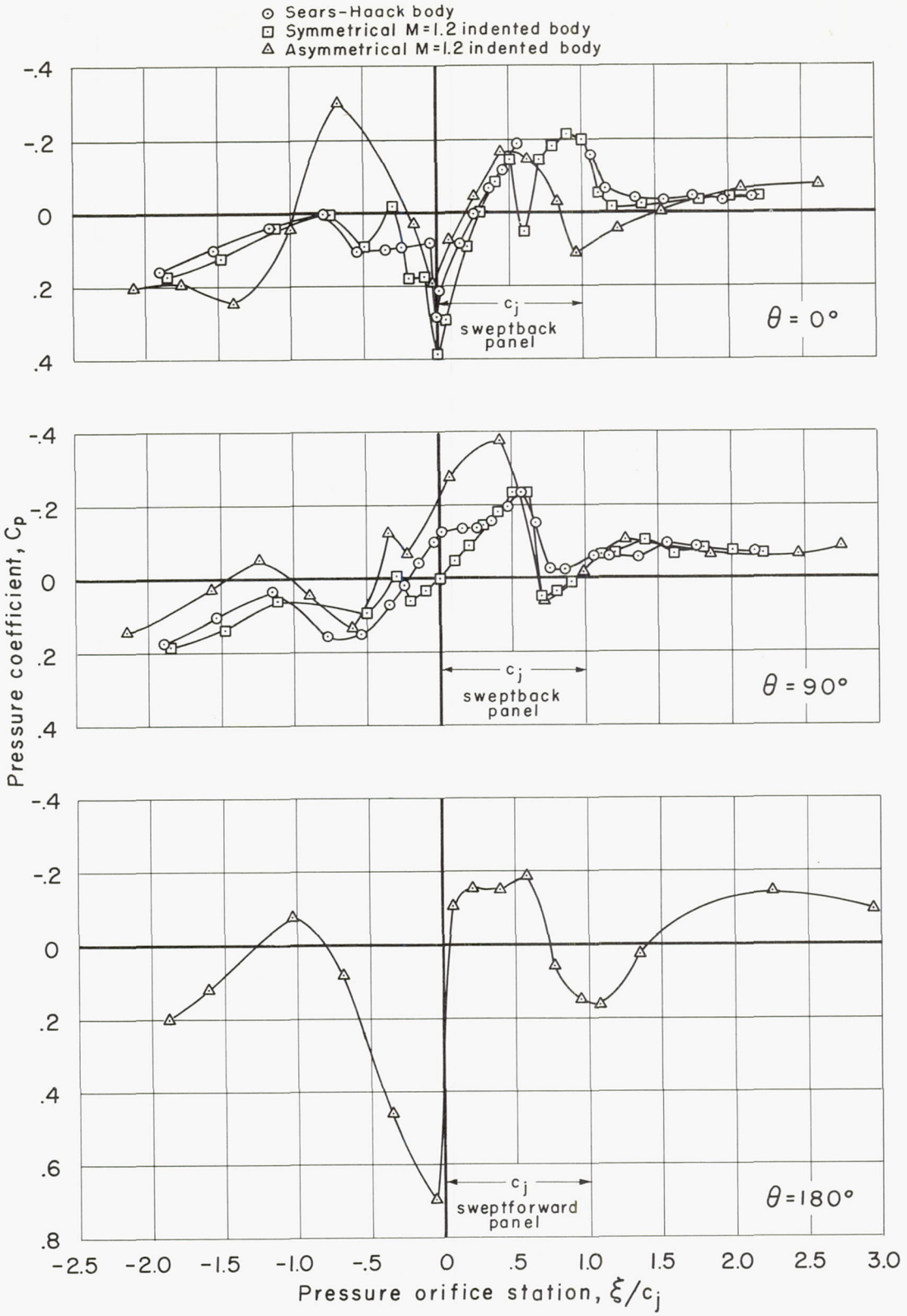

(g) M = 1.20

Figure 33.- Concluded.

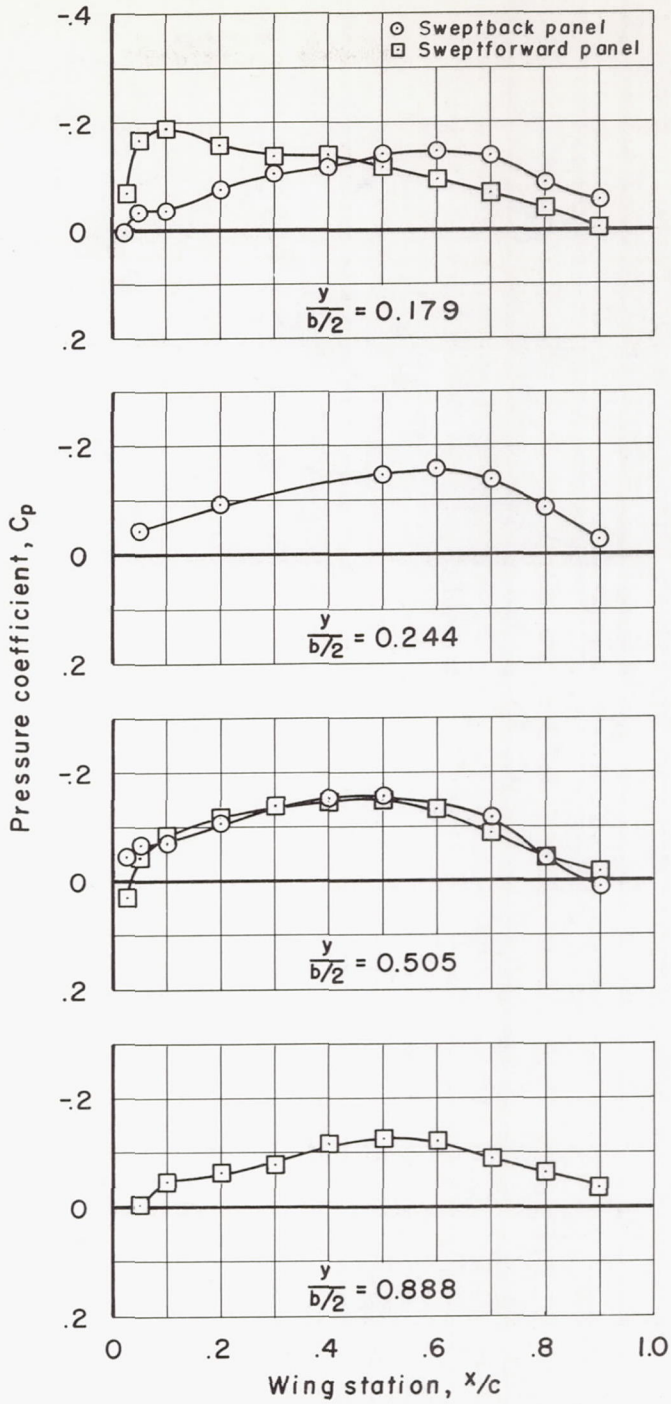

(a) M = 0.80; Sears-Haack body

Figure 34.- Wing pressure coefficients at zero lift for the aspect-ratio-3 yawed wing with a Sears-Haack body.

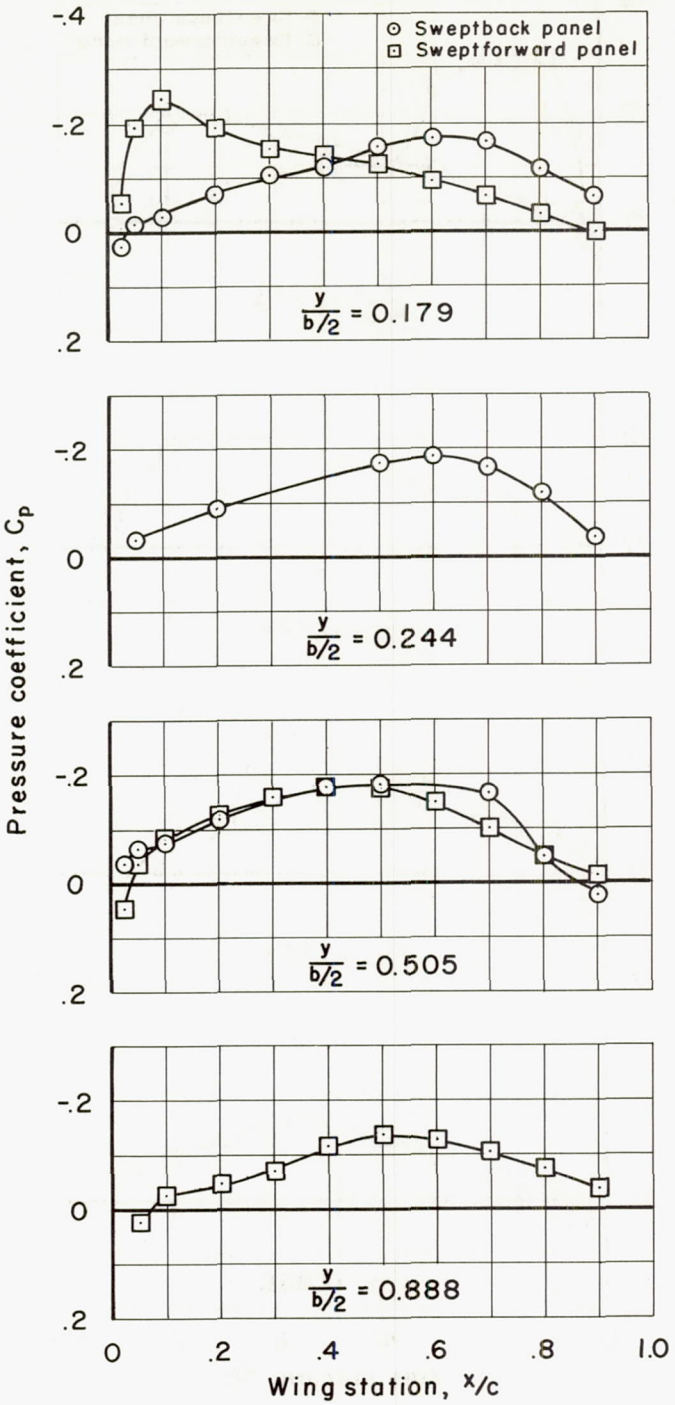

(b) M = 0.90; Sears-Haack body

Figure 34.- Continued.

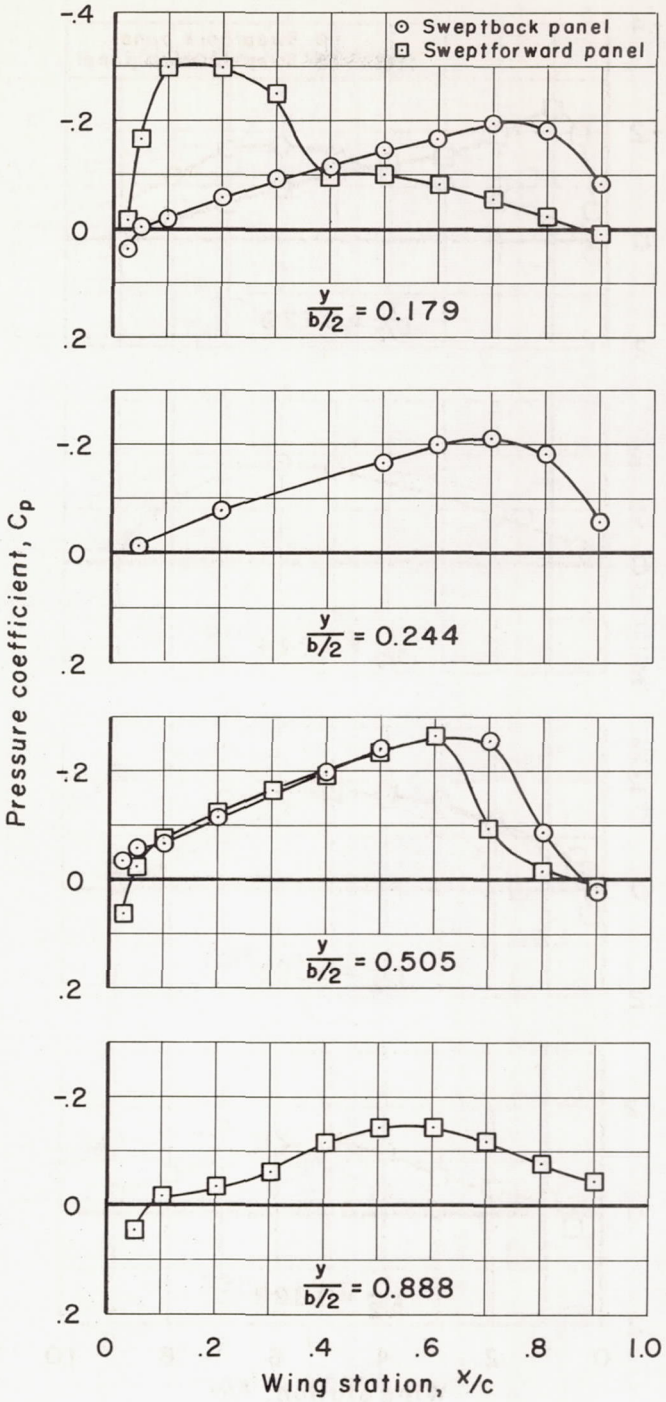

(c) M = 0.95; Sears-Haack body

Figure 34.- Continued.

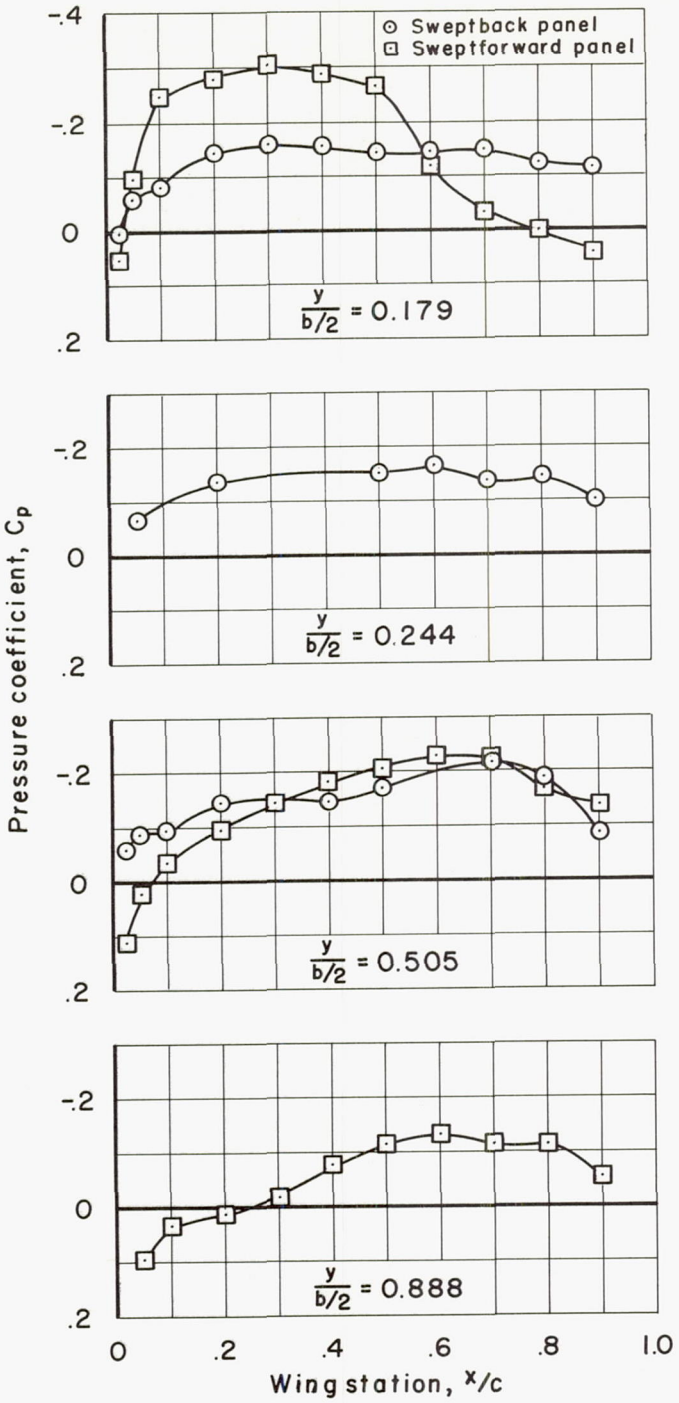

(d) M = 1.00; Sears-Haack body

Figure 34.- Continued.

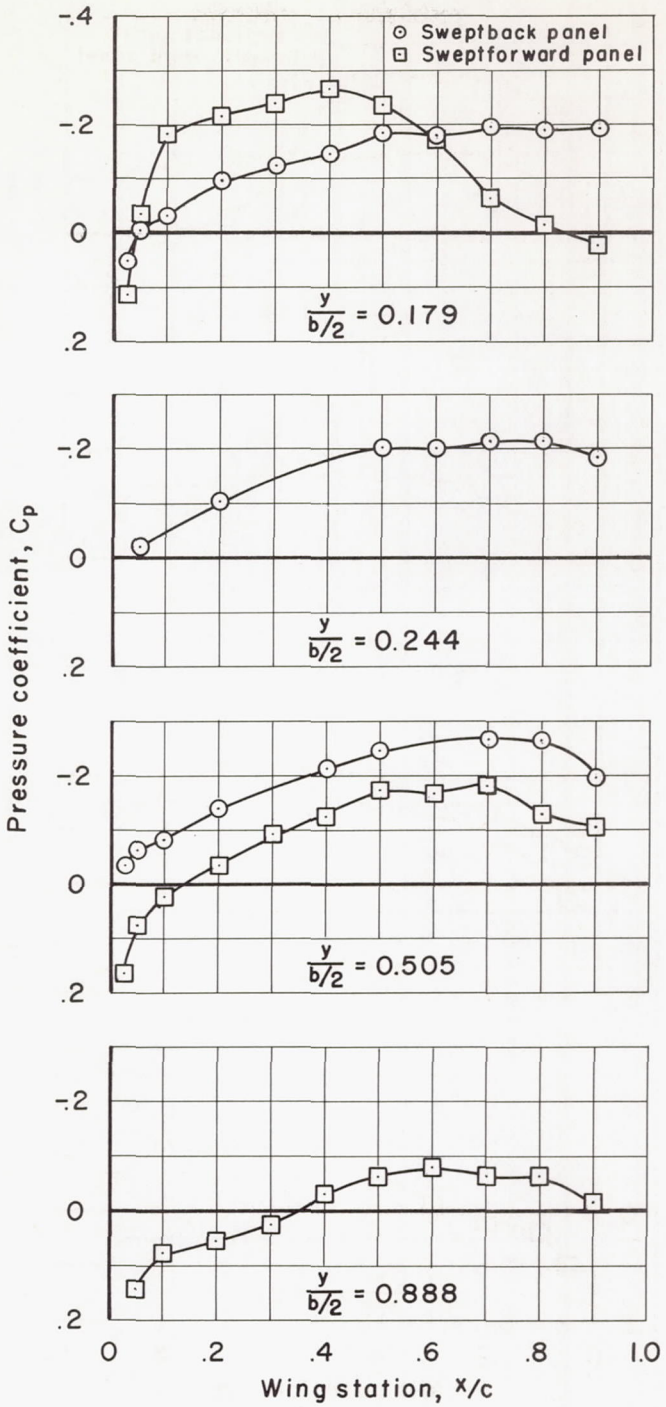

(e) M = 1.05; Sears-Haack body

Figure 34.- Continued.

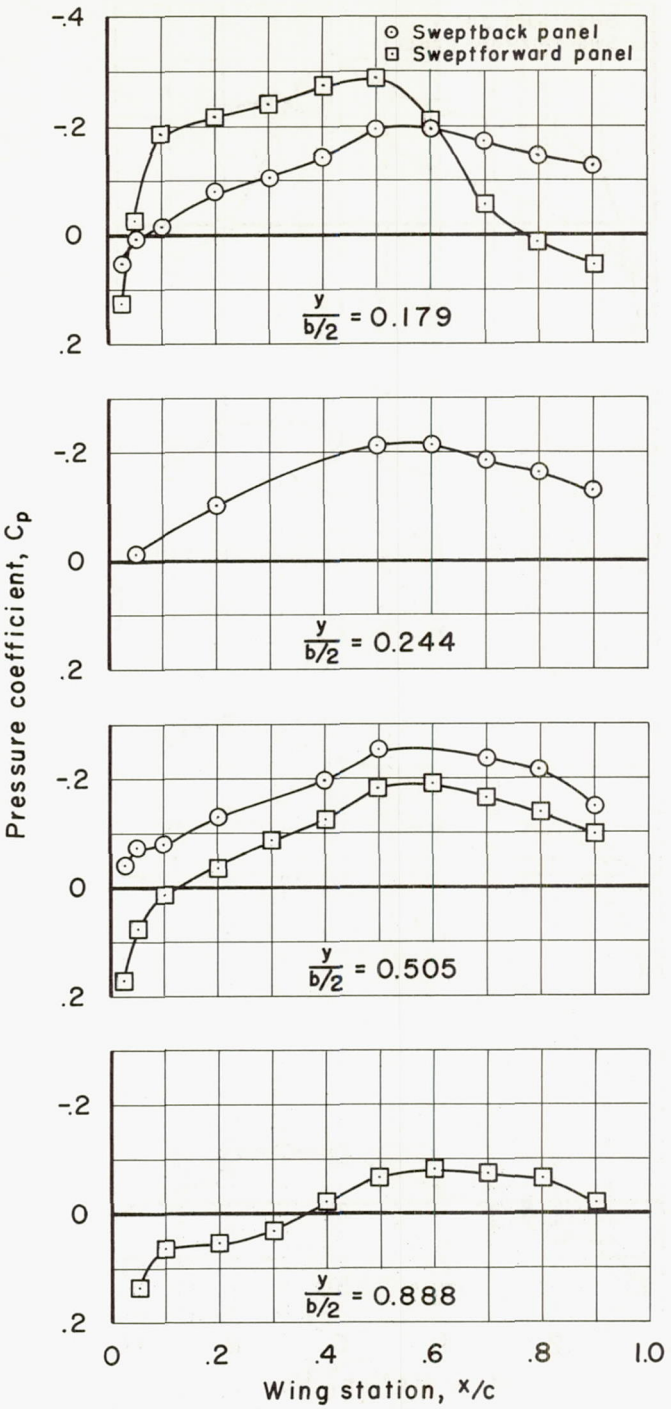

(f) M = 1.10; Sears-Haack body

Figure 34.- Continued.

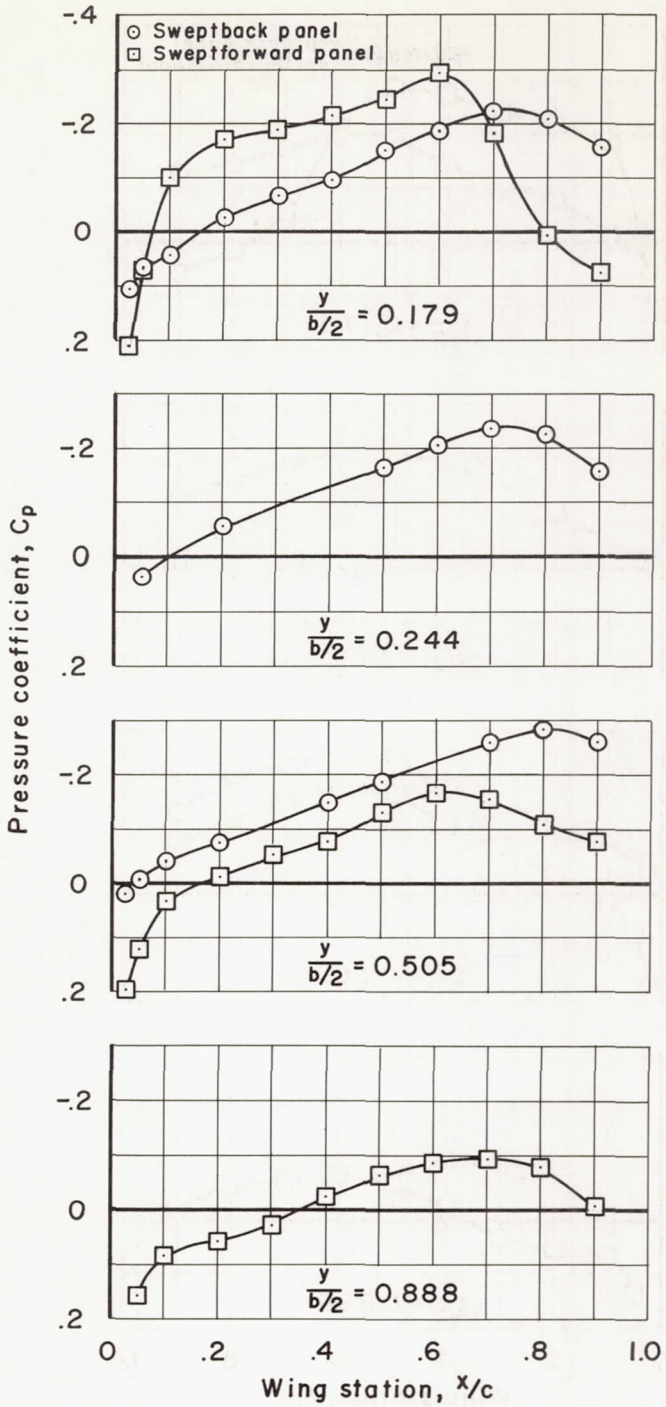

(g) M = 1.20; Sears-Haack body

Figure 34.- Concluded.

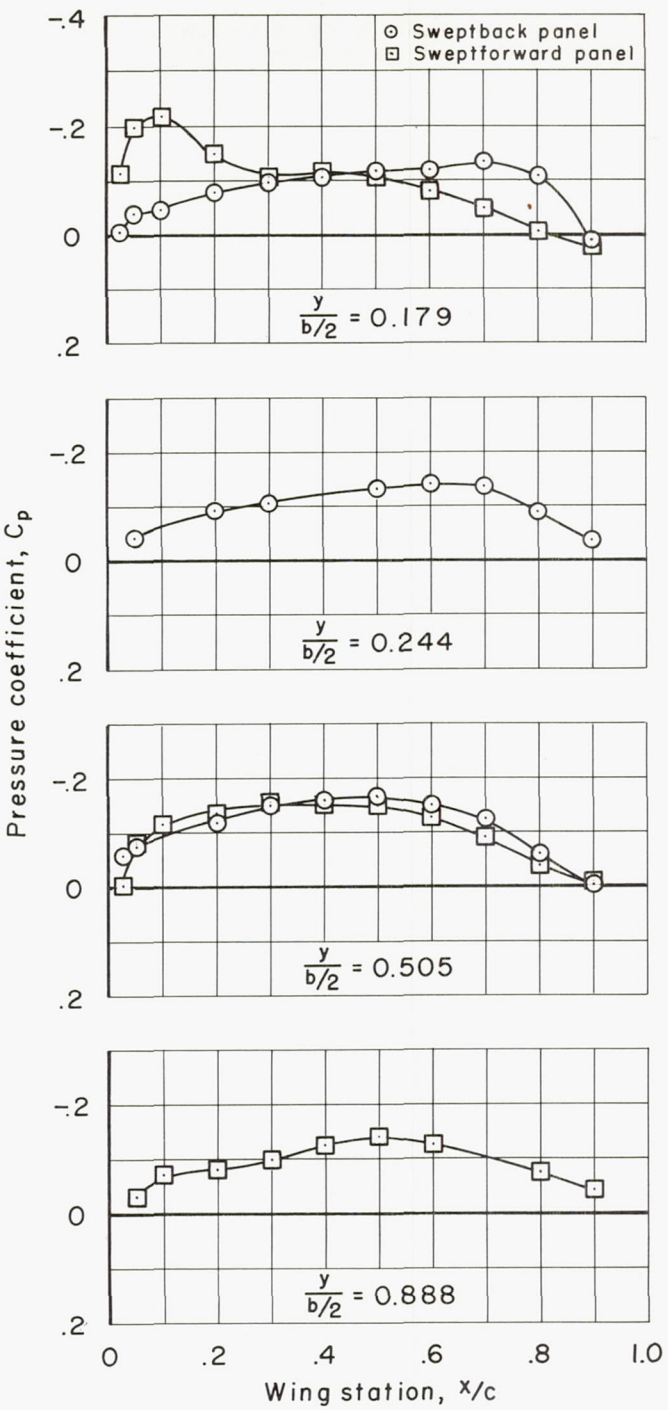

(a) M = 0.80; symmetrical M = 1.20 indented body

Figure 35.- Wing pressure coefficients at zero lift for the aspect-ratio-3 yawed wing with a symmetrical M = 1.20 indented body.

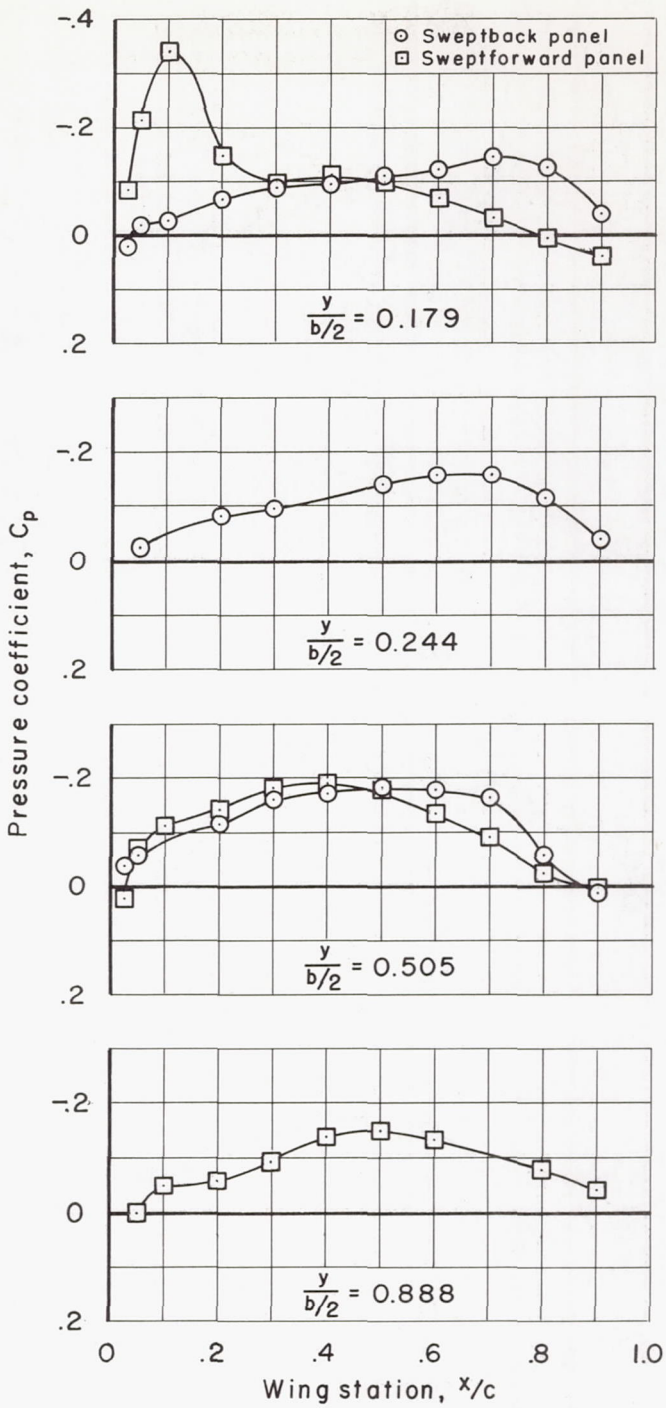

(b) M = 0.90; symmetrical M = 1.20 indented body

Figure 35.- Continued.

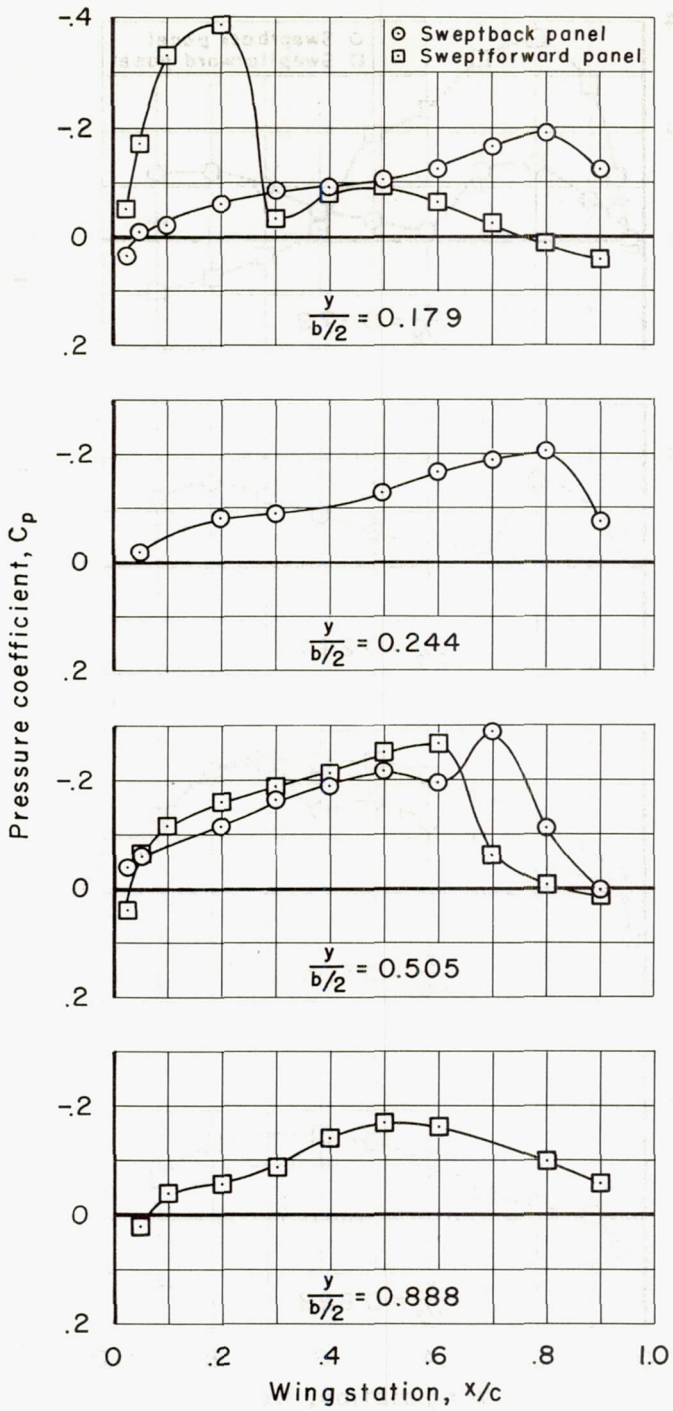

(c) M = 0.95; symmetrical M = 1.20 indented body

Figure 35.- Continued.

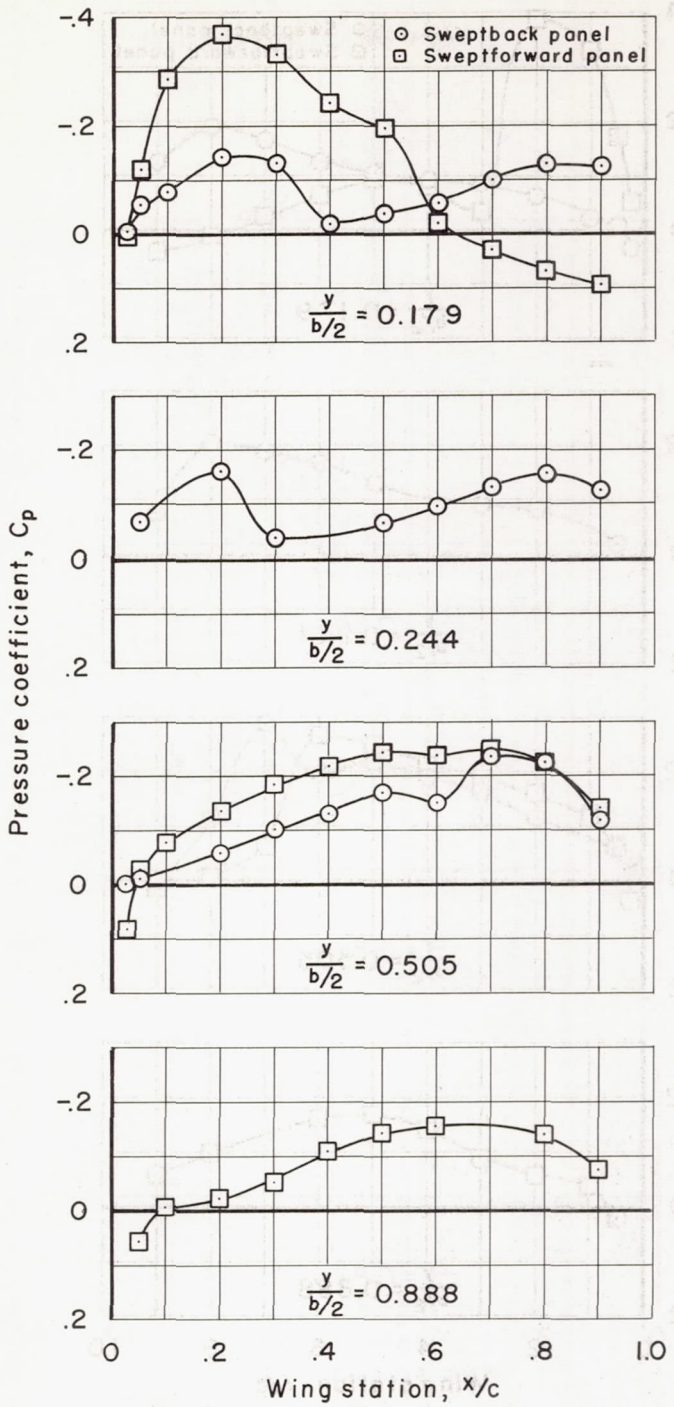

(d) M = 1.00; symmetrical M = 1.20 indented body

Figure 35.- Continued.

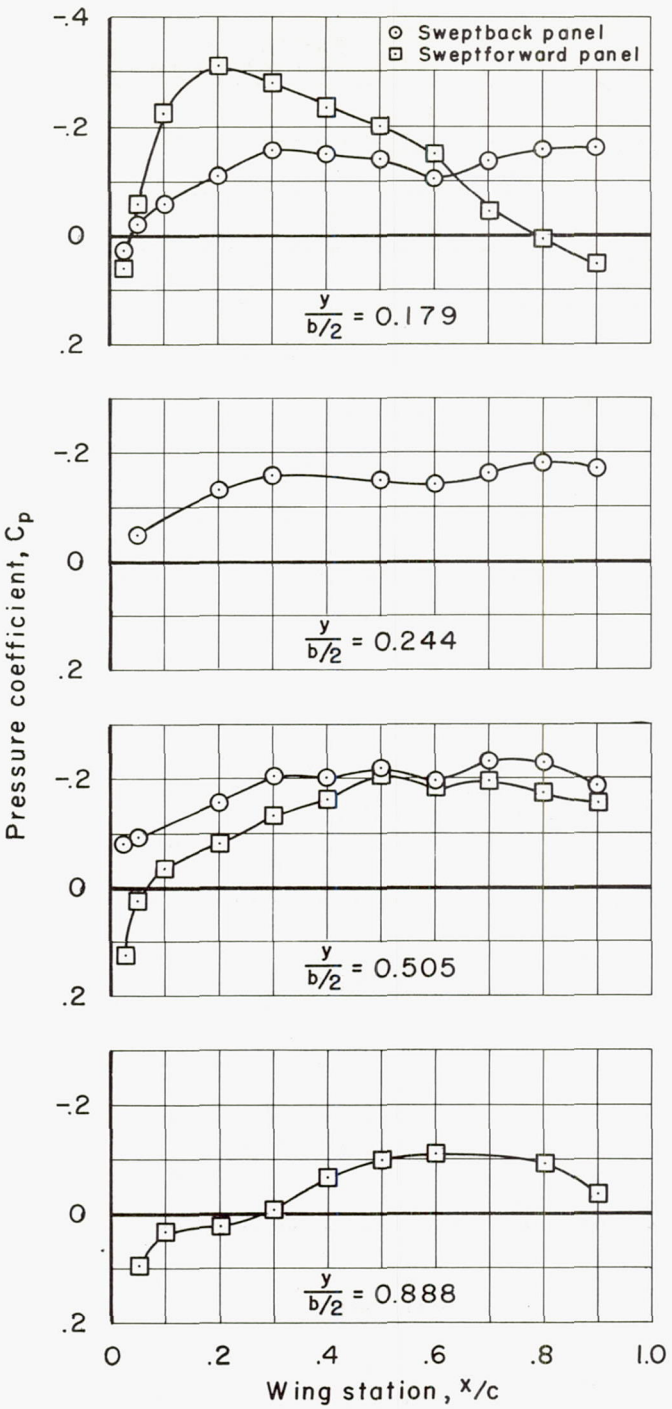

(e) M = 1.05; symmetrical M = 1.20 indented body

Figure 35.- Continued.

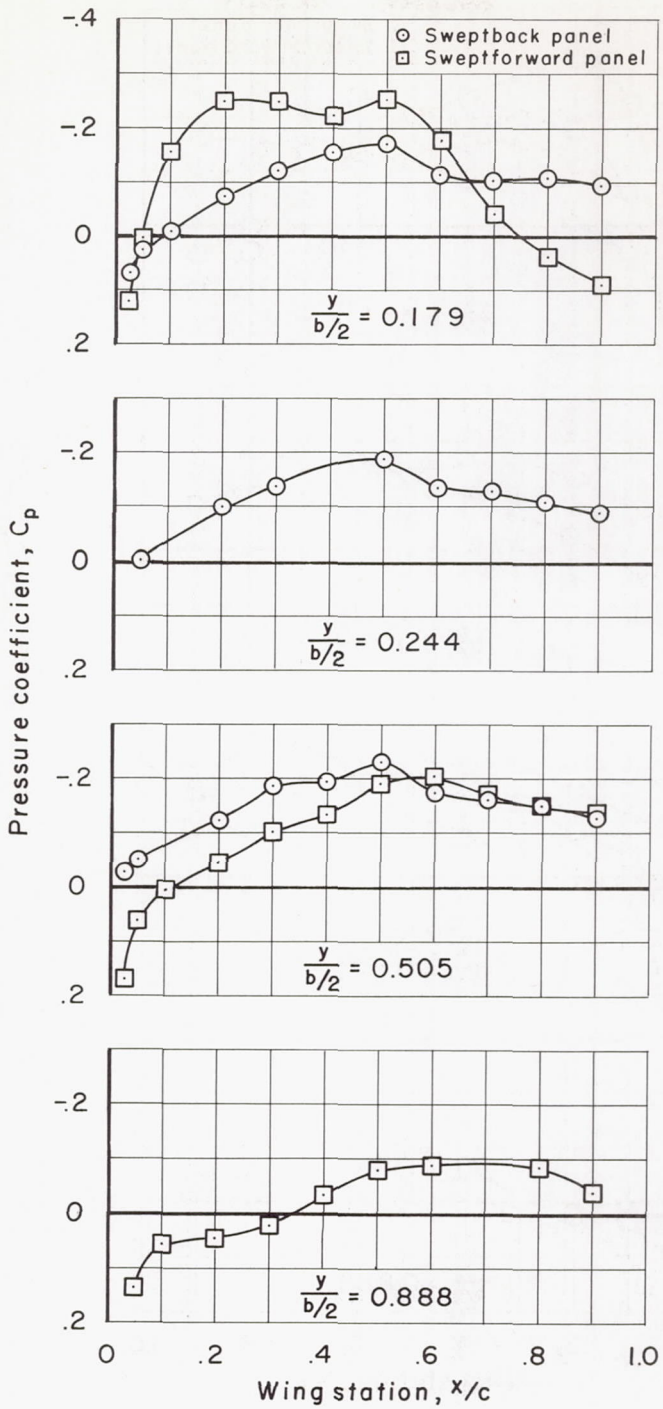

(f) M = 1.10; symmetrical M = 1.20 indented body

Figure 35.- Continued.

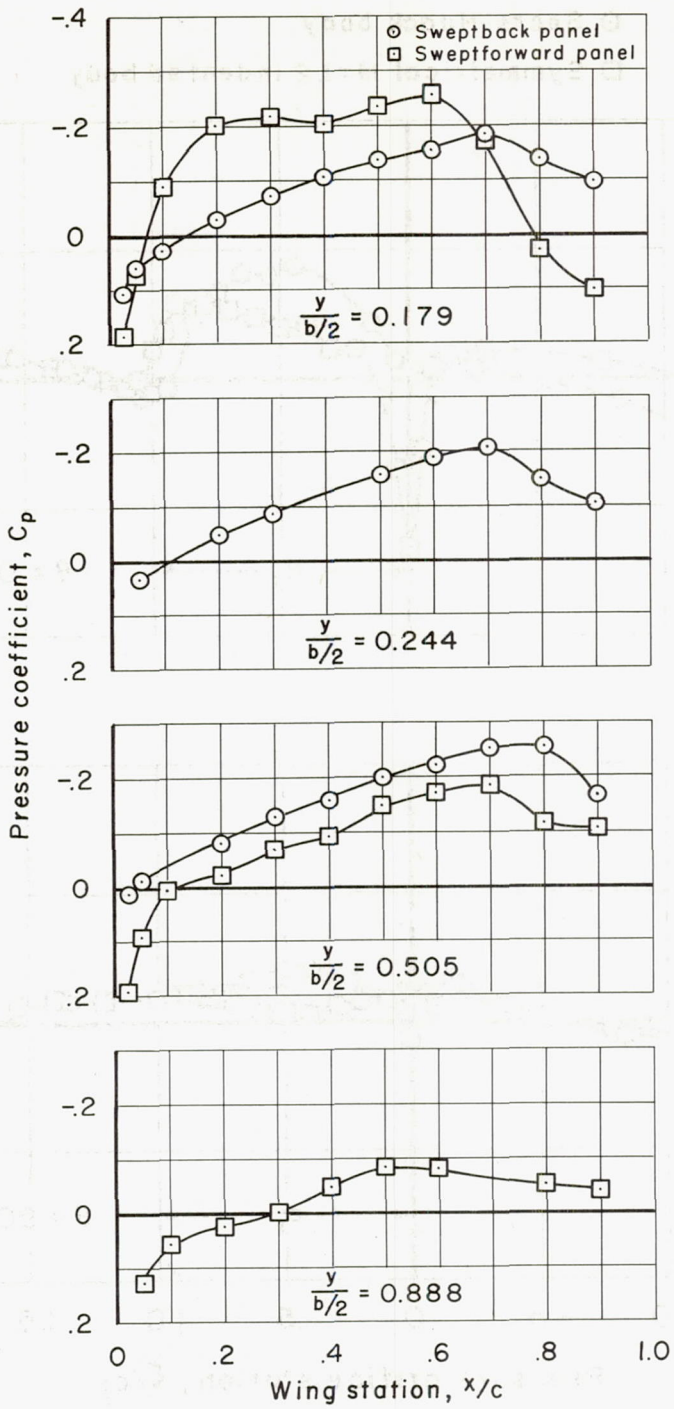

(g) M = 1.20; symmetrical M = 1.20 indented body.

Figure 35.- Concluded.

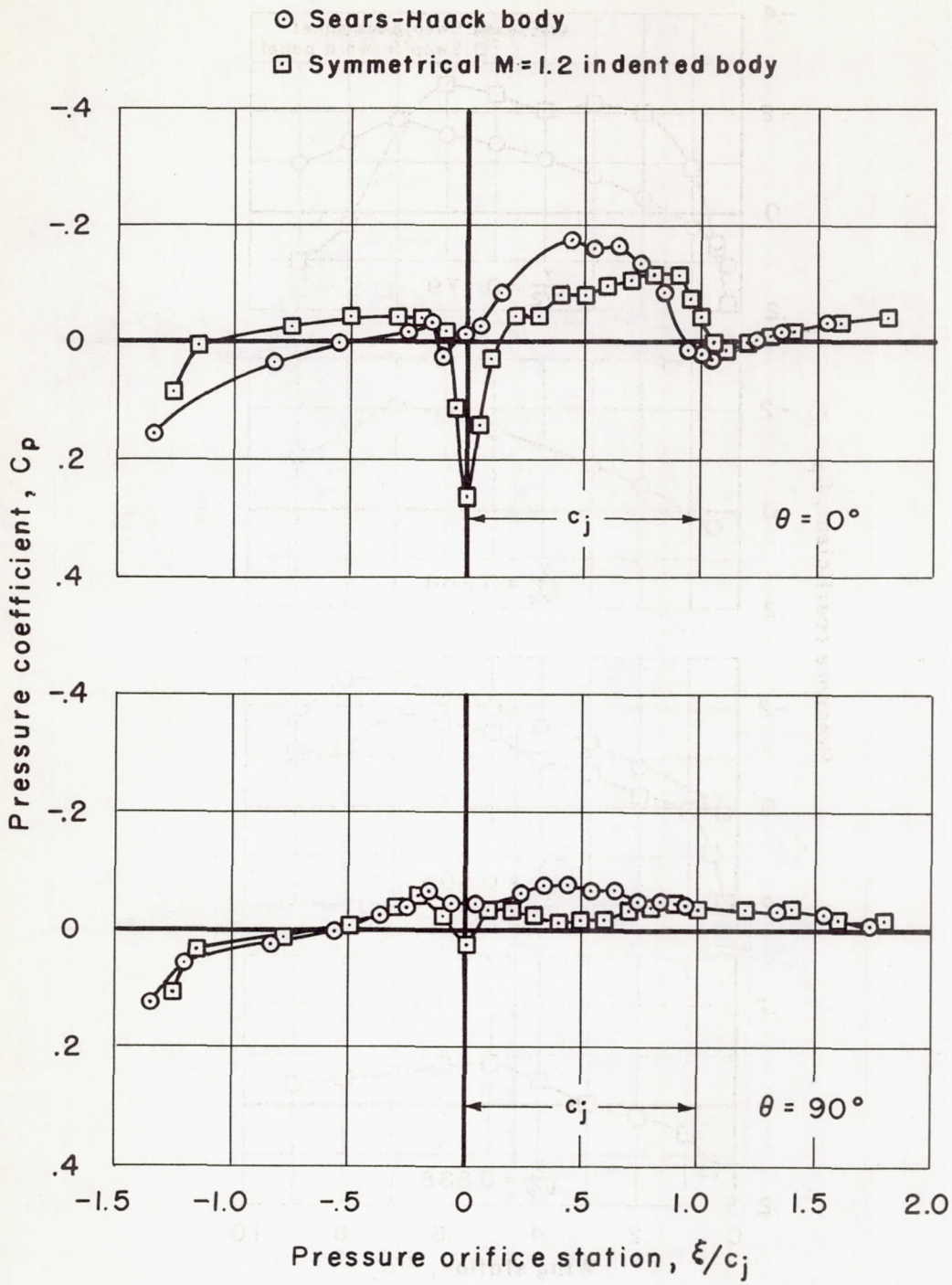

(a) M = 0.80

Figure 36.- Body pressure coefficients at zero lift for the aspect-ratio-3 yawed wing with a Sears-Haack body and a symmetrical M = 1.20 indented body.

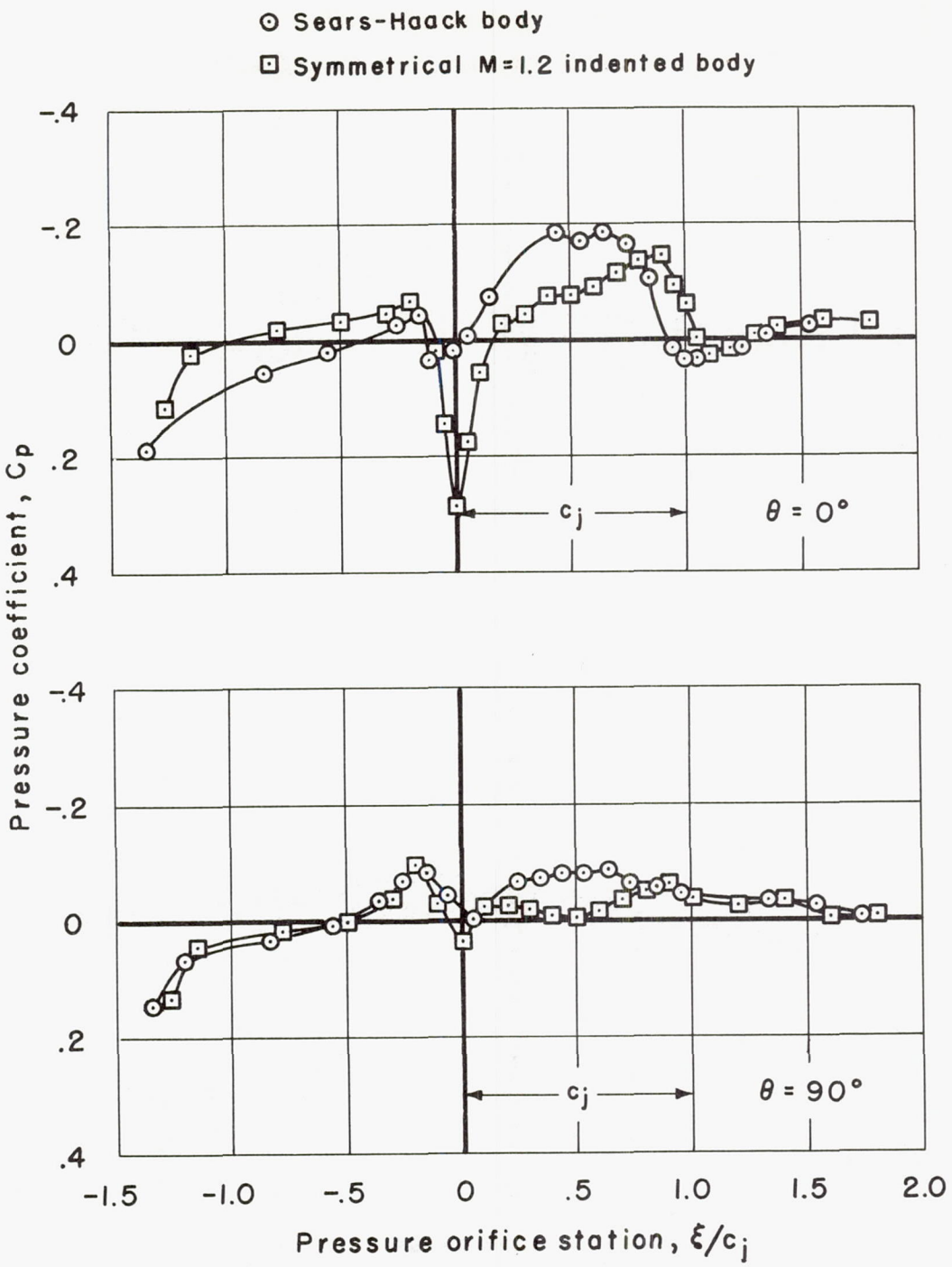

(b) M = 0.90

Figure 36.- Continued.

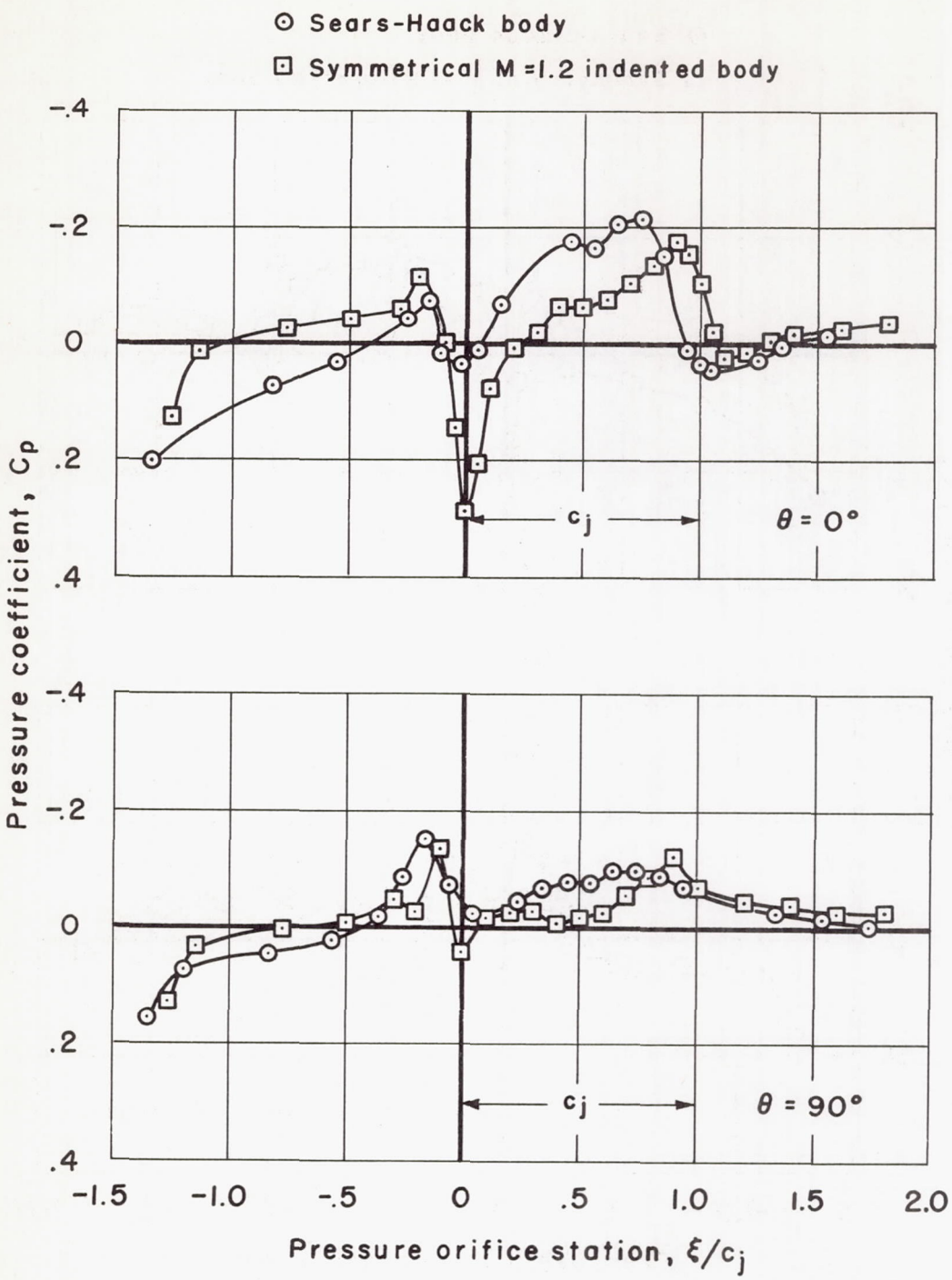

(c) M = 0.95

Figure 36.- Continued.

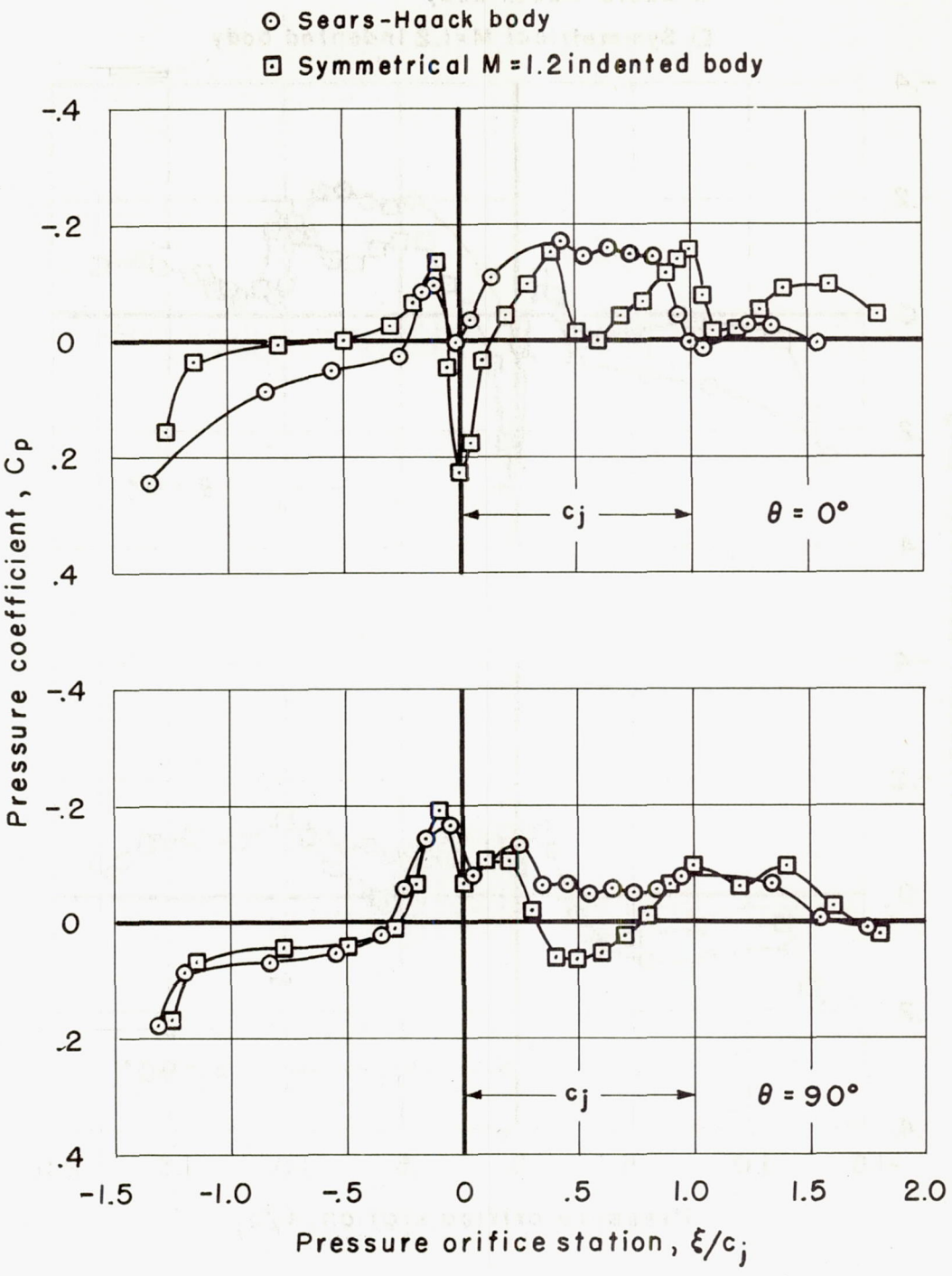

(d) M = 1.00

Figure 36.- Continued.

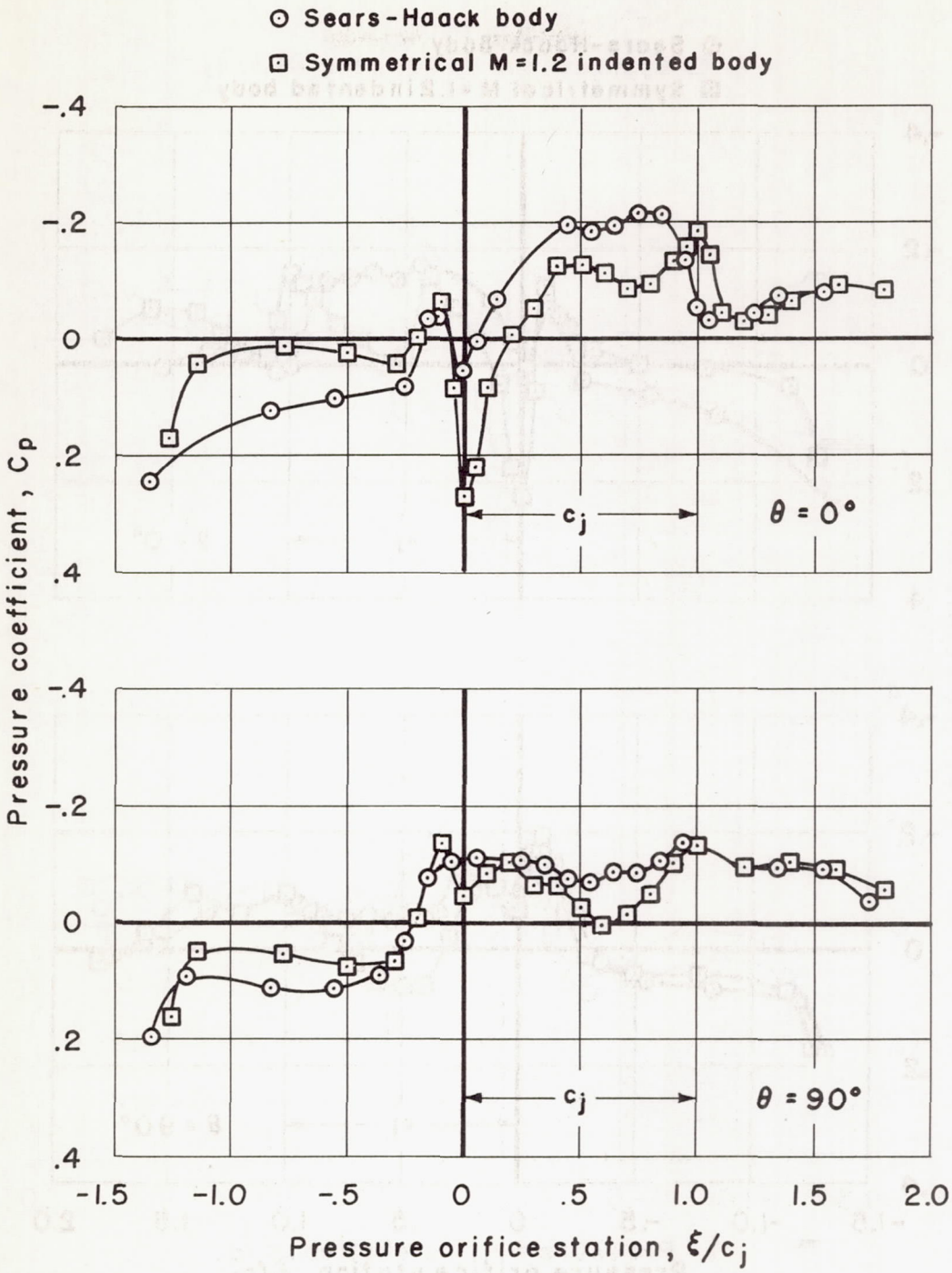

(e) M = 1.05

Figure 36.- Continued.

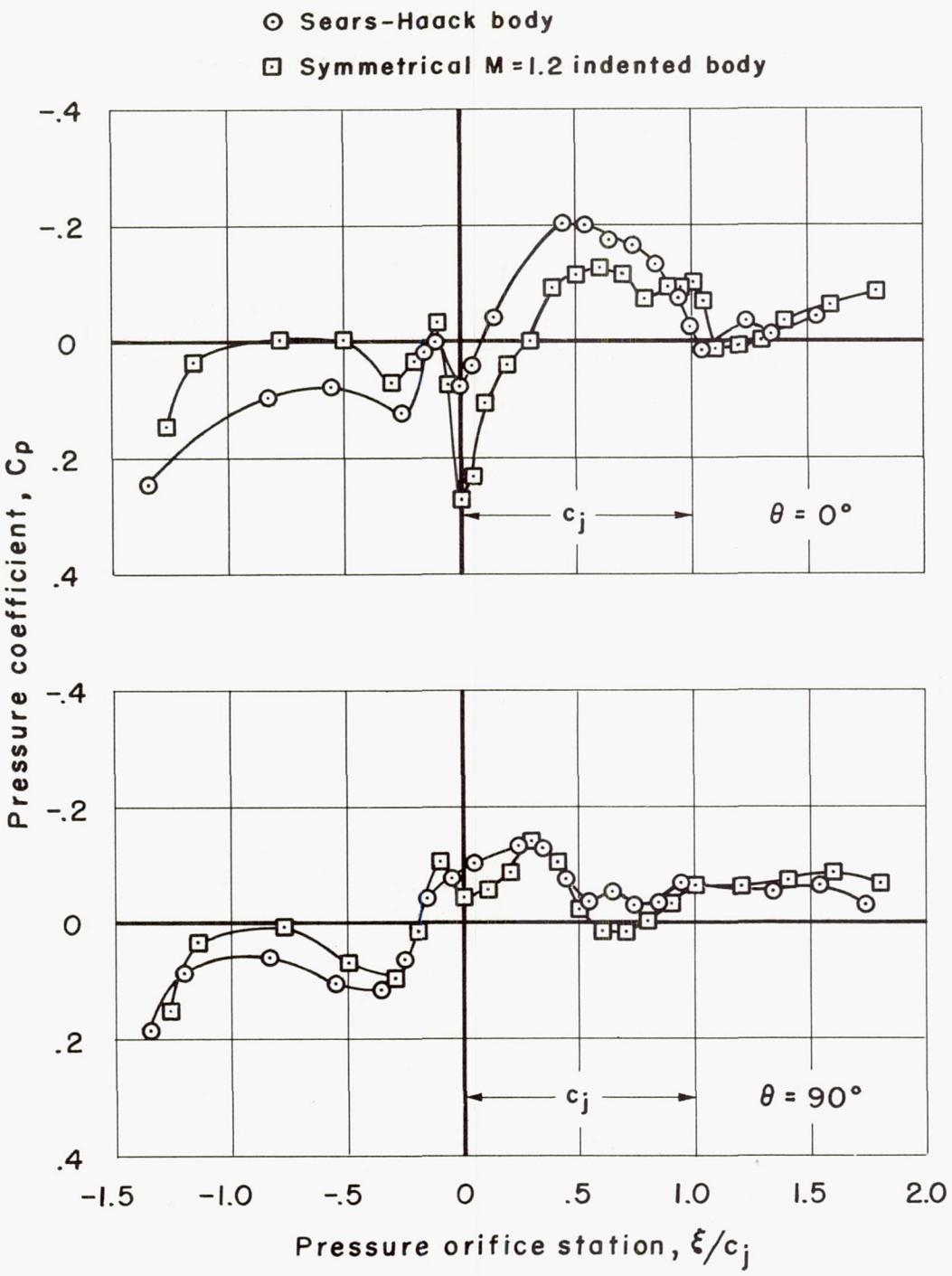

(f) M = 1.10

Figure 36.- Continued.

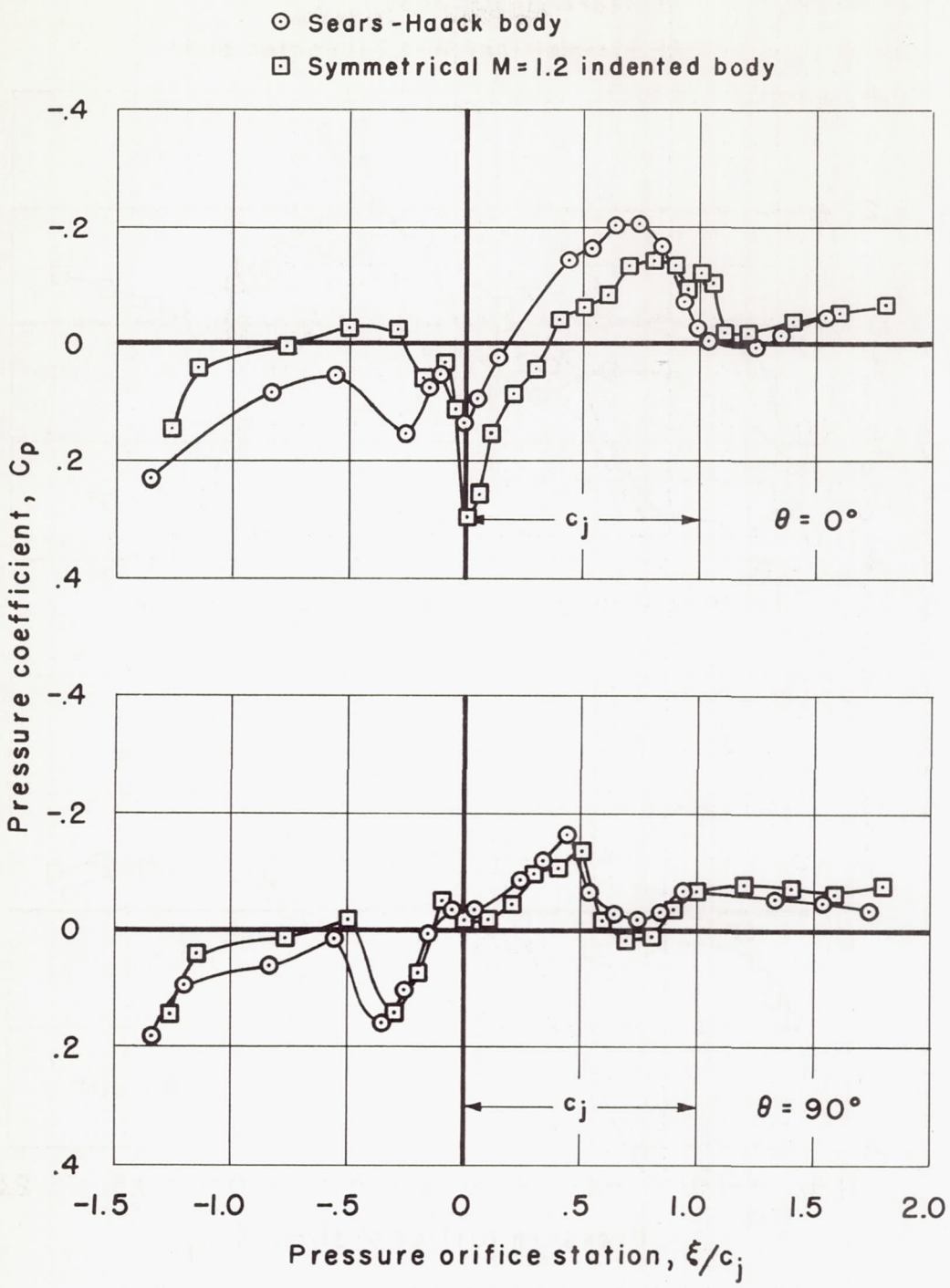

(g) M = 1.20

Figure 36.- Concluded.

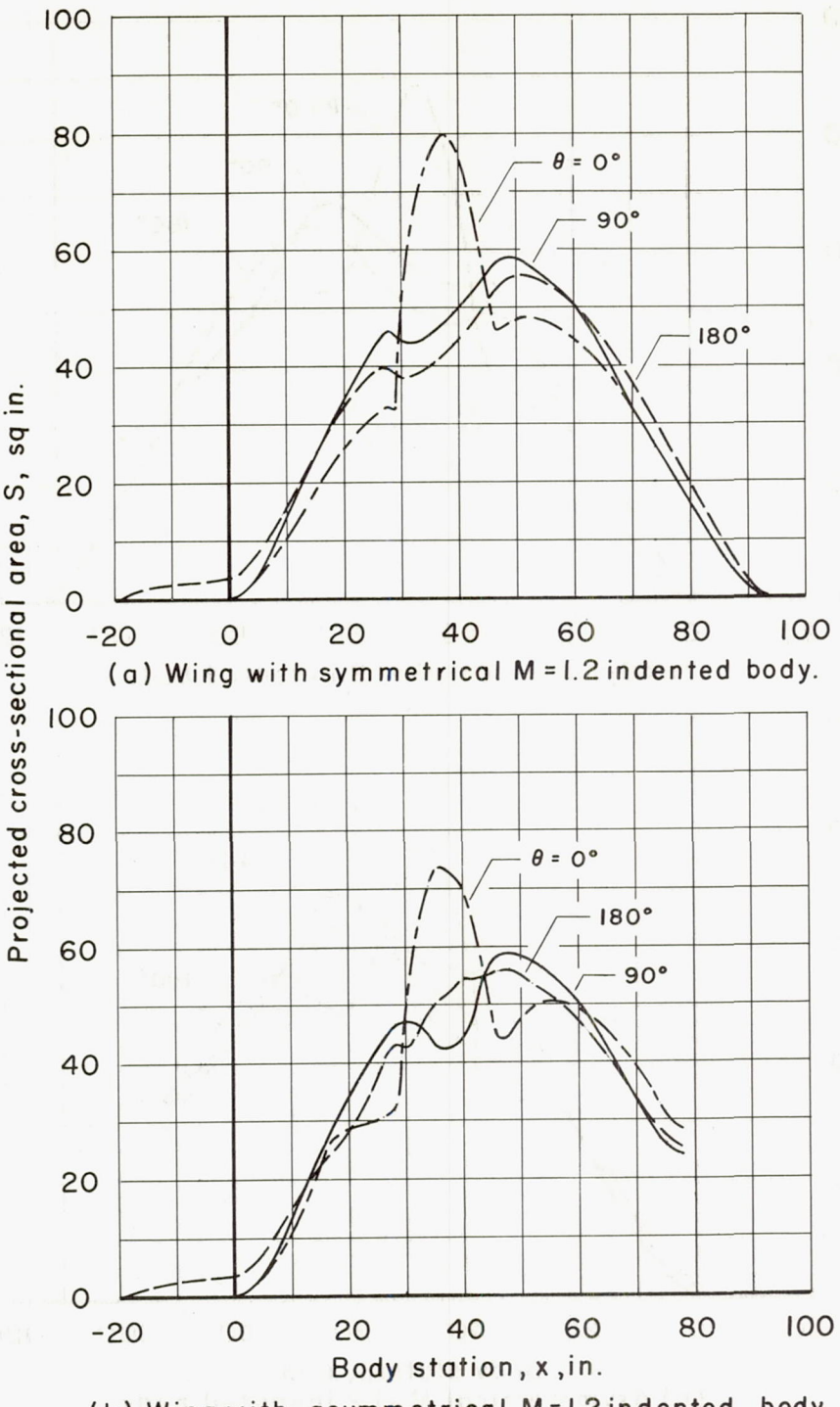

Figure 37.- Projected area distributions for the aspect-ratio-6 yawed wing with symmetrical and asymmetrical M = 1.20 indented bodies for cutting angles of $\theta = 0^\circ$, 90°, and 180° for M = 1.20.

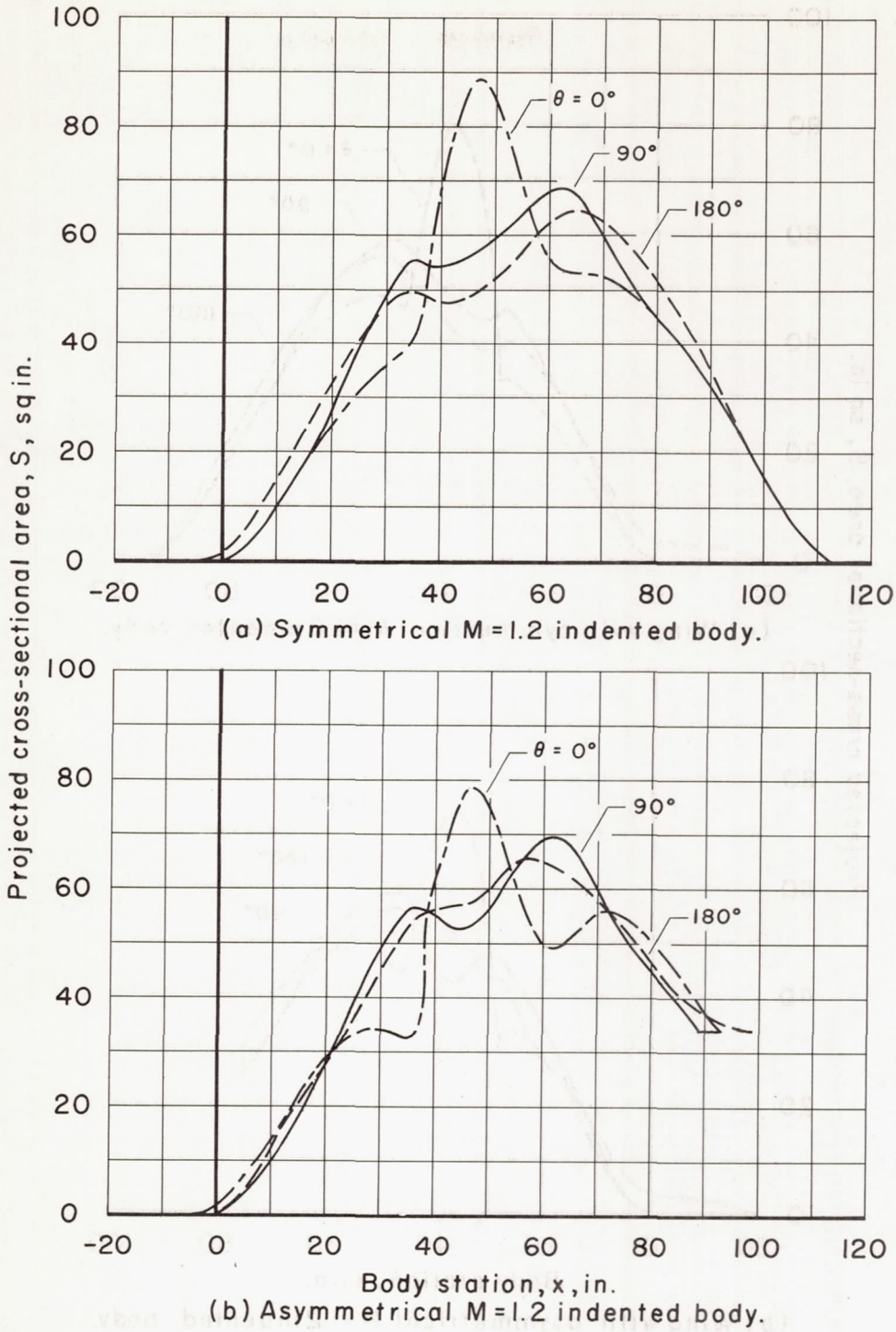

Figure 38.- Projected area distributions for the aspect-ratio-3 yawed wing with symmetrical and asymmetrical M = 1.20 indented bodies for cutting angles of $\theta = 0^{\circ}$, 90°, and 180° for M = 1.20.

NACA - Langley Field, Va.